Electrochemical Energy Reviews (2019) 2:277–311
https://doi.org/10.1007/s41918-019-00032-8

REVIEW ARTICLE

Li-Rich Layered Oxides and Their Practical Challenges: Recent Progress and Perspectives

Sijiang Hu[1,2] · Anoop. S. Pillai[1] · Gemeng Liang[1] · Wei Kong Pang[1] · Hongqiang Wang[3] · Qingyu Li[3] · Zaiping Guo[1]

Received: 15 December 2018 / Revised: 7 February 2019 / Accepted: 28 February 2019 / Published online: 19 March 2019

Abstract

Lithium-rich layered oxides (LLOs), also known as $Li_{1+x}M_{1-x}O_2$ or xLi_2MnO_3-$(1–x)LiMO_2$ (M = Ni, Co, Mn), have been regarded as some of the highest capacity lithium cathodes and have attracted increasing attention from battery researchers and engineers in recent years. This is because LLOs possess maximum possible capacities of ~ 280 to 310 mAh g^{-1} with a high working potential of ~ 3.7 V (vs. Li^+/Li^0) and an astounding energy density of ~ 900 Wh kg^{-1}. Despite these promising properties, these technologically important cathodes have not yet been successfully commercialized due to low initial Coulombic efficiency, poor rate capabilities and gradual capacity/voltage fade during electrochemical cycling as well as further complications from continuous structural changes during cycling. Here, researchers have concluded that these issues mainly originate from the electrochemical activation of Li_2MnO_3 components, which, although it provides anomalously high capacity performances, also causes associated complex anionic redox activities of O and irreversible structural and phase transformations during charging at potentials greater than 4.5 V (vs. Li^+/Li^0). To provide perspectives, this review will summarize various attempts made towards addressing these issues and present the connections between electrochemical properties and structural change. In addition, this review will discuss redox chemistries and mechanistic behaviours during cycling and will provide future research directions to guide the commercialization of LLOs.

Keywords Li-rich layered oxide · Surface coating · Voltage fade · Oxygen activities · Lithium-ion battery

1 Introduction

Lithium-ion batteries (LIBs) have experienced major breakthroughs in battery technology since being commercialized less than 3 decades ago. Since then, LIBs have been successfully applied in electrified vehicles (EVs) and are integral to daily life, with demand for higher energy density ever increasing. The International Energy Agency reported that the number of EVs (including battery electric vehicles (BEVs) and plug-in hybrid electric vehicles (PHEVs)) surpassed 3 million in 2017, which is a 56% increase from 2016 [1] and that this is a strong driving force for breakthroughs and evolution in battery technologies, in which aside from battery costs and safety [2], long-range BEVs require higher volumetric and gravimetric energy density (*i.e.* 750 Wh L^{-1} and 350 Wh kg^{-1}) [3].

However, cathodes in LIBs are intrinsic bottlenecks that restrict LIBs capacities and energy performances and current commercial cathode materials for BEVs and PHEVs such as $LiFePO_4$, $LiNi_{0.8}Co_{0.15}Al_{0.05}O_2$ (NCA) and the $LiNi_{1-x-y}Co_xMn_yO_2$ ($x+y<0.5$) (NCM) family

Sijiang Hu and Anoop. S. Pillai have contributed equally to this work.

✉ Wei Kong Pang
wkpang@uow.edu.au

✉ Zaiping Guo
zguo@uow.edu.au

[1] Institute for Superconducting and Electronic Materials, Australian Institute for Innovative Materials, University of Wollongong, Innovation Campus, North Wollongong, NSW 2500, Australia

[2] Hubei Key Laboratory for Processing and Application of Catalytic Materials, College of Chemistry and Chemical Engineering, Huanggang Normal University, Huanggang 438000, China

[3] School of Chemistry and Pharmaceutical Sciences, Guangxi Normal University, Guilin 541004, China

[*e.g.* $LiNi_{0.6}Co_{0.2}Mn_{0.2}O_2$ (NCM622), $LiNi_{0.8}Co_{0.1}Mn_{0.1}O_2$ (NCM811)] exhibit gravimetric energy densities lower than 800 Wh kg^{-1} [4]. In addition, the overall energy density of LIBs is further reduced by battery packaging.

To address these issues, considerable research has been conducted on the optimization and design of new cathode materials with high capacities (*e.g.* > 200 mAh g^{-1}) or high voltage (e.g. ⩾4 V vs. Li^+/Li^0) [5–11] with prospective high-voltage candidates including high-voltage spinel oxides ($LiNi_{0.5}Mn_{1.5}O_4$), lithium-rich layered oxides (LLOs) ($Li_{1+x}M_{1-x}O_2$, M = Ni, Co, Mn, etc.), nickel-rich layered oxides ($LiNi_{1-x}M_xO_2$, M = Co, Mn and Al) and high-voltage sulphate-, phosphate- or silicate-based polyanionic compounds (Fig. 1). And in particular, $Li_{1+x}M_{1-x}O_2$ or xLi_2MnO_3-$(1-x)LiMO_2$ (M = Ni, Co, Mn), known as LLOs, has attracted immense attention from researchers because they can deliver the highest energy density (~ 900 Wh kg^{-1}) thus far as compared with other conventional cathode materials.

The concept of LLO cathode materials originated from Thackeray et al. who investigated rock-salt-phase $Li_{1.09}Mn_{0.91}O_2$ and later introduced a strategy to design new cathode materials with high capacities (> 200 mAh g^{-1}) [13, 14]. Since then, the discharge capacity of LLOs has improved substantially, reaching above 300 mAh g^{-1} [15]. However, several issues still need to be addressed for LLOs before commercialization, including low initial Coulombic efficiency (ICE), capacity and voltage fade and poor rate capability [16–18]. And although numerous strategies have been applied to overcome these challenges, such as surface modification [19], lattice doping [20, 21] and more recently the alteration of O activities [22], the fundamental origins of the crystal structural change related to these issues, especially the voltage fade, and the mechanisms of how these changes contribute to such fading during cycling have not been elucidated clearly. Until recently, however, few studies have achieved breakthroughs in the understanding of the fundamental origin of the crystal structural changes [23–28] and most reviews have mainly focused on the structure [29], electrochemical performance [30], synthesis methods [31] or characterization technique [32] of LLO materials. Therefore, this review will comprehensively present the structure-function relationship of LLO materials along with explanations of their modifying strategy-issue connection from a fundamental perspective. In addition, this review will provide suggestions for ongoing high-energy cathode research.

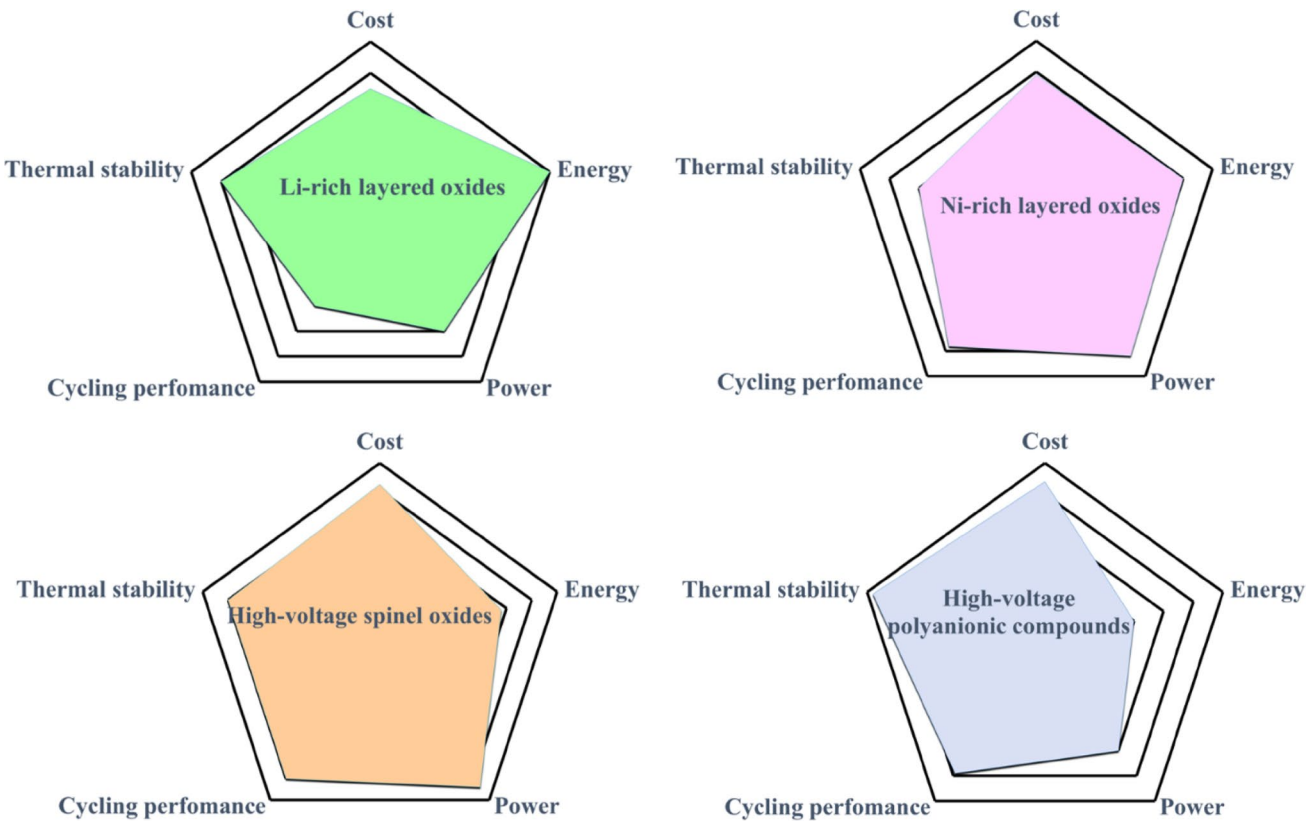

Fig. 1 Radar plot comparing the volumetric energy density, power, cycling performance, thermal stability and costs of various high-voltage cathode materials. *Source*: Reproduced with permission from Ref. [12]

2 Crystal Structures and Mechanistic Reactions

2.1 Crystal Structure

LLOs can be categorized into the xLi_2MnO_3-$(1-x)LiMO_2$ model (M stands for transition metals (TMs)) based on a two-phase model first proposed by Thackeray et al. [14, 33] and the $Li(Li_xM_{1-x})O_2$ model based on a solid solution model with a homogeneous long-range order as proposed by Dahn et al. [34, 35]. Here, both models are widely used in the literatures, and currently, the optimal model is still a matter of debate with no agreement being reached on the definition of the original structure of LLOs [36].

For the two-phase (xLi_2MnO_3-$(1-x)LiMO_2$) model, LLOs are regarded as composites in which a monoclinic symmetry Li_2MnO_3 phase (space group $C2/m$) is structurally integrated with a trigonal symmetry $LiMO_2$ phase (space group $R\bar{3}m$) at the atomic level [14] due to the similar O3-type layered structures of the two phases [37] with Li atom sites occupying octahedral sites in the structure with three MO_6 octahedral layers (Fig. 2a, b). Here, Mn and excess Li atoms (at a Li/Mn ratio of 1:2) form the MO_6 octahedral layers in the structure of the Li_2MnO_3 phase [37], and therefore, Li_2MnO_3 can be reformulated as $Li(Li_{1/3}Mn_{2/3})O_2$ [29]. Furthermore, the distances between the close-packed layers of the (001) plane in the Li_2MnO_3 monoclinic phase and the (003) plane in the $LiMO_2$ trigonal phase are both ~ 4.7 Å, allowing for the compatible integration of the two phases at the atomic level [38].

And as a result of the high compatibility of these two phases, researchers have also proposed that the MO_6 octahedral layers can contribute to a monoclinic superstructure with one LiO_6 octahedron surrounded by six MnO_6 octahedra to form a hexagonal $LiMn_6$ honeycomb in the Mn-rich layer, allowing for a solid solution ($Li_{1+x}M_{1-x}O_2$) model (Fig. 2c) [39] in which the cation ordering-derived superstructure can produce broad and weak peaks in the 2θ range of 20°–30° in the X-ray diffraction (XRD) patterns of LLOs (Fig. 2d).

Different synthetic methods have been suggested to be the cause of the discrepancy in the two LLO models. Based on this, Table 1 summarizes competing two-phase and single-phase models of LLOs through comparisons of experimental evidence and synthesis methods of various compounds reported in the literature in which 30% of the reported literature supports the two-phase composite model and 70% considers LLOs as a solid solution of either $R\bar{3}m$ or $C2/m$. Here, much of the literature suggesting a phase composite model is solely based on selected characterization techniques and their conclusions do not appear to be reliable due to the structural complexity and similarity between the two phases of LLOs, and in their final analyses, a unique reference structure for the LLOs cannot be fully established because of the strong correlation to synthesis conditions and compositions.

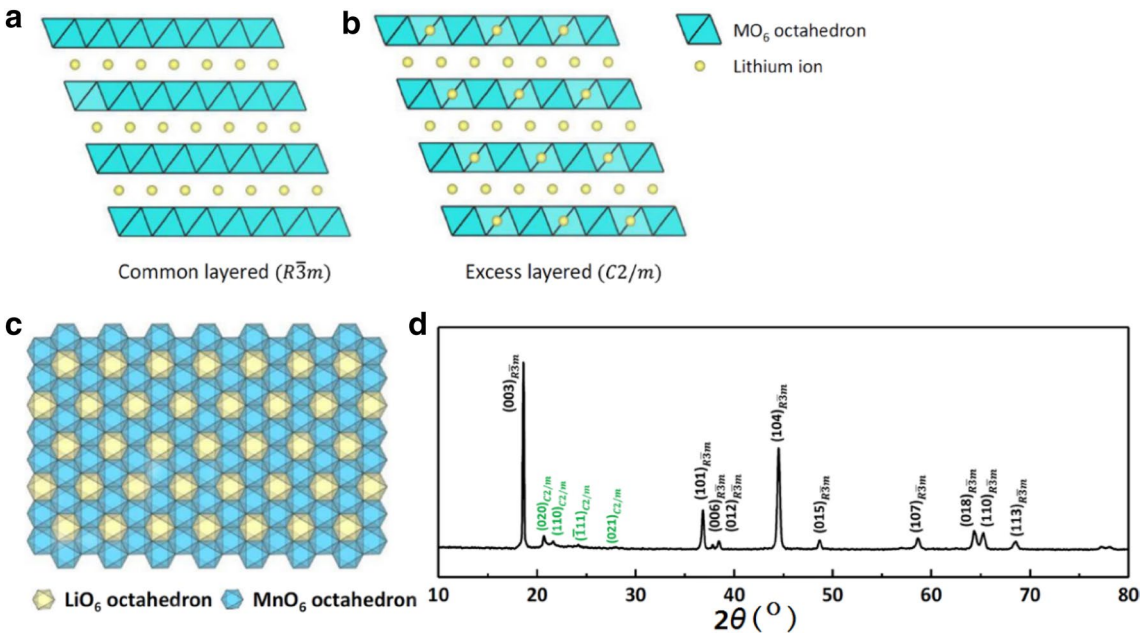

Fig. 2 Schematic of structure crystallography. **a** $LiMO_2$ structure ($R\bar{3}m$), **b** monoclinic Li_2MnO_3 ($C2/m$), **c** Li/Mn atom ordering in LiM_2 layer in Li_2MnO_3, **d** XRD pattern of layered $0.5Li_2MnO_3$-$0.5LiMn_{0.5}Ni_{0.5}O_2$ material. *Source*: Reproduced with permission from Ref. [37]

Table 1 Summary of reported LLO materials with notations based on competing models

	Material composition; notation	Characterization techniques	Synthesis method/sintering conditions	Ref.
Two-phase ($R\bar{3}m$+ $C2/m$) composite	$Li_{1.2}Mn_{0.55}Ni_{0.15}Co_{0.10}O_2$; $0.5LiCo_{0.25}Mn_{0.375}Ni_{0.375}O_2$-$0.5Li_2MnO_3$	NPD, magnetic susceptibility studies	Co-precipitation Commercial powder (Toda HE5050)	[40]
	$Li_{1.5}Ni_{0.25}Mn_{0.75}O_{2.5}$	In situ XRD, HAADF-STEM	Co-precipitation, 600 °C-6 h and 900 °C-14 h	[41]
	$Li_{1.2}Mn_{0.61}Ni_{0.18}Mg_{0.01}O_2$; $0.6Li(Li_{1/3}Mn_{2/3})O_2$-$0.4LiNi_{0.45}Mn_{0.525}Mg_{0.025}O_2$	SXRPD, HAADF-STEM, NBED, EELS	Solid-state reaction, 1000 °C for 24 h	[42]
	$0.5Li_2MnO_3$-$0.5LiMn_{0.42}Ni_{0.42}Co_{0.16}O_2$	SXRPD	Solid-state reaction 1000 °C for 20 h	[43]
	$Li_{1.19}Ni_{0.25}Mn_{0.56}O_2$; $Li_{1.25}Ni_{0.17}Mn_{0.61}O_2$: $Li_{0.85}Ni_{0.57}Mn_{0.55}O_2$ (74: 26 wt%)	SXRPD, NPD	Single-step one-pot method, 850 °C for 6 h at 1 °C/min	[44]
	$Li_{1.2}Ni_{0.2}Mn_{0.6}O_2$	La-APT, STEM-EDS	–	[45]
	$Li_{1.2}Co_{0.4}Mn_{0.4}O_2$; ~ 0.5 Li_2MnO_3-0.5 $LiCoO_2$	HAADF-STEM, SAED, EELS, EXAFS	900 °C for 12 h	[46]
	$Li_{1.2}Mn_{0.567}Ni_{0.166}Co_{0.067}O_2$	ABF/HAADF-STEM	Solid-state reaction 1000 °C for 20 h	[38]
	$Li[Li_{(1-x)/3}Co_xMn_{(2-2x)/3}]O_2$ ($0 \leqslant x \leqslant 1$)	Monte Carlo simulation	Combinatorial synthesis, 900 °C/800 °C cooling rate of 1 °C/min	[47]
	$Li(Li_{0.2}Ni_{0.2}Mn_{0.6})O_2$	HAADF-STEM, EELS	Co-precipitation, 900 °C-24 h	[48]
	$Li_{1.2}Mn_{0.55}Ni_{0.15}Co_{0.10}O_2$;	AC-STEM, EELS	Commercial powder (Toda HE5050)	[49]
	$Li_{1.2}Ni_{0.16}Mn_{0.51}Al_{0.05}Co_{0.08}O_2$	XRD, HRTEM, NBED, Raman Spectroscopy	Solution combustion reaction, 700 °C-1 h and 900 °C-20 h	[50]
	$Li_{1.2}Ni_{0.23}Co_{0.12}Mn_{0.5}O_2$	NPD, XRD	Co-precipitation, 900 °C-16 h	[51]
	$Li_{1.2}Ni_{0.2}Mn_{0.6}O_2$; $0.5Li_2MnO_3$-$0.5LiNi_{0.5}Mn_{0.5}O_2$	ED, HAADF-STEM, EELS, XEDS	Co-precipitation, 900 °C-15 h	[52]
	$Li_{1.2}Ni_{0.2}Mn_{0.6}O_2$	XRD, HRTEM, HAADF-STEM, SAED, EELS, XEDS	Co-precipitation, 900 °C-6 h	[53]
	$Li_{1.2}Ni_{0.2}Mn_{0.6}O_2$; 0.5 Li_2MnO_3-$0.5Li(Ni_{0.5}Mn_{0.5})O_2$	NPD	Co-precipitation, 900 °C-6 h	[54]
	$Li(Li_{0.2}Ni_{0.2}Mn_{0.6})O_2$	XRD	Co-precipitation, 900 °C-15 h	[55]
	$Li_{1.2}Mn_{0.4}Fe_{0.4}O_2$; $(1-x)Li_2MnO_3$-$xLiFeO_2$($x=0.5$)	STEM-EELS, NBED, HRTEM	Co-precipitation, mixed alkaline hydrothermal method (220 °C-8 h, 850 °C-1 h) and cooled by quenching	[56]
	NMC.Li_2MnO_3 composite and multilayer films	HAADF-STEM, SAED, HRTEM	Pulsed laser deposition(750 °C)	[57]
$C/2m$ Single phase	$0.5Li_2MnO_3$-$0.5LiNi_{0.8}Co_{0.1}Mn_{0.1}O_2$	ABF/HAADF-STEM, XRD, Raman Spectroscopy	Co-precipitation, 450 °C-6 h and 850 °C-12 h	[58]
	$Li(Li_{0.19}Ni_{0.16}Co_{0.08}Mn_{0.57})O_2$	XRD, HRTEM, SAED	Co-precipitation, 900 °C-10 h	[59]
	$Li_{(2x+2)/(2+x)}Ni_{(2-2x)/(6+3x)}Co_{(2-2x)/(6+3x)}Mn_{(2+4x)/(6+3x)}O_2$ ($0 \leqslant x \leqslant 1$)	XRD, HRTEM, Raman Spectroscopy	Spray pyrolysis, 900 °C-10 h	[60]
	$Li(Ni_{0.17}Li_{0.2}Co_{0.07}Mn_{0.56})O_2$	XRD, HRTEM, SAED	Solid-state reaction, 800 °C-10 h and 900 °C-12 h	[61]
	$Li_{1.2}Ni_{0.15}Co_{0.1}Mn_{0.55}O_2$; $Li(Ni_{0.375}Co_{0.25}Mn_{0.375})O_2$-$Li(Li_{1/3}Mn_{2/3})O_2$	XRD, SAED, TEM, EXAFS, HAADF-STEM, STEM-EDS	–	[18]
	xLi_2MnO_3-$(1-x)LiNi_{2/3}Co_{1/6}Mn_{1/6}O_2$	XRD, Raman Spectroscopy, TEM	Sol-gel, 950 °C-12 h	[62]
	$Li_{1.200}Mn_{0.540}Ni_{0.130}Co_{0.13}0O_{2+\delta}$	XRD, HRTEM	Electrospinning, 800 °C-12 h	[63]
	$Li_{1.16}Mn_{0.6}Co_{0.12}Ni_{0.12}O_2$	Raman Spectroscopy, XRD	Hydrothermal (180 °C-12 h, 450 °C-6 h, 650 °C-24 h)	[63]
	$Li_{1.2}Mn_{0.54}Ni_{0.13}Co_{0.13}X_{0.03}O_2$ (X = Si and Sn)	XRD, HAADF/ABF-STEM	Sol-gel, 450 °C-5 h and 900 °C-12 h	[64]

Table 1 (continued)

	Material composition; notation	Characterization techniques	Synthesis method/sintering conditions	Ref.
	xLi_2MnO_3-$(1-x)Li(Mn_{0.375}Ni_{0.375}Co_{0.25})O_2$ $(0 \leqslant x \leqslant 1)$	XRD, HRTEM	Auto-combustion route, 800 °C-12 h	[65]
	$Li[Ni_xLi_{(1/3-2x/3)}Mn_{(2/3-x/3)}]O_2$	XRD	Mixed hydroxide method, 480 °C-3 h and 900 °C-3 h	[35]
	$Li_{1.2}Ni_{0.2}Mn_{0.6}O_2$	XRD	Co-precipitation 750 °C-12 h	[36]
	xLi_2MnO_3-$yLiNi_{1/2}Mn_{1/2}O_2$-$(1-x-y)$ $LiNi_{1/3}Co_{1/3}Mn_{1/3}O_2$	STEM-EELS, TEM, XRD	Co-precipitation, 900 °C-12 h	[66]
	$Li[Li_{(1-2x)/3}Ni_xMn_{2/3-x/3}]O_2$	NMRS, XRD, DIFFaX simulation	Double mixed hydroxide method, 480 °C-12 h and 1000 °C-3 days	[67]
	$Li(Li_{0.2}Ni_{0.2}Mn_{0.6})O_2$; $Li[Ni_xLi_{(1/3-2x/3)}Mn_{(2/3-x/3)}]O_2$	HAADF-STEM, D-STEM, XRD, NBED	EDTA and citric acid compl-exation route, 850 °C-5 h	[68]
	$Li_{1.2}Mn_{0.55}Ni_{0.15}Co_{0.1}O_2$	HAADF-STEM, EELS, XEDS	Co-precipitation, commercial powder (Toda HE5050)	[69]
	$Li(Li_{0.2}Ni_{0.2}M_{0.6})O_2$	HAADF-STEM, XEDS	Hydrothermal assisted, 900 °C-24 h	[70]
	$Li_{1.25}Mn_{0.56}Ni_{0.19}O_{1.93}$	XRD, HAADF-STEM, EELS	Solid-phase calcination method, 900 °C-12 h	[71]
	$Li_{1.2}Mn_{0.6}Ni_{0.2}O_2$	SXRPD, HRTEM	Solid-state reaction	[28]
	$Li(Li_{0.20}Ni_{0.20}Mn_{0.60})O_2$	HAADF-STEM, EELS	Hydrothermal assisted, 900 °C and cooling by quenching	[72]
	$Li_{1.95}Mn_{0.9}Co_{0.15}O_3$	XRD, NPD	Co-precipitation, 900 °C-12 h	[73]
	$Li_{1.2}(Ni_{0.13}Mn_{0.54}Co_{0.13})O_2$; Li_yMO_2, $y>1$, M = Mn, Co and Ni and Mn > Ni > Co	HAADF-STEM, XEDS, EELS	Molten salt method	[69]
	$Li_{1.2}Ni_{0.13}Mn_{0.54}Co_{0.13}O_2$	XRD, HAADF-STEM, NMRS	–	[74]
	$Li(Li_{0.23}Ni_{0.15}Mn_{0.62})O_2$	XRD	Solid-state reaction, 900 °C-8 h	[75]
	$Li(Li_{0.2}Ni_{0.13}Mn_{0.54}Co_{0.13})O_2$	XRD, ABF/HAADF-STEM	Co-precipitation, 500 °C-5 h and 850 °C-12 h	[76]
	$Li_{1.85}Mn_{0.7}Co_{0.45}O_3$, $Li_{1.95}Mn_{0.9}Co_{0.15}O_3$; $Li_{2-\delta}(Mn_{1-x}Co_x)_{1+\delta}O_3$	XRD, HREM, TEM, ED	Co-precipitation, 950 °C-12 h	[77]
	$Li(Li_{0.20}Mn_{0.58}Ni_{0.18}Co_{0.04})O_2$	XRD, HAADF-STEM	Co-precipitation, 1000 °C-12 h, different cooling rates	[78]
$R\bar{3}m$ Single phase	$Li_{1.20}Mn_{0.54}Co_{0.13}Ni_{0.13}O_2$	XRD, NPD	Sol-gel, (800-1000) °C	[79]
	$Li(Co_{1-x}Li_{x/3}Mn_{2x/3})O_2$ $(0 \leqslant x \leqslant 1)$	XRD	Solid-state reaction, 900 and 1000 °C-20 h	[80]
	$Li\ [Ni_xMn_{\ (2-x)/3}Li_{\ (1-2x)/3}]\ O_2$ $(0 \leqslant x \leqslant 0.5)$	XRD, NMRS, first-principles computations	Co-precipitation, 900 °C-24 h	[81]
	$Li(Ni_xLi_{1/3-2x/3}Mn_{2/3-x/3})O_2$ $(0 \leqslant x \leqslant 0.5)$	SXRPD, TEM, ED	Co-precipitation 900 °C-24 h, cooled by quenching	[82]
	$Li[Li_{(1-x)/3}Co_xMn_{(2-2x)/3}]O_2$ $(0 \leqslant x \leqslant 1)$	Monte Carlo simulation	Combinatorial synthesis, quenched from 900/800 °C	[47]
	$Li_{1.20}Mn_{0.54}Co_{0.13}Ni_{0.13}O_2$	HAADF-STEM, electron nanodif-fraction	Sol-gel, 900 °C	[83]
	$Li(Li_{x/3}Co_{1-x}Mn_{2x/3})O_2$ $(0.5 \leqslant x \leqslant 1)$	XRD	Spray drying, 750 –950 °C-15 h	[84]
	$Li_{1.17}Mn_{0.56}Ni_{0.135}Co_{0.135}O_2$	XRD	Carbonate synthesis route, 500 °C-3 h and 900 °C-18 h, cooling by quenching	[85]
	$Li[Ni_xLi_{(1/3-2x/3)}Mn_{(2/3-x/3)}]O_2$ ($x = 1/2$, 2/7 and 1/5)	XRD, FT-IR	Co-precipitation, 500 °C-12 h and 1000 °C-12 h	[86]

Table 1 (continued)

Material composition; notation	Characterization techniques	Synthesis method/sintering conditions	Ref.
$Li(Li_{0.144}Ni_{0.136}Co_{0.136}Mn_{0.544})O_2$	NPD, HRTEM, EELS	Co-precipitation, 500 °C-5 h and 800 °C-15 h	[15]
$Li_{1.7}Mn_{0.4}Co_{0.9}O_3$; $Li_{1.6}Mn_{0.2}Co_{1.2}O_3$; $Li_{2-\delta}(Mn_{1-x}Co_x)_{1+\delta}O_3$	XRD, HREM, TEM, ED	Co-precipitation, 950 °C-12 h	[77]
$Li_{1.2}Ni_{0.175}Co_{0.1}Mn_{0.52}O_2$	XRD, Raman Spectroscopy	Co-precipitation commercial powder (Toda)	[87]
$Li(Ni_{0.183}Li_{0.20}Co_{0.022}Mn_{0.583})O_2$	XRD, HAADF-STEM	Co-precipitation, 1000 °C	[88]
xLi_2MnO_3-$(1–x)LiNi_{0.5}Mn_{0.5}O_2$ ($x = 0.7$ and 0.3)	Raman Spectroscopy, XRD	Co-precipitation, 900 °C-12 h	[87]

XRD: X-ray powder diffraction, NPD: neutron powder diffraction, SXRPD: Synchrotron X-ray powder diffraction, HAADF-STEM: high-angle annular dark-field scanning transmission electron microscopy, ABF-STEM: annular bright-field scanning transmission electron microscopy, AC-STEM: aberration-corrected scanning transmission microscopy, ED: electron diffraction, FT-IR: fourier transform infrared microscopy, NMRS: nuclear magnetic resonance spectroscopy, HRTEM: high-resolution transmission electron microscopy, XEDS: X-ray energy-dispersive spectroscopy, NBED: nanobeam electron diffraction, EELS: electron energy loss spectroscopy, La-APT: laser-assisted atom probe tomography, HREM: high-resolution electron microscopy, SAED: selected area electron diffraction

2.2 Mechanistic Reactions of LLOs

Although the structure of LLOs is still debated, Mn-containing LLOs do possess unique mechanistic behaviours based on highly compatible intergrown structures in which it is generally accepted that the mechanistic behaviours and corresponding structural and phase evolutions are similar for all LLOs [14]. Therefore, by using the two-phase notation as a model and the composition triangle originating from Thackeray et al. [14], the mechanistic reactions of layered $0.3Li_2MnO_3$-$0.7LiMn_{0.5}Ni_{0.5}O_2$ (as an example) can be clearly described by using its typical initial two cycles and corresponding incremental capacity (dQ/dV) plots (Fig. 3a) [14, 89]. Here, upon charging to 4.4 V, Li extraction occurs with the redox couple of Ni^{2+}/Ni^{4+} in the electrochemically active $LiMn_{0.5}Ni_{0.5}O_2$ component based on a solid solution reaction mechanism to form $0.3Li_2MnO_3$-$0.7Mn_{0.5}Ni_{0.5}O_2$ [14, 90]. During this stage, the Li_2MnO_3 component is electrochemically inactive and can act as a Li reservoir to compensate for Li extraction from the active layer through Li migration from the octahedral sites in the MO_6 octahedral layers to the tetrahedral sites in the Li-consuming layers, thus ensuring integrated structural stability (Fig. 3b) [14]. In addition, the existence of Li in both tetrahedral and octahedral sites in the Li-consuming layer can endow LLO materials with more interstitial Li spacing and enhance reaction kinetics. Furthermore, as charging voltage increases to above 4.4 V, a long flat plateau can be observed which can be associated with the activation process of the Li_2MnO_3 phase involving Li loss and O release from the monoclinic structure [39]. Here, the product obtained at the end of the charging process is a metastable MnO_2 phase, implying a two-phase reaction mechanism. And upon discharge, Li can intercalate into MnO_2 and MO_2 lattices to form rock-salt-type $LiMnO_2$ and $LiMO_2$ phases, respectively [14, 22]. Overall, as described in the composition triangle (Fig. 3c) [14], the mechanistic reactions of LLO electrodes in the initial cycles can be illustrated as follows:

$$xLi_2MnO_3\text{-}(1-x)LiMO_2 \xrightarrow{\text{Charging} < 4.4\ \text{V}} xLi_2MnO_3\text{-}(1-x)MO_2 + (1-x)Li \quad (1)$$

$$xLi_2MnO_3\text{-}(1-x)MO_2 \xrightarrow{\text{Charging} > 4.4\ \text{V}} xMnO_2\text{-}(1-x)MO_2 + xLi_2O \quad (2)$$

$$xMnO_2\text{-}(1-x)MO_2 + Li \xrightarrow{\text{Discharging} \sim 2.0\ \text{V}} xLiMnO_2\text{-}(1-x)LiMO_2 \quad (3)$$

Here, the process of Li^+ extraction (Eq. 2) along with O evolution during Li_2MnO_3 activation in the first cycle [16, 25, 54, 91, 92] is a one-off reaction behaviour that is not only linked with initial irreversibility but also linked with the highly anomalous reversible capacity involving the anionic redox species, O, which can coordinate with metal ions (*i.e.* Mn, Ni or Li) or form peroxo-like O_2^{n-} species [39]. In their study, Koga et al. [93] proposed that all cations were in the oxidation state of +4 after charging and recovered to their normal state after discharging, implying that TM cation redox cannot fully explain the observed extra capacity. Here, the researchers concluded that lattice oxygen could undergo reversible redox reactions within the bulk and that irreversible O loss occurred at the surface [94]. Furthermore, researchers have conducted theoretical and experimental studies and have reported that the anionic redox reactions of O anions can not only lead to extra capacity, but also affect the mechanistic behaviour and electrochemical performance of LLOs [22, 95]. In addition,

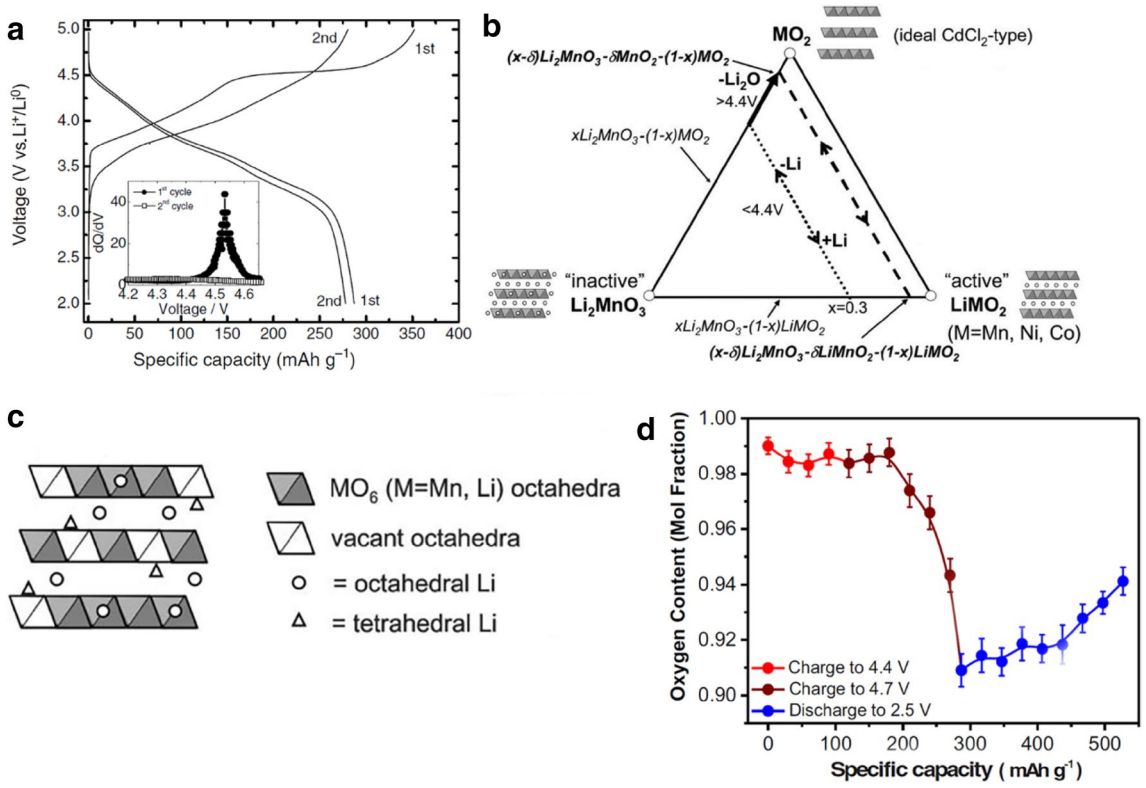

Fig. 3 **a** Typical voltage profiles and d*Q*/d*V* plots (inset) of $0.3Li_2MnO_3$-$0.7LiMn_{0.5}Ni_{0.5}O_2$ electrode. **b** Compositional phase diagram illustrating the electrochemical reaction pathways at different voltages in LLO electrodes. **c** Schematic of diffusion from octahedral sites to tetrahedral sites. **d** Oxygen content in $0.4Li_2MnO_3$–$0.6LiMn_{0.5}Ni_{0.5}O_2$ electrode during the first cycle. *Source*: **a** Reproduced with permission from Ref. [89]. **b**, **c** Reproduced with permission from Ref. [14]. **d** Reproduced with permission from Ref. [96]

Armstrong et al. [54] were the first to track oxygen evolution using in situ differential electrochemical mass spectrometry (DEMS) and powder neutron diffraction (NPD). Here, the researchers demonstrated that O_2 was released from LLOs during charging and suggested that this surface oxygen loss can lead to structural changes, with Li from octahedral sites migrating into Li layers and creating vacancies which were subsequently occupied by TM ions, simulating the formation of metastable rock-salt MnO_2. In later studies, Hy et al. [91] used in situ surface-enhanced Raman spectroscopy (SERS) to confirm the formation of a Li_2O phase and Muhammad et al. [96] reported significant drops in the O content in a $0.4Li_2MnO_3$-$0.6LiMn_{0.5}Ni_{0.5}O_2$ electrode during the first charge (190–280 mAh g^{-1}) (*e.g.* 4.4–4.7 V) (Fig. 3d). Here, the decomposition of conventional electrolyte solutions can also occur, especially at high-voltage operations (> 4.4 V).

In general, the mechanistic behaviours of LLOs are complex and are closely related to performance. However, significant research is required to elucidate these behaviours. In addition, although researchers have reported that anionic oxygen redox reactions and oxygen evolution give rise to the extra capacity in LLOs, the relationship between these two oxygen activities is not fully understood. However, the phase evolution and electrochemical performance of LLOs are obviously linked to the activities associated with the Li_2MnO_3 activation process. Overall, the precise understanding of high-voltage (> 4.4 V) mechanisms and corresponding effects on electrochemical performance is attainable through a combination of advanced characterization tools to explain bulk and surface reactions of LLOs.

3 Challenges and Strategies

To address the challenging issues of LLOs (*i.e.* low ICE, capacity and voltage fade and poor rate capability), it is vital to understand the origin of such issues, which are closely connected to underlying mechanistic reactions and structural/chemical evolutions. Here, many methods have been attempted by researchers, and surface modifications and lattice doping have been reported to be useful. In this review, various surface modifications and lattice doping strategies for LLOs are summarized, along with corresponding effects on the issues of low ICE, capacity/voltage fade and poor rate capability (Tables 2, 3).

3.1 Low Initial Coulombic Efficiency (ICE)

3.1.1 The Origins of Low ICE

All LLOs suffer from low ICE, which is unfavourable in real-world applications [16, 28, 54, 73, 97]. For example, Wu et al. [98] reported that LLOs generally suffered from an initial capacity loss in the range of 60–120 mAh g^{-1}, implying an ICE of ~ 65% to 83%, based on a systematic investigation of surface modifications on LLOs. Similarly, Rozier et al. [29] reported an ICE of 25% for a $Li_{1.2}Ni_{0.2}Mn_{0.6}O_2$ electrode (Fig. 4a), Thackeray et al. [89] reported an ICE of 81.3% for a $0.3Li_2MnO_3$-$0.7LiMn_{0.5}Ni_{0.5}O_2$ electrode and West et al. [99] reported an ICE of 27% for a $Li_{1.2}Ni_{0.175}Mn_{0.52}O_2$ electrode, indicating that ICEs vary with LLO composition.

Mechanistically, the mechanisms for these low ICEs or the initial irreversible capacity loss are typically a combination of irreversible Li and O loss from the LLO lattice in conjunction with possible electrolyte decomposition at high voltage (Eq. 2) [15, 28, 100, 101]. For example, Kang et al. [102] reported that acid treatment can be applied to $0.5Li_2MnO_3$-$0.5LiNi_{0.44}Co_{0.25}Mn_{0.31}O_2$ to remove Li_2O from the Li_2MnO_3 component before cycling and can greatly improve ICE. And although this approach is not considered to be fully successful because the acid-leached samples demonstrated worse cycling performances and rate capabilities as compared with pristine samples, this approach does confirm the origin of low ICE and can guide researchers. Furthermore, researchers also proposed a combination of LLOs with Li receptor oxides such as V_2O_5 [103] and MnO_2 [104], which can act as intercalation hosts to "catch" isolated Li^+ for reinsertion back into the layered lattice after the initial charge, to improve ICE. Alternatively, Xu et al. [28] used in situ DEMS to characterize two LLOs ($Li_{1.2}Ni_{0.2}Mn_{0.6}O_2$ and Mn-free $Li_{1.2}Ni_{0.2}Ru_{0.6}O_2$) by monitoring gas ($O_2$ and CO_2) evolutions at 4.5 V during the first charge and suggested that O_2 evolution only contributed to less than half of the total capacity loss, whereas non-volatile electrolyte decomposition played a major role in this context (Fig. 4b). However, from the perspective of this review, low ICE mainly arises from the loss of Li and O because high ICE values (90%–95%) can be achieved through O activity (anionic redox) modifications and Li diffusion enhancements without targeting electrolyte decomposition/passivation [101, 105].

3.1.2 Efforts to Improve ICE

3.1.2.1 Particle Size Control The use of nanocomposites and nanometre-thick coatings has proved to dramatically impact electronic and ionic conduction pathway optimizations [106, 107], which are closely related to the Coulombic efficiency (CE) of LIB electrode materials. And because nanoparticles typically possess higher surface areas that are directly exposed to electrolytes, there are higher rates of side reactions. Therefore, it is important to keep primary particle sizes at an appropriate scale for LLOs [108, 109]. This was demonstrated by Li et al. [110] and Yabuuchi et al. [111], both of whom claimed that particle size can greatly affect LLO structural evolutions and electrochemical properties. In the study by Li et al. [110], the researchers compared the charge-discharge profiles of LLO electrodes with large and small particle sizes at different cycles and their corresponding structural evolutions during cycling using in situ XRD (Fig. 5a, b) and reported that the large-particle LLO exhibited a two-phase reaction mechanism, whereas the small-particle LLO exhibited no phase separation upon charging to above 4.5 V (Fig. 5a, b). Here, the researchers suggested that O loss occurred throughout the bulk of small-particle LLO, whereas O loss only occurred on the surface of large-particle LLO, resulting in smaller capacity loss and higher ICE for the large-particle LLO. Despite these results, this study sacrificed the completeness of the reactions and the deliverable capacity to increase the ICE and cycling performance of the LLOs and did not show a solid improvement to the ICE. Nevertheless, there is no doubt that particle size can affect LLOs through its effects on structural evolution during cycling [108–111].

3.1.2.2 Surface Modification Because O loss occurs at the electrode/electrolyte interface and is accompanied by various side reactions [110, 112–114], surface modification has become one of the most effective approaches to improve ICE, in which surface modifications can act as a protective layer or a source of surface structure modification to positively influence ICE. For example, Wu et al. [98] investigated ICE based on a series of protective coatings on LLOs (Fig. 6a, b) and reported that the coated samples, in particular those with Al_2O_3 and $AlPO_4$ coatings, exhibited higher ICE and discharge capacities than pristine samples. In another study, Sun et al. [59] reported that a thin AlF_3 coating can effectively enhance the electrochemical performance of $Li(Li_{0.19}Ni_{0.16}Co_{0.08}Mn_{0.57})O_2$ (Fig. 6c) and hypothesized that the improvement can be attributed to the transformation of the Li_2MnO_3 component to a spinel phase resulting from the effects of Li chemical leaching by the AlF_3 layer. Here, the researchers suggested that the coating-induced changes to the original structure/composition can alter mechanistic behaviours and vary O activities during O evolution and Li_2MnO_3 activation, thus reducing Li and O loss and improving ICE. Furthermore, the researchers also hypothesized that this improvement arose from the increased retention of oxide ion vacancies in the lattice after the initial charge, particularly in the Al_2O_3- and $AlPO_4$-modified samples. Overall, a wide range of materials, including other oxides and electron and ion conductive materials, have been employed as coatings to improve the ICE of different LLOs.

Table 2 Surface modification strategies to improve ICE

Type of coating	Surface coating	LLOs	First cycle (DC, CE at 0.1 C) (pristine)	First cycle (DC, CE at 0.1 C) (modified)	Capacity retention (modified)	Rate performance ($DC_{pristine}$, $DC_{modified}$, C rate)	Ref.
Surface gradient doping	Na^+	$0.5Li_2MnO_3$-$0.5LiNi_{1/3}Co_{1/3}Mn_{1/3}O_2$	187, 63%	286, 87%	~88% after 100 cycles at 0.2 C	128, 182, 2 C	[116]
	PO_4^{3-}	$Li_{1.17}Mn_{0.5}Ni_{0.17}Co_{0.16}O_2$	276, 72%	300, 86%	95% after 100 cycles at 0.1 C	17, 128, 6 C	[117]
	Nb^{5+}	$Li_{1.2}Mn_{0.54}Ni_{0.13}Co_{0.13}O_2$	276, 81%	320, 87%	94.5% after 100 cycles at 0.1 C	175, 200, 2 C	[118]
	Si^{4+}	$Li_{1.2}Mn_{0.54}Ni_{0.13}Co_{0.13}O_2$	283, 78.8%	286.5, 81.4%	70.4% after 100 cycles at 1 C	13.2, 50, 10 C	[64]
	Sn^{4+}	$Li_{1.2}Mn_{0.54}Ni_{0.13}Co_{0.13}O_2$	283, 78.8%	279.3, 82.1%	86.2% after 100 cycles at 1 C	13.2, 127, 10 C	[64]
Typical surface coating	AlF_3	$Li(Li_{0.19}Ni_{0.16}Co_{0.08}Mn_{0.57})$	227.6, 82.8%	240.6, 96.3%	91.6% after 100 cycles at 0.5 C	164.2, 190, 2 C	[59]
	$PrPO_4$	$Li(Li_{0.19}Ni_{0.16}Co_{0.08}Mn_{0.57})$	282.8, 81.8%	286.9, 90%	89.3% after 100 cycles at 0.5 C	80.6, 124.2, 10 C	[64]
	Al_2O_3	$Li_{1.2}Ni_{0.13}Mn_{0.54}Co_{0.13}O_2$	283, 84.5%	248, 84.1%	82% after 50 cycles at C/3	–	[119]
	TiO_2	$Li_{1.2}Ni_{0.13}Mn_{0.54}Co_{0.13}O_2$	283, 84.5%	287, 87.1%	78% after 50 cycles at C/3	–	[119]
	Zr phosphate	$Li(Li_{0.2}Ni_{0.17}Co_{0.07}Mn_{0.56})O_2$	202, 71%	216, 80%	91% after 100 cycles at 0.1 C	80, 125, 2 C	[120]
	$LiFePO_4$	$Li_{1.2}Mn_{0.54}Ni_{0.13}Co_{0.13}O_2$	243, 70.5%	267, 63%	88% after 20 cycles at 0.1 C	–	[121]
	Al_2O_3	$Li_{1.2}Mn_{0.54}Ni_{0.13}Co_{0.13}O_2$	243, 70.5%	285, 51%	80% after 20 cycles at 0.1 C	–	[121]
	(rGO^)/$AlPO_4$	$Li(Li_{0.190}Mn_{0.54}0Co_{0.143}Ni_{0.127})O_2$	218, 75.69%	240, 83.6%	95% after 100 cycles at 0.1 C	50, 110, 5 C	[122]
	$FePO_4$	$Li_{1.2}Ni_{0.13}Co_{0.13}Mn_{0.54}O_2$	250.3, 78.3%	271.7, 85.1%	95% after 100 cycles at 0.5 C	150, 166, 2 C	[123]
	$LiCoPO_4$	$Li_{1.2}Ni_{0.18}Mn_{0.59}Co_{0.03}O_2$	251, 75.83%	250, 82.5%	98% after 40 cycles at 20 mA g^{-1}	25, 90, 2 C	[124]
	CaF_2	$Li_{1.2}Mn_{0.54}Ni_{0.13}Co_{0.13}O_2$	275.8, 76%	277.3, 89.6%	91.2% after 80 cycles at 0.2 C	85, 141, 3 C	[125]
	$AlPO_4$	$Li_{1.2}Ni_{0.13}Mn_{0.54}Co_{0.13}O_2$	249, 76.2%	261.9, 85.2%	~97% after 40 cycles at 01 C	–	[126]
	MnO_x	$Li(Ni_{0.2}Li_{0.2}Mn_{0.6})O_2$	265.1, 71.6%	298.1, 90.2%	88.9% after 30 cycles at 0.1 C	205, 222, 2 C	[127]
	TiO_2	$Li(Li_{0.2}Mn_{0.54}Co_{0.13}Ni_{0.13})O_2$	241.3, 76.5%	258.3, 86%	75% after 80 cycles at 0.1 C	–, 105, 5 C	[128]

Table 2 (continued)

Type of coating	Surface coating	LLOs	First cycle (DC, CE at 0.1 C) (pristine)	First cycle (DC, CE at 0.1 C) (modified)	Capacity retention (modified)	Rate performance ($DC_{pristine}$, $DC_{modified}$, C rate)	Ref.
	MgO	$Li(Li_{0.2}Mn_{0.54}Ni_{0.13}Co_{0.13})O_2$	79.65%	282.2, 80.8%	96% after 100 cycles at 200 mA g^{-1}	–	[129]
	Sm_2O_3	$Li(Li_{0.2}Mn_{0.56}Ni_{0.16}Co_{0.08})O_2$	298.1, 86%	287.7, 86%	92% after 80 cycles at 200 mA g^{-1}	125, 153, 2000 mA g^{-1}	[130]
	ZrO_2	$Li(Li_{0.2}Mn_{0.54}Ni_{0.13}Co_{0.13})O_2$	254.7, –	253.1, –	94.9% after 50 cycles at 0.5 C	–	[130]
	FeF_3	$Li(Li_{0.2}Mn_{0.54}Ni_{0.13}Co_{0.13})O_2$	260, 72%	280, 80%	95% after 100 cycles at 0.5 C	80, 110, 5 C	[131]
	La_2O_3	$Li_{1.2}Mn_{0.54}Ni_{0.13}Co_{0.13}O_2$	242.2, –	276.9, –	71% after 100 cycles at 0.1 C	33, 90, 5 C	[132]
	CeF_3	$Li_{1.2}Mn_{0.54}Ni_{0.13}Co_{0.13}O_2$	229, 72%	222.8, 80%	91.7% after 50 cycles at 0.1 C	82.2, 103.1, 5 C	[133]
	Pr_6O_{11}	$Li_{1.2}Mn_{0.54}Ni_{0.13}Co_{0.13}O_2$	290.1, 79.8%	283.7, 85.6%	97.9% after 50 cycles at 0.2 C	132.5, 162.2, 5 C	[134]
	MgF_2	$Li(Li_{0.2}Ni_{0.17}Co_{0.07}Mn_{0.56})O_2$	211, 70.4%	220, 76%	86% after 50 cycles at 0.1 C	110, 130, 2 C	[135]
	BiOF	$Li(Li_{0.18}Ni_{0.15}Co_{0.15}Mn_{0.52})O_2$	248, 75%	292, 92%	92% after 100 cycles at 0.2 C	–, 78, 25 C	[136]
	$MWCNT^+$	$Li_{1.17}Ni_{0.17}Co_{0.1}Mn_{0.56}O_2$	234.8, ~ 84%	241.5, 87%	75.7% after 50 at 0.2 C	24, 103, 10 C	[137]
	C	$Li_{1.2}Mn_{0.54}Ni_{0.13}Co_{0.13}O_2$	253, 84.3%	263, 96.7%	92% after 100 cycles at 0.2 C	13, 54, 20 C	[138]
	C	$0.33Li_2MnO_3{\cdot}0.67Li(Mn_{1/3}Ni_{1/3}Co_{1/3})O_2$	290.2, 78%	334.5, 92.2%	~ 90% after 50 cycles at 1 C	55.3, 122.3, 30 C	[139]
	ZnO	$0.3Li_2MnO_3$-$0.7LiNi_{5/21}Co_{5/21}Mn_{11/21}O_2$	283, 81.7%	316, 89.1%	78.8% after 50 cycles at 1 C	112, 124, 5 C	[140]
	PEDOT:PSS*	$Li_{1.17}Mn_{0.56}Co_{0.095}Ni_{0.175}O_2$	265, 89.8%	260, 89.7%	67.3% after 50 cycles at 1 C	20, 83, 9 C	[141]
	PEDOT:PSS*	$Li_{1.2}Ni_{0.2}Mn_{0.6}O_2$	265.6, 77.18%	286.5, 77.9%	~ 80% after 100 cycles at 1 C	62, 135. 2 C	[142]
	Graphene	$Li_{1.2}Mn_{0.54}Ni_{0.13}Co_{0.13}O_2$	256, 69%	~ 290, 74%	90% after 100 at 0.5 C	–, 50, 12 C	[143]
	Polyaniline	$Li_{1.2}Mn_{0.54}Ni_{0.13}Co_{0.13}O_2$	291.9, 81.31%	313.5, 89.0%	~ 100% at 0.1 C	60, 199, 10 C	[144]
	rGO^	$Li_{1.2}Mn_{0.54}Ni_{0.13}Co_{0.13}O_2$	284, 76.5%	313, > 100%	94.5% after 70 cycles at 40 mA g^{-1}	50, 125, 10 C	[145]
	Li_3PO_4	$Li(Li_{0.2}Mn_{0.54}Ni_{0.13}Co_{0.13})O_2$	241, –	215.6, –	87% after 200 cycles at 150 mA g^{-1}	71, 121, 10 C	[146]
	Li_3PO_4/C	$Li_{1.2}Ni_{0.13}Mn_{0.54}Co_{0.13}O_2$	266, 83.3%	–, 88.3%	100% after 50 cycles at 0.2 C	83, 124, 1000 mA g^{-1}	[147]

Table 2 (continued)

Type of coating	Surface coating	LLOs	First cycle (DC, CE at 0.1 C) (pristine)	First cycle (DC, CE at 0.1 C) (modified)	Capacity retention (modified)	Rate performance ($DC_{pristine}$, $DC_{modified}$, C rate)	Ref.
	$(NH_4)_3AlF_6$	$0.5Li_2MnO_3{\cdot}0.5LiNi_{1/3}Co_{1/3}Mn_{1/3}O_2$	269.1, 69.62%	277.9, 76.4%	85% after 50 cycles at 0.2 C	109, 143, 5 C	[148]
	Li–Ni–PO_4	$0.5Li_2MnO_3{\cdot}0.5LiNi_{0.44}Co_{0.25}Mn_{0.31}O_2$	240, 81%	260, 87%	74.4% after 50 cycles at 0.1 C	175, 200, 1 C	[149]
	$AlPO_4$	$Li(Li_{0.2}Fe_{0.1}Ni_{0.15}Mn_{0.55})O_2$	246.2, 66.5%	267.2, 78.9%	88.95% after 100 cycles at 1 C	56, 136, 10 C	[150]
	$LiAlSiO_4$	$Li(Li_{0.17}Ni_{0.2}Co_{0.05}Mn_{0.58})O_2$	262.5, 78.3%	273, 84.1%	Improved	124, 163, 5 C	[151]
	Li_2TiF_6	$Li_{1.17}Ni_{0.17}Co_{0.1}Mn_{0.56}O_2$	263.9, 87.3%	260.2, 89%	94.3% after 100 cycles at 0.05 C	20, 93, 10 C	[152]
	LiV_3O_8	$Li(Li_{0.17}Ni_{0.17}Co_{0.10}Mn_{0.56})O_2$	253.9, 85.81%	250.1, 98.3%	92% after 100 cycles at 1 C	99, 158, 2 C	[153]
	Li_3VO_4	$Li_{1.18}Co_{0.15}Ni_{0.15}Mn_{0.52}O_2$	253, 77.5%	276.4, 87.7%	78% after 100 cycles at 5 C	74, 124, 5 C	[154]
	Zr-abundant	$Li_{1.2}Ni_{0.13}Mn_{0.54}Co_{0.13}O_2$	245, 70.3%	245, 70.9%	85% after 300 cycles at 6 A g^{-1}	105, 130, 10 C	[155]
	$LiMnPO_4$	$Li(Li_{0.17}Ni_{0.25}Mn_{0.58})O_2$	260.8, 80.7%	293.3, 85.5%	~88.9% after 80 cycles at 30 A g^{-1}	98, 141, 5 C	[156]
	Li_2ZrO_3	$Li_{1.2}Ni_{0.13}Mn_{0.54}Co_{0.13}O_2$	235, 71%	225, 74%	85% after 100 cycles at 0.2 C	30, 55, 3 C	[157]
	MnO_2	$Li_{1.2}Mn_{0.567}Ni_{0.167}Co_{0.066}O_2$	280, 77%	299, 88%	93% after 50 cycles at 0.5 C	115, 157, 5 C	[158]
	$LiAlO_2$	$Li_{1.5}Ni_{0.25}Mn_{0.75}O_{2.5}$	221.3, 66.8%	257.6, 82.9%	96.5% after 50 cycles at 1 C	23, 88, 10 C	[159]
	MoO_3	$Li[Li_{0.2}Mn_{0.54}Ni_{0.13}Co_{0.13}]O_2$	271.9, 76.9%	272.7, 99.6%	88.5% after 50 cycles at 0.1 C	–	[160]
	MoS_2	$Li_{1.2}Mn_{0.54}Ni_{0.13}Co_{0.13}O_2$	236.9, 76.1%	228.5, 83.9%	92.7% after 100 cycles at 0.5 C	91, 129, 5 C	[161]
	P(VDF–TrFE)[#]	$Li_{1.2}Mn_{0.54}Ni_{0.13}Co_{0.13}O_2$	240.2, 70.3%	275.5, 79.1%	87.8% after 100 cycles at 0.5 C	91, 117, 5 C	[162]

CE: coulombic efficiency (%), DC: discharge capacity (mAh g^{-1})

[^]Reduced graphene oxide

[+]Multi-walled carbon nanotube

*Poly(3, 4-ethylenedioxythiophene)-poly(styrene sulphonate)

[#]Poly(vinylidene fluoride-trifluoroethylene)

Table 3 Doping strategies to improve ICE

Dopant	LLOs	First CE (pristine)^	First CE (modified)^	First DC (pristine)^^	First DC (modified)^^	Capacity retention (modified)	Rate performance ($DC_{pristine}$, $DC_{modified}$, C rate)	Ref.
Na^+	$Li(Li_{0.2}Mn_{0.54}Ni_{0.13}Co_{0.13})O_2$	–	–	241.9	215.6	–	66, 136, 5 C	[163]
K^+	$Li_{1.2}Mn_{0.54}Co_{0.13}Ni_{0.13}O_2$	74	77	302	315	85% after 110 cycles at 20 mA g^{-1}	142, 197, 1000 mA g^{-1}	[164]
K^+	$Li_{1.232}Mn_{0.615}Ni_{0.154}O_2$	76	87	266	299	94% after 100 cycles at 0.5 C	90, 133, 10 C	[165]
Mg^{2+}	$Li_{1.5}(Mn_{0.75}Ni_{0.25})O_{2+\delta}$	77.5	87.9	–	248.6	94.2% after 200 cycles at 0.5 C	65, 130, 10 C	[166]
Al^{3+}	$Li_{1.5}Mn_{0.675}Ni_{0.1675}Co_{0.1675}O_2$	72.9	81.2	278.7	323.7	~78% after 100 cycles at 0.5 C	60, 120, 20 C	[167]
Fe^{3+}	$Li_{1.2}Ni_{0.13}Co_{0.13}Mn_{0.54}O_2$	77.4	87.8	237	230	90.4% after 50 cycles at 0.1 C	–	[168]
Cr^{3+}	$Li_{1.2}Mn_{0.567}Ni_{0.167}Co_{0.066}O_2$	~77	~77	~262	~258	~90% after 200 cycles at 0.1 C	–	[51]
Y^{3+}	$Li_{1.2}Mn_{0.6}Ni_{0.2}O_2$	~73	79	272.3	281	95.6% after 40 cycles at 1 C	50, 98, 5 C	[169]
Sn^{4+}	$Li(Li_{0.17}Ni_{0.25}Mn_{0.58})O_2$	78.1	77	257.3	232.2	86% after 400 cycles at 30 mA g^{-1}	98, 112, 5 C	[170]
Ti^{4+}	$Li_{1.2}Mn_{0.54}Co_{0.13}Ni_{0.13}O_2$	–	~73		> 320	71% after 300 cycles at 0.2 C	81, 136, 5 C	[171]
Zr^{4+}	$Li_{1.2}Mn_{0.54}Ni_{0.13}Co_{0.13}O_2$	70.3	70.9	233	242	~95% after 100 cycles at 25 mA g^{-1}	145, 159, 250 mA g^{-1}	[172]
Ru^{4+}	$Li_{1.2}Ni_{0.13}Co_{0.13}Mn_{0.54}O_2$	–	–	268	268	98.1% after 100 cycles at 0.1 C	80, 150, 5 C	[173]
Ru^{4+}	$0.55Li_2MnO_3{\cdot}0.45LiNi_{1/3}Co_{1/3}Mn_{1/3}O_2$	77.5	87.7	253	276.4	~92.5% after 50 cycles at 2 C	152, 181, 2 C	[174]
Nb^{5+}	$Li(Li_{0.2}Ni_{0.2}Mn_{0.6})O_2$	61	77	220	254	92.3% after 100 cycles at 0.1 C	80, 106, 5 C	[175]
W^{6+}	$Li_{1.13}Ni_{0.3}Mn_{0.57}O_2$	69	81	251	284	~78% after 100 cycles at 1 C	30, 90, 40 C	[176]
SO_4^{2-}	$Li(Li_{0.17}Ni_{0.20}Co_{0.05}Mn_{0.58})O_2$	81.1	83.2	288.3	282.2	~80% after 400 cycles at 30 mA g^{-1}	130, 160, 1500 mA g^{-1}	[175]
SiO_4^{4-}	$Li(Li_{0.17}Ni_{0.20}Co_{0.05}Mn_{0.58})O_2$	81.1	83.5	288.3	261.2	~83% after 400 cycles at 30 mA g^{-1}	130, 150, 1500 mA g^{-1}	[175]
F^-	$Li_{1.2}Mn_{0.567}Ni_{0.167}Co_{0.066}O_2$	~77	~86	~262	~274	70% after 200 cycles at 0.5 C	–	[51]

CE: Coulombic Efficiency (%) at 0.1 C^, DC: Discharge capacity (mAh g^{-1}) at 0.1 C^^

3.1.2.3 Lattice Doping In addition to surface modification, lattice doping with cationic and anionic ions has also been introduced to improve ICE for LLOs [21, 115]. For example, Qing et al. [116] employed gradient Na^+ doping to boost the kinetics of LLOs using a molten salt method (Fig. 7a) and reported the Na-doped LLO not only exhibited a higher ICE (87 vs. 63%), but also a higher discharge capacity (286 vs. 228 mAh g^{-1}) during testing at 25 mA g^{-1} in the range of 2.0–4.7 V (Fig. 7b, c). Here, the researchers attributed the noticeably better electrochemical performance of the doped LLO to the pinning effect of Na ions towards the stabilization of the LLO structure and the consequent improvements in electronic and ionic conductivities. In another study, Zhao et al. [117] employed gradient PO_4^{3-} doping and developed a spinel-like hierarchical structure on LLOs composed of a PO_4^3-enriched spinel-like surface and a PO_4^3-doped LLO core (Fig. 7d). Here, the optimal modified sample showed an enhanced ICE of 86% as compared with 72% for the pristine sample, indicating faster Li^+ diffusion and reduced irreversible Li_2O due to the increased PO_4^{3-} polyanions (Fig. 7e).

Researchers have also reported the use of cationic and anionic ions as dopants in LLO lattices and reported that the performance effects were varied. For example, Pang et al. [51] reported that anionic doping with F^- can promote larger lattice sizes and stimulate faster Li diffusions, whereas cationic doping with Cr^{3+} can enhance structural stabilities but sacrifice capacity through reduced redox centres and

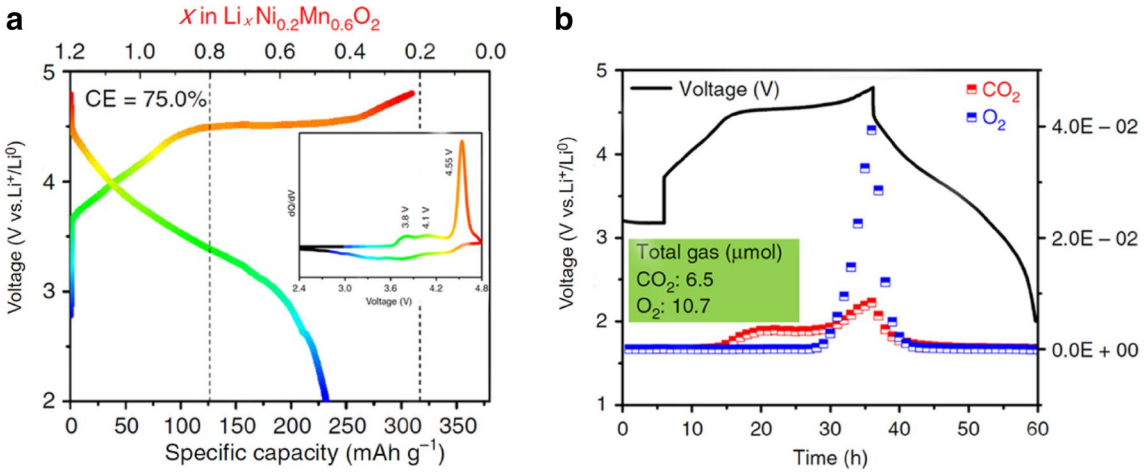

Fig. 4 **a** First charge-discharge characteristics and dQ/dV plots. **b** Gas evolution rates of $Li_{1.2}Ni_{0.2}Mn_{0.6}O_2$ electrode. *Source*: **a**, **b** Reproduced with permission from Ref. [28]

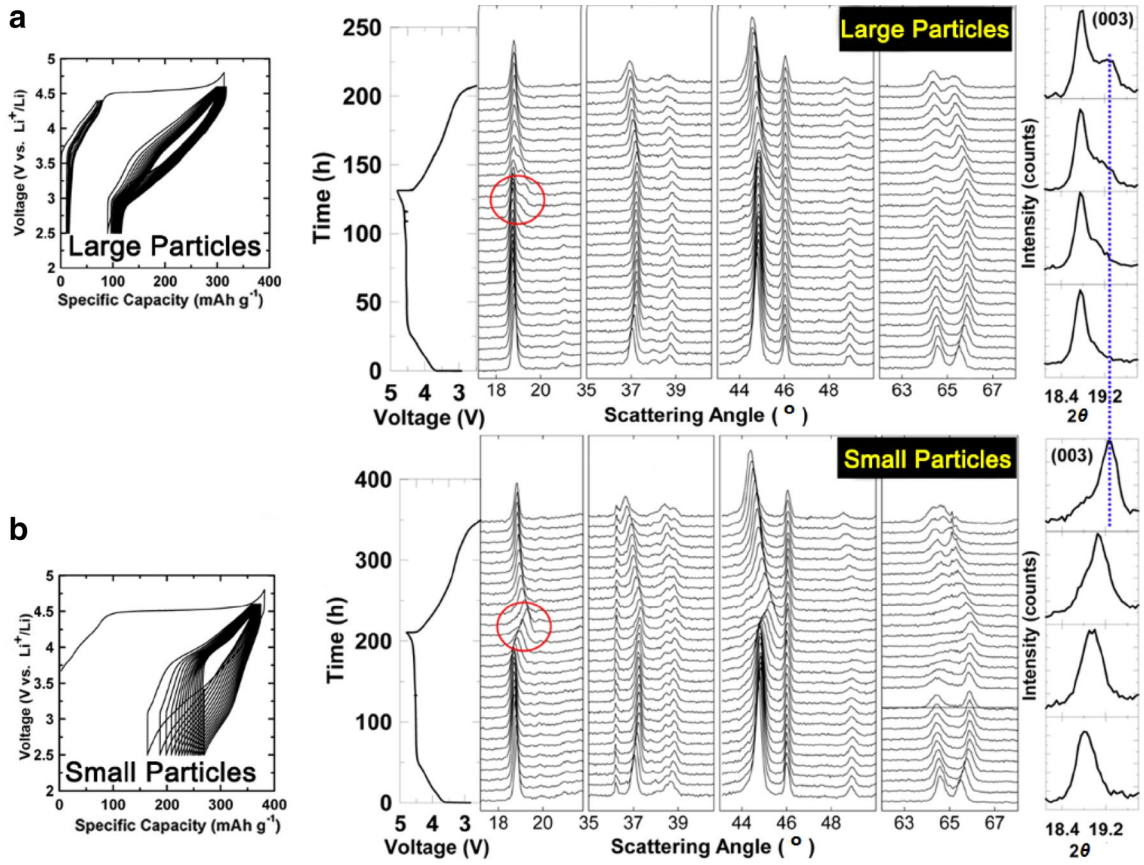

Fig. 5 Cell voltage as a function of capacity and selected in situ individual diffraction patterns during the first cycle of **a** large-particle and **b** small-particle LLOs. The cells were tested in a potential window of 2.0–4.8 V versus Li/Li$^+$ at a current of C/100. *Source*: Reproduced with permission from Ref. [110]

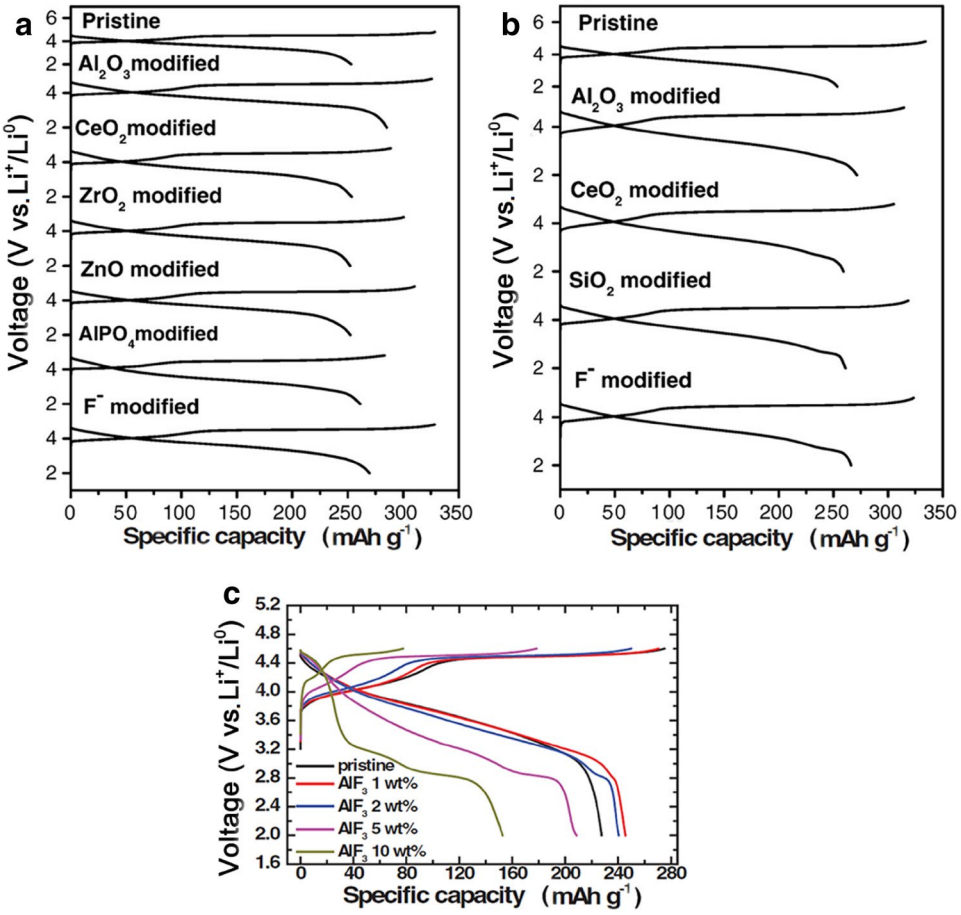

Fig. 6 Initial charge-discharge profiles of **a** $0.6Li(Li_{1/3}Mn_{2/3})O_2$-$0.4Li(Mn_{1/3}Ni_{1/3}Co_{1/3})O_2$ and **b** $0.6Li(Li_{1/3}Mn_{2/3})O_2$-$0.4Li(Mn_{1/6}Ni_{1/6}Co_{2/3})O_2$ with various coatings and F doping. **c** Initial charge-discharge curves of pristine and AlF_3-modified $Li(Li_{0.19}Ni_{0.16}Co_{0.08}Mn_{0.57})O_2$ electrodes. **d** Initial charge-discharge profiles of $Li(Li_{0.2}Mn_{0.54}Ni_{0.13}Co_{0.13})O_2$, V_2O_5-modified samples and V_2O_5. *Source*: **a**, **b** Reproduced with permission from Ref. [98]. **c** Reproduced with permission from Ref. [59]

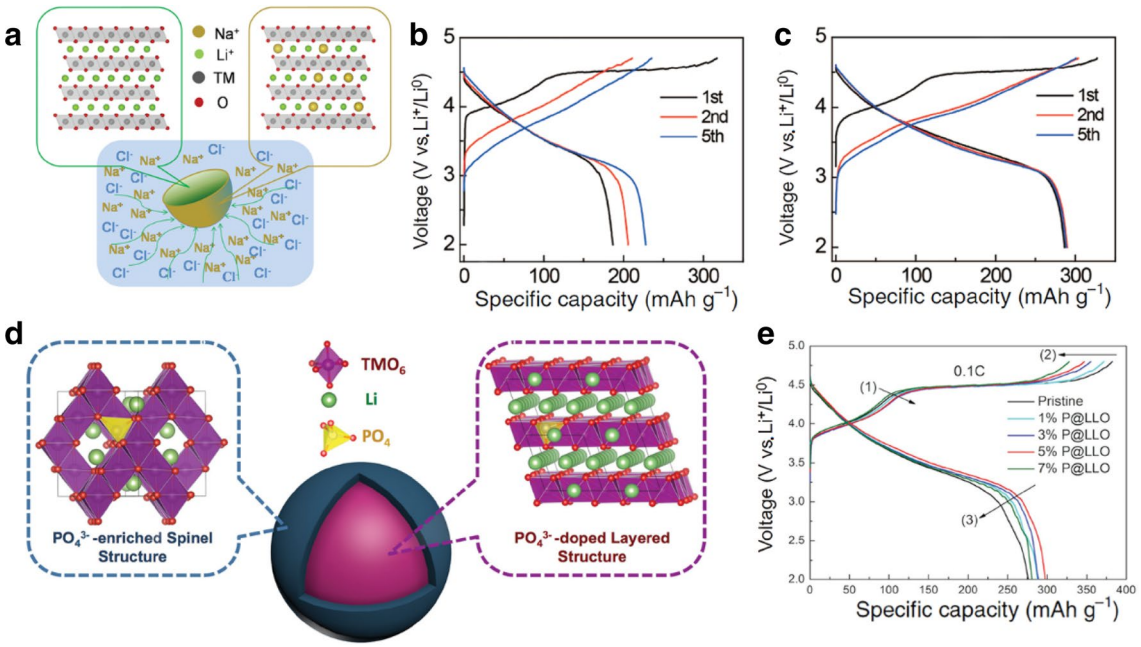

Fig. 7 **a** Schematic of gradient surface Na^+ doping in LLOs and the initial charge-discharge profiles of **b** pristine and **c** Na-doped LLOs. **d**, **e** Schematic of gradient polyanion doping in LLOs and the first charge-discharge curves of pristine and PO_4^{3-}-doped LLOs. *Source*: **a**–**c** Reproduced with permission from Ref. [116]. d, e Reproduced with permission from Ref. [117]

therefore suggested that co-doping can be a viable strategy to combine the benefits of various dopants to achieve optimal electrochemical performances. Overall, by regulating the loss of Li and O in LLOs, ICE can be improved, in which particle size control, surface coating and lattice doping prove to be useful in the reconstruction of surface structures, leading to possible stabilization of bulk structures, and are therefore feasible strategies.

3.2 Capacity and Voltage Fade

The capacity and voltage fade in LLOs, especially sustained average voltage, decreases during electrochemical cycling, significantly lowers energy efficiency and complicates corresponding battery management systems. Therefore, capacity and voltage fade has been thoroughly studied to achieve a better fundamental understanding. And because capacity fade is often coupled with voltage fade in LLOs, they will be reviewed simultaneously.

3.2.1 The Origins of Capacity and Voltage Fade

Capacity and voltage fade is a key issue in the practical application of LLOs and has been extensively investigated. Here, fading is believed to be caused by (1) TM/Li migration/layered-spinel transition/O redox, (2) the valence drop of TM ions and (3) porogenic behaviours or cracking, and all of these are closely linked to each other [48, 52, 97, 177].

3.2.1.1 TM/Li Migration/Layered-Spinel Transition/O Redox TM migration is an intrinsic feature of the electrochemical process in LLOs which causes an increase in trapped TM ions in interstitial tetrahedral sites, and cation migration from a TM slab to a Li slab is closely associated with the layered-spinel transition and the formation of spinel-like structures and is known to be associated with voltage fade [178–183]. In one study, Dogan et al. [184] used ^{6}Li magic angle spinning (MAS) nuclear magnetic resonance (NMR) spectroscopy to confirm that TM migration in LLOs was a limited reversible process that could cause gradual decay of LLO capacity and voltage during cycling. Moreover, recent studies have also shown that there is a close coupling between TM migration and the anion redox reactions of O [27, 97, 181, 185, 186] and this was further supported by first-principles calculations (Fig. 8) [23]. In a further study, Kleiner et al. [177] experimentally demonstrated that the host structure of $Li_{1.17}Ni_{0.19}Co_{0.10}Mn_{0.54}O_2$ could undergo an irreversible transition metal-ion migration during long-term cycling (Fig. 9a), resulting in a high capacity drop (50 mAh g^{-1}) between the initial two cycles and ~ 0.4 mAh g^{-1} drop per cycle in the following cycles (Fig. 9b). In another study, Zheng et al. [72] combined aberration-corrected scanning transmission electron microscopy (AC-STEM) with electron energy loss spectroscopy (EELS) to probe the structural changes in $Li(Li_{0.2}Ni_{0.2}Mn_{0.6})O_2$ during cycling (Fig. 9c) and revealed that the layered structure experienced phase transformations, including a defect spinel-like structure and a disordered rock-salt structure. Finally, Yan et al. [187] combined STEM with density functional theory (DFT) calculations to investigate the structural evolution of $Li_{1.2}Ni_{0.2}Mn_{0.6}O_2$ during cycling and concluded that the successive phase transitions of *C2/m*, *I*41 and spinel occurred after extended cycling (Fig. 9d, e). And based on these results, it is clear that TM migration, layered-spinel transition and O redox are closely connected to each other and contribute to the capacity and voltage decay of LLOs.

3.2.1.2 Valence Drops of TM Ions During Cycling Alternatively, Hu et al. [25] achieved better fundamental understandings of voltage fade and suggested that the origin of voltage fade may arise not only from changes in TM migration and O redox activity, but also from the valence drop process of TM ions as induced by O release based on structural changes in $Li_{1.2}Ni_{0.15}Co_{0.1}Mn_{0.55}O_2$. Here, the researchers noticed that lower-voltage Mn^{3+}/Mn^{4+} and Co^{2+}/Co^{3+} redox couples became major contributors to capacity in extended cycling, which was directly linked to voltage fade (Fig. 10a), and that the shift of redox couples from O and Ni to Mn and Co had dramatic influences on voltage profiles (Fig. 10b, c). This finding was also supported by other researchers. For example, Zheng et al. [48] examined the structural changes of $Li(Li_{0.2}Ni_{0.2}Mn_{0.6})O_2$ electrodes and ascribed the capacity fading to the irreversible formation of Mn^{2+} species from the disproportionate reaction of Mn^{3+} (Fig. 11), in which Mn^{2+} species dissolved in the electrolyte and the number of redox centres in the LLOs was permanently reduced.

3.2.1.3 Porogenic Behaviours and Cracking Issues In addition to Mn^{2+} dissolution, particle fragmentation of LLO particles can be induced by spinel grain formations (Fig. 11). In addition, the formation of cracks or porogenic behaviours on the surface or in the bulk of LLO materials has also been proposed and is directly related to high strain and high-voltage cycling [185, 188]. For example, Chen et al. [97] used *operando* neutron powder diffraction and transmission X-ray microscopy methods to reveal that generated cracks, possibly occurring alongside the two-phase and Li_2MnO_3 reactions during the charge process (Fig. 12a), accounted for capacity fade, and suggested that controlling phase separation and O evolution can prevent capacity fade in LLOs. Similarly, Liu et al. [74] found that layered-spinel transition was an irreversible behaviour that occurred not only on the surface, but also in the internal bulk structure of $Li_{1.2}Ni_{0.13}Mn_{0.54}Co_{0.13}O_2$ during cycling (Fig. 12b) and can induce surface cracking and bulk fragmentation. Here, the researchers suggested that surface degradation and drastic bulk evolution were the main degradation mechanisms and

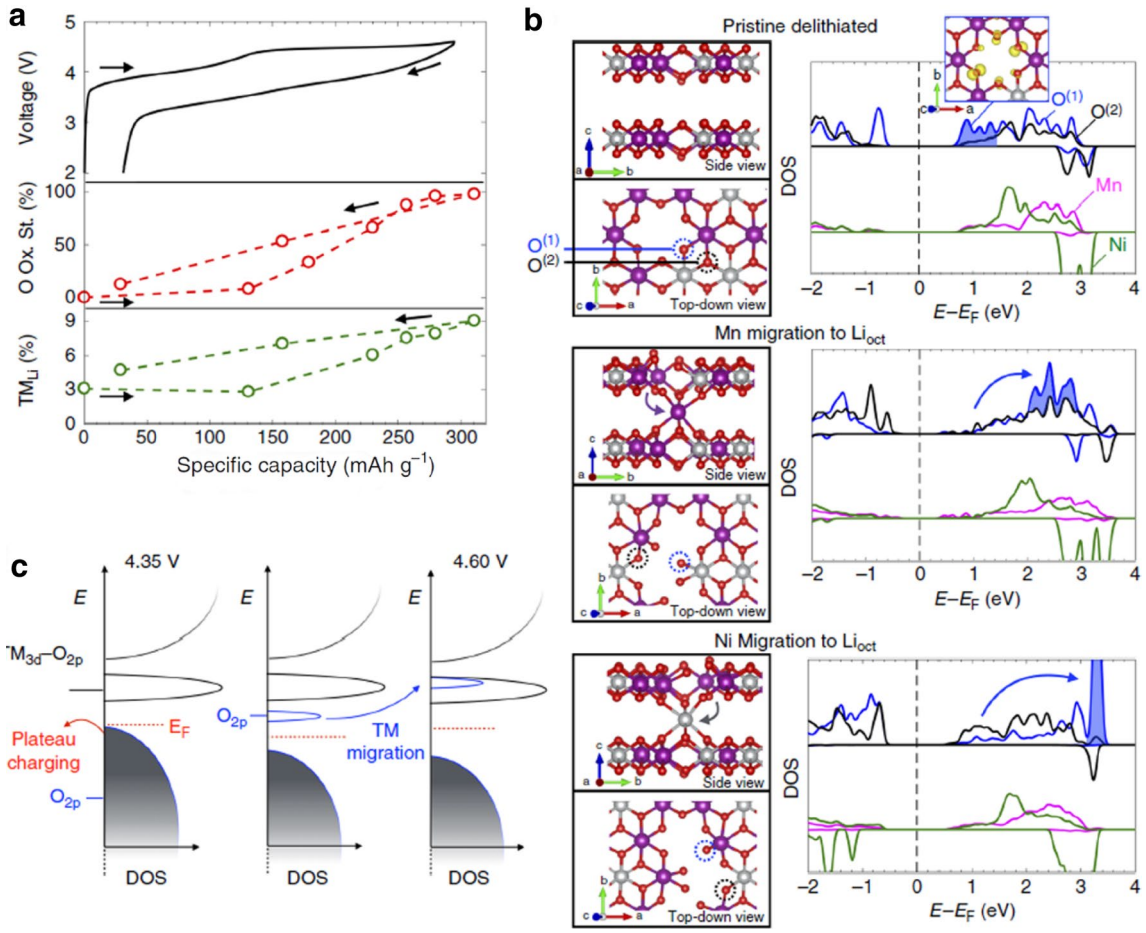

Fig. 8 Electronic structure related to cation migration. **a** Plot of the O fractional oxidation state and the migrated TM fraction as a function of capacity. **b** Projected density of states (pDOS) for TMs and two-coordinate ($O^{(1)}$) and three-coordinate ($O^{(2)}$) oxygen environments in the pristine delithiated state (top) and after Mn (middle) and Ni (bottom) migration into octahedral sites in the Li layer. **c** Schematic of the reorganization of the electronic structure resulting from TM migration. *Source*: **a**–**c** Reproduced with permission from Ref. [23]

were the sources of the rapid failure of their LLO electrodes. In addition, by using in situ Bragg coherent diffractive imaging (BCDI) techniques, Singer et al. [26] directly captured structural evolution during cycling in primary particles and observed large quantities of dislocations and grain boundary movements, inducing strains between the grains and causing particle cracking in LLO electrodes (Fig. 12c). Overall, all these results suggest that porogenic behaviours and cracking issues are intrinsic properties of typical LLOs.

Alternatively, researchers have also reported that the release of O in the irreversible process of O redox activity can result in bulk/surface cracking [61, 97, 189] and can contribute to LLO capacity/voltage fade. In addition, researchers have also reported that pores can form within bulk structures through nucleating vacancies which can worsen LLO cracking issues in which nucleating vacancies are thought to be formed through the release of O during charging and exposed through the pathways of O diffusion [25]. Overall, deeper fundamental understandings of the capacity and voltage fade of LLOs need to be achieved with direct detection and quantification of TM and oxygen activities through *operando* techniques such as in situ neutron powder diffraction, X-ray absorption spectroscopy and Raman spectroscopy. And in particular, correlations between fundamental reaction mechanisms and structure-property relationships are needed for further improvement.

3.2.2 Strategies to Suppress Voltage Fade

To mitigate capacity and voltage fade, electrolyte and binder modulation, surface modification and lattice doping are the most commonly used strategies.

3.2.2.1 Electrolyte and Binder Modulation Aside from intrinsic mechanistic issues, the instability and possible decomposition of conventional electrolytes can also affect the capacity and voltage fade of LLOs due to the need for high-voltage charging (> 4.7 V). Because of this, conven-

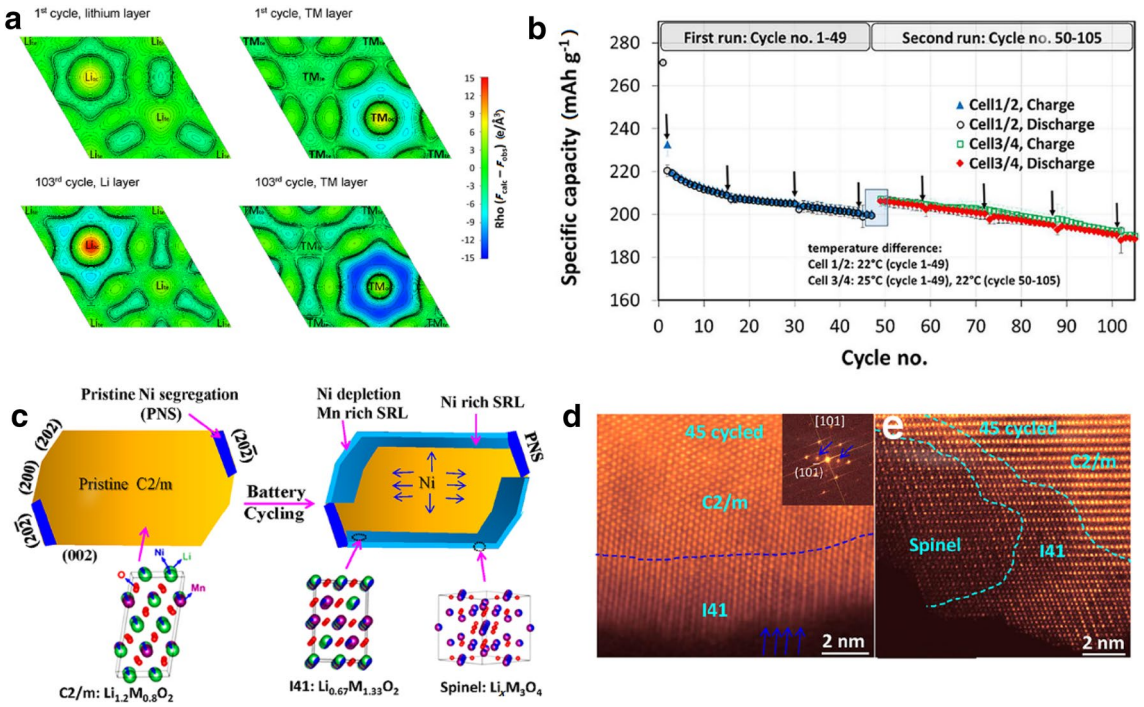

Fig. 9 **a** Difference Fourier maps of the *ab* plane of discharged LLOs after the first cycle. **b** Mean specific capacity of LLOs in pouch cells upon cycling. **c** Schematic of cycling-induced surface layer evolution. **d**, **e** [101] and [010] zone axis STEM-HAADF images and fast Fourier transformation (FFT) image of LLO electrodes after 45 cycles. *Source*: **a**, **b** Reproduced with permission from Ref. [177]. **c**–**e** Reproduced with permission from Ref. [187]

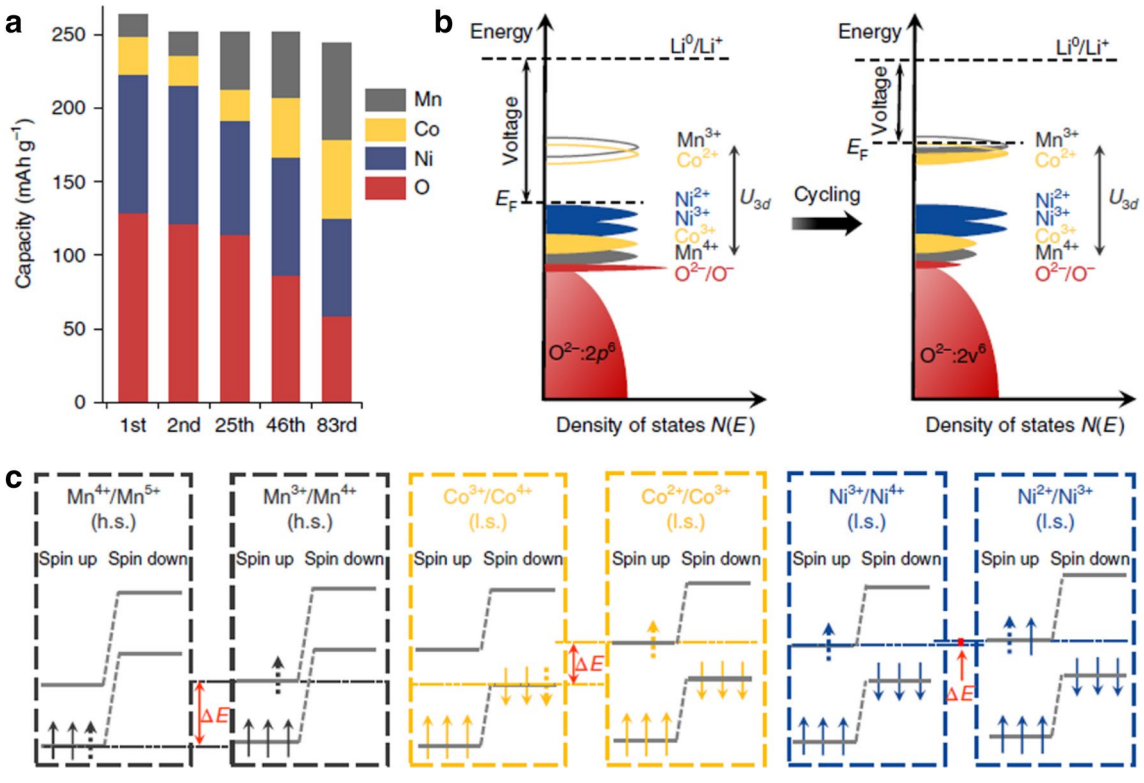

Fig. 10 Evolution of redox couples in $Li_{1.2}Ni_{0.15}Co_{0.1}Mn_{0.55}O_2$ upon cycling. **a** Contribution towards the discharge capacity of Ni, Co, Mn and O redox at various cycles. **b** Effects of electronic structure change on the Fermi level. **c** Diagram of the correlation between redox couple and energy level of each element. *Source*: **a**–**c** Reproduced with permission from Ref. [25]

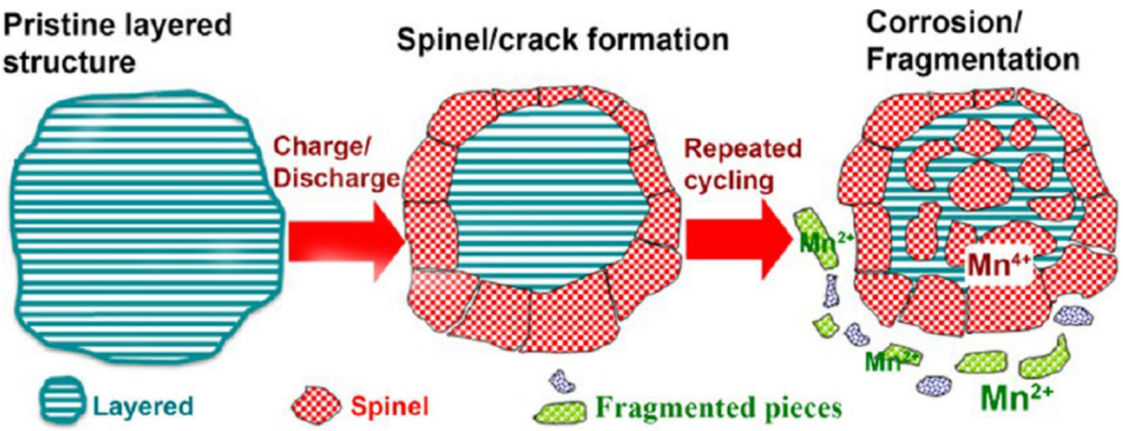

Fig. 11 Schematic of corrosion/fragmentation-related capacity/voltage fade upon electrochemical cycling in $Li(Li_{0.2}Ni_{0.2}Mn_{0.6})O_2$. *Source*: Reproduced with permission from Ref. [48]

tional electrolytes and binders cannot meet the demands of high-voltage operations for LLOs; therefore, optional solvents (*e.g.* ionic liquids [190], suberonitrile [191]) and additives (*e.g.* tris(pentafluorophenyl) borane (TPFPB) [192], lithium bis(oxalate) borate (LiBOB) [193], dimethyl phenylphosphonite (DMPP) [194], lithium difluoro(oxalate) borate (LiDFOB) [195, 196], triethyl phosphite (TEP) [197], tris(trimethylsilyl)borate (TMSB) [198, 199], (trimethylsilyl)methanesulphonate (TMSOMs) [199], 1,3,6-hexanetricarbonitrile [200], tripropylborate (TPB) [201], phenyl vinyl sulphone (PVS) [200], tris(2,2,2-trifluoroethyl) phosphite (TTFP) [202], tri(hexafluoro-iso-propyl)phosphate (HFiP) [203]) have been frequently applied to achieve better electrolyte stability at such high working voltages. Here, most additives can improve capacity retention and even discharge voltage fade by forming protective solid electrolyte interphase (SEI) films on cathode surfaces to prevent direct contact between cathode surfaces and electrolytes. For example, Zheng et al. [192] reported that TPFPB as an anion receptor can be used as an electrolyte additive in $Li(Li_{0.2}Ni_{0.2}Mn_{0.6})O_2$ to effectively improve capacity retention and reduce voltage fade through the capture of oxygen species generated during Li_2MnO_3 activation. In another example, Nayak et al. [193] reported that LiBOB as an electrolyte additive could slow down Li_2MnO_3 activation and that the subsequent structural stabilization could restrict layered-spinel transition in $Li_{1.2}Mn_{0.56}Ni_{0.16}Co_{0.08}O_2$. In addition, various binders other than the commonly used polyvinylidene fluoride (PVDF) have been found to able to enhance LLO electrochemical performances [63, 204]. For example, Zhang et al. [205] used sodium carboxymethyl cellulose (CMC) as a binder in $Li_{1.2}Ni_{0.13}Co_{0.13}Mn_{0.54}O_2$ and reported excellent suppression of voltage fade (Fig. 13), revealing that the CMC binder could not only prevent the detachment of electrode materials from the current collector, but also possibly introduce Na^+ doping through an ion exchange process during discharge.

3.2.2.2 Surface Modification As for surface modifications, they can not only protect, but also enhance electronic/ionic conductivities and alter mechanistic behaviours of LLOs in terms of capacity and voltage fade. For example, Liu et al. [206] modified $Li_{1.17}Ni_{0.17}Co_{0.17}Mn_{0.5}O_2$ with a hybrid surface coating layer composed of Mg^{2+} pillars and Li-Mg-PO_4 (Fig. 14a) and reported significantly enhanced cycling performances (capacity of 180 mAh g^{-1} after 250 cycles at 60 °C) and average discharge voltage retention of 88.7% after extended cycling (Fig. 14b-c). In another example, Prakasha et al. [157] used Li_2ZrO_3, a well-known ion conductor, as a coating layer for LLOs to promote the migration of Li^+ and resist the diffusion of Mn^{2+} and reported greatly suppressed layered-spinel transitions and voltage fade during cycling. Similarly, Wu et al. [150] modified $Li(Li_{0.2}Fe_{0.1}Ni_{0.15}Mn_{0.55})O_2$ with an $AlPO_4$ coating and reported that the coating reduced side reactions between the electrolyte and the electrode surface, decreased O vacancy mobility and promoted Li diffusion, leading to improved LLO electrochemical performances. In a further example, Kim et al. [207] modified the surface structure of LLOs to form a Li_2MnO_3-like coating on the surface and reported that the Li_2MnO_3-like layer possessed high atomic-level structural compatibility and exhibited a seamless surface–bulk connection with the core LLO structure. In addition, the researchers reported that compared with other coating materials, their Li_2MnO_3-like coating not only provided facile Li diffusion, but also suppressed layered-spinel transition, hence ameliorating the voltage fade problem of LLOs (Fig. 15a–c), in which the suppression of the layered-spinel transition was attributed to the unique atomic coordination of Li/Ni mitigating TM mixing (Fig. 15d).

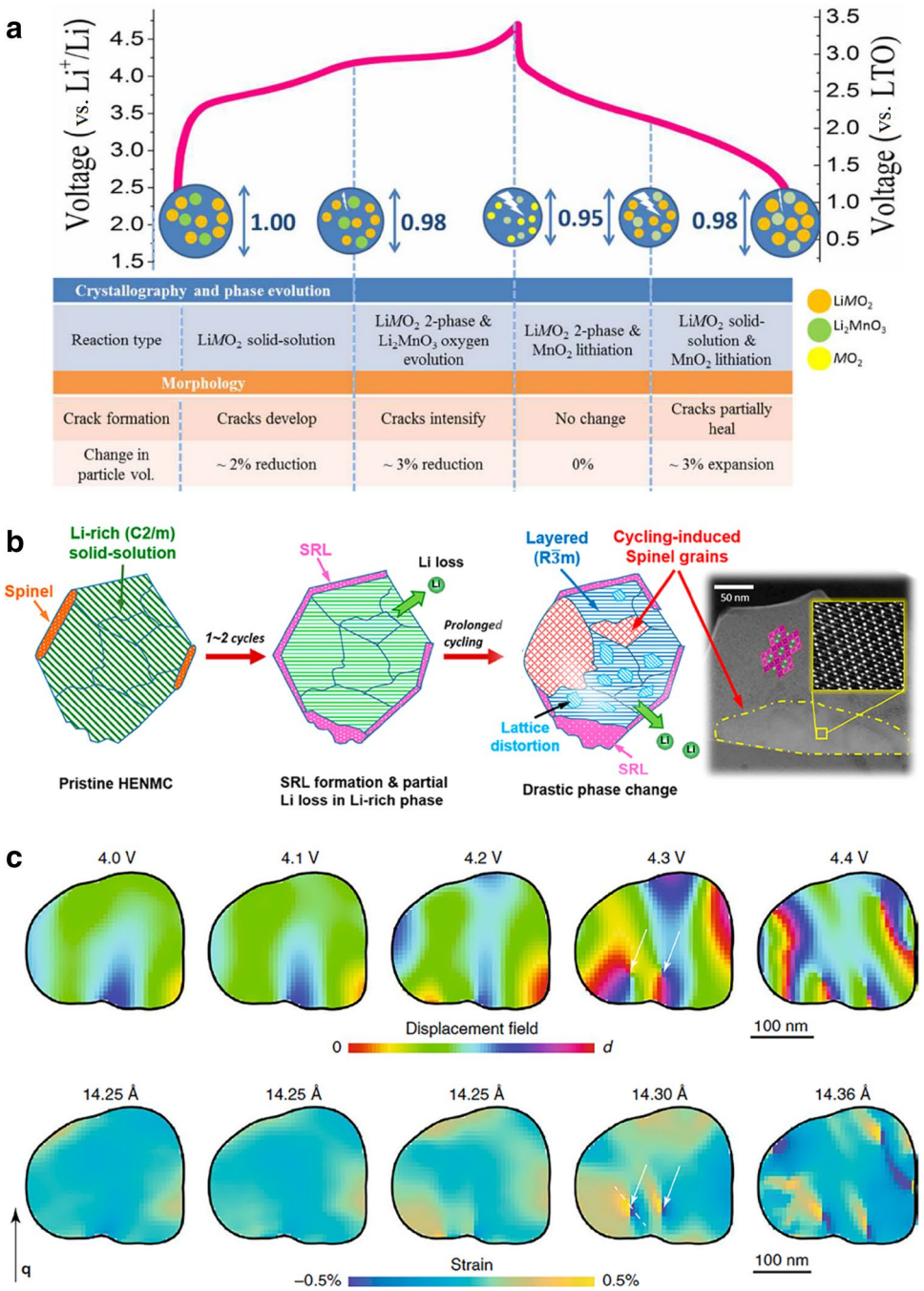

Fig. 12 **a** Summary of the changes related to electrochemistry and morphology in $Li_2MnO_3{\cdot}LiMO_2$ electrodes during cycling based on a combination of *operando* NPD and TXM results. **b** Schematic of the structural evolution of $Li_{1.2}Ni_{0.13}Mn_{0.54}Co_{0.13}O_2$ electrodes during electrochemical cycling. **c** Changes in the displacement field along ***q*** in a plane in LLO nanoparticles during charge and the strain along the (001) direction (perpendicular to the layers) inside the LLO nanoparticles calculated from 3D displacement fields. *Sources*: **a** Reproduced with permission from Ref. [97], **b** Reproduced with permission from Ref. [74]. **c** Reproduced with permission from Ref. [26]

3.2.2.3 Lattice Doping Lattice doping is the most common approach used by researchers to reduce voltage fading through the blocking of TM migration and the stabilization of LLO structures [208, 209]. For example, Nayak et al. [50] replaced Mn ions with Al^{3+} ions in $Li_{1.2}Ni_{0.16}Mn_{0.56}Co_{0.08}O_2$ and reported that the doped sample demonstrated noticeably reduced capacities and voltage fade and that this effect increased with Al doping amounts (Fig. 16). Here, Raman spectroscopy results suggested that Al doping can stabilize the layered structure during the charge-discharge process in LLOs. In another example, Yu et al. [210] introduced Ti^{4+} doping into an LLO structure to investigate its effects towards LLO voltage fade suppression and reported that Ti^{4+} doping can prevent the migration of Mn ions and therefore stabilize the layer structure. Furthermore, in addition to TM site doping, Li site doping with alkali cations (such as Na^+ and K^+) [116, 164] and O site doping with F^- [115, 211] have also been investigated by researchers with promising results.

Overall, it is generally accepted that oxygen activities play an important role in the suppression of capacity and voltage fade in LLOs. And although lattice doping and the

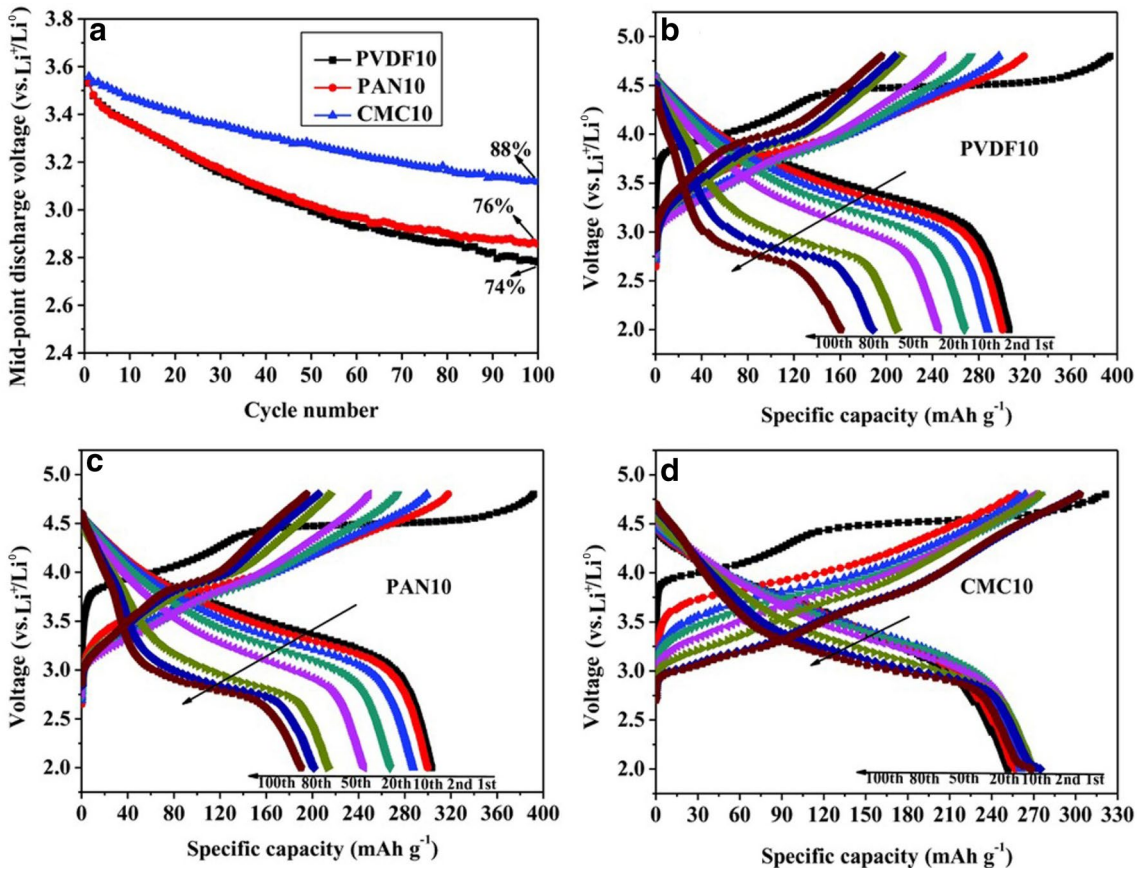

Fig. 13 **a** Mid-point discharge voltage fade curves of LLOs and **b–d** voltage profiles of LLOs with 10 wt% PVDF, PAN and CMC binders. *Source*: **a–d** Reproduced with permission from Ref. [205]

control of synthesis conditions have been shown to affect oxygen activities, more precise control has yet to achieve and a deep understanding into this control is lacking. More importantly, more cost-effective methods for the large-scale synthesis of optimal LLOs in full cells are required for real-world applications.

3.3 Poor Rate Capability

The rate capability of an electrode is an important parameter in application for high-power applications such as EVs. In LLOs, rate performance is linked to Li diffusion kinetics within crystal structures and interfacial charge transfer reactions [55].

3.3.1 The Origins of Poor Rate Capability

LLOs suffer from structural instabilities (TM migration and lattice dislocation) and complex O activities during cycling and therefore hinder Li diffusion, resulting in poor rate capabilities. Here, rate capability is determined by the Li mobility within cells, and for LLOs, the Li_2MnO_3 component with the *C*2/*m* monoclinic structure possesses relatively low Li diffusion kinetics as compared with other layered oxides [55, 212]. In a study, Zheng et al. [55] used galvanostatic intermittent titration technique (GITT) to confirm that the sluggish Li diffusion kinetics in Li_2MnO_3 and MnO_2 components was the rate-determining factor of $Li(Li_{0.2}Ni_{0.2}Mn_{0.6})O_2$ and limited the discharge capacity of LLOs at high rates. Similar results have also been reported in literature [31, 213, 214]. Furthermore, although the activation of Li_2MnO_3 in LLOs is the origin of their anomalously high capacities and energy densities, it also causes surface structure transformations, which can increase interfacial resistances, impede Li diffusion kinetics and induce poor rate capabilities [18, 215, 216]. In addition, the oxidation of organic electrolytes at high voltage can induce the formation of undesirable surface passivation layers, which block Li diffusion and contribute to poor rate capabilities.

3.3.2 Strategies for Improving Rate Performance

Various successful methods have been reported in the enhancement of LLO rate performances, and in this review,

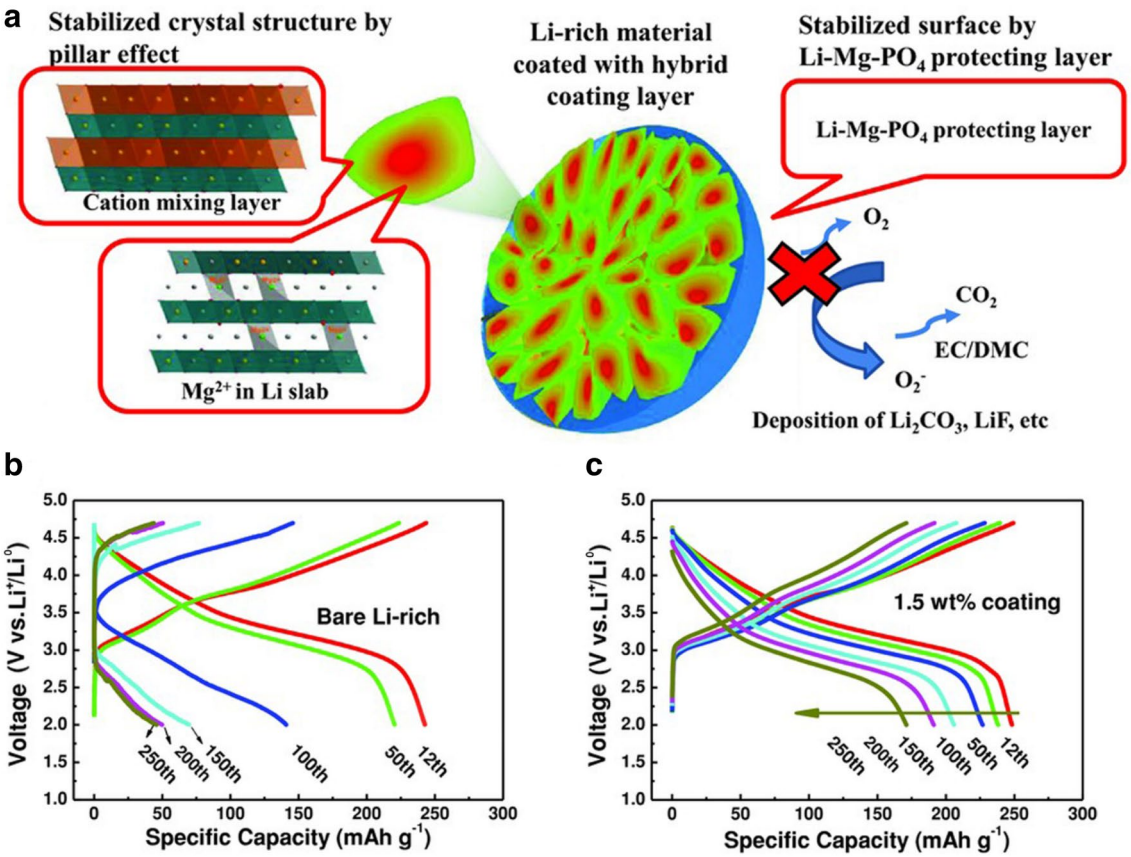

Fig. 14 **a** Schematic of $Li_{1.17}Ni_{0.17}Co_{0.17}Mn_{0.5}O_2$ particles with surface modification. **b**, **c** Charge-discharge curves of bare and surface-modified LLOs at various cycles. *Source*: **a**-**c** Reproduced with permission from Ref. [206]

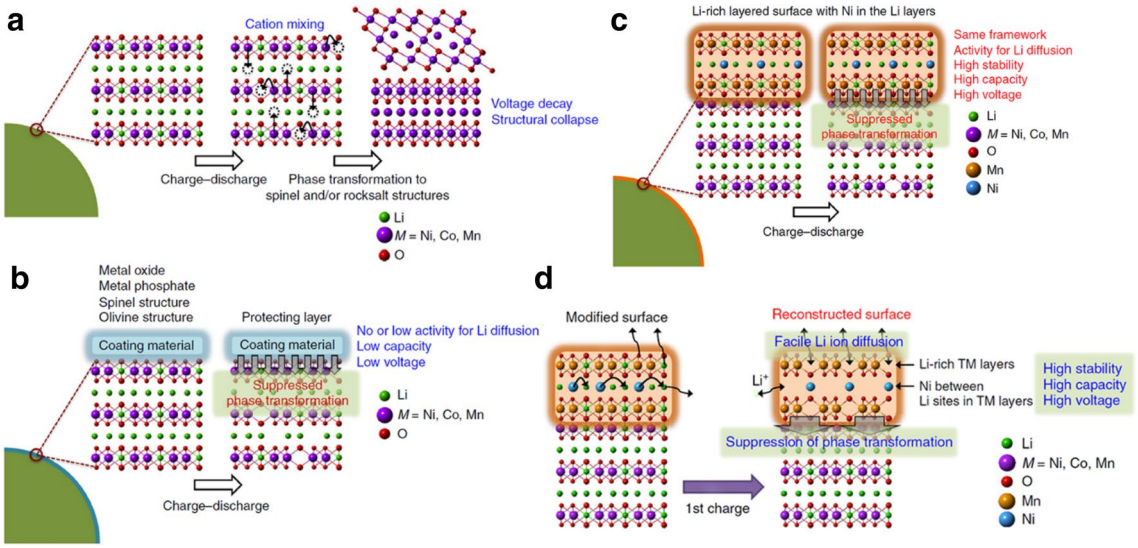

Fig. 15 Surface crystal structure of LLOs and the effects of surface modification: **a** pristine sample, **b** with conventional surface coating and **c** with unique surface modifications in which Ni is located between Mn layers. **d** Schematic of the effects of surface modification. *Source*: **a**–**d** Reproduced with permission from Ref. [207]

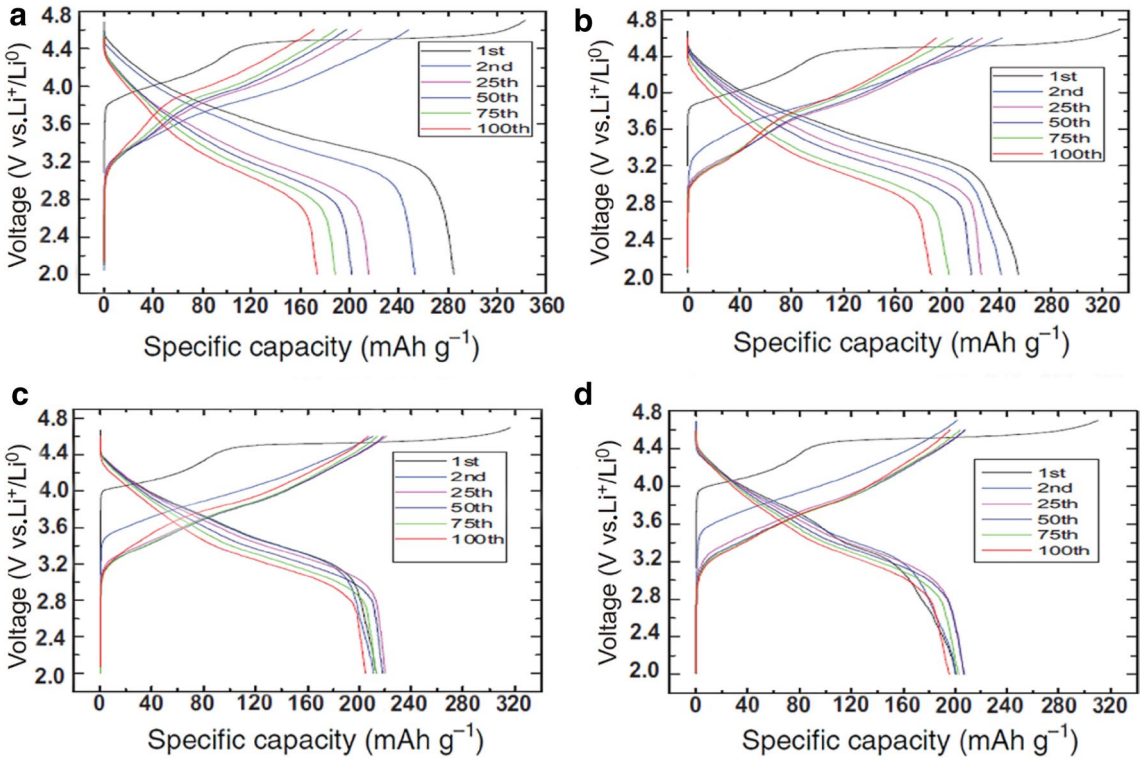

Fig. 16 Charge-discharge curves of LLOs: **a** $Li_{1.2}Ni_{0.16}Mn_{0.56}Co_{0.08}O_2$, **b** $Li_{1.2}Ni_{0.16}Mn_{0.54}Al_{0.02}Co_{0.08}O_2$, **c** $Li_{1.2}Ni_{0.16}Mn_{0.51}Al_{0.05}Co_{0.08}O_2$ and **d** $Li_{1.2}Ni_{0.16}Mn_{0.48}Al_{0.08}Co_{0.08}O_2$. *Source*: **a**–**d** Reproduced with permission from Ref. [50]

various enhancement strategies will be presented to assist with understanding and discussion.

3.3.2.1 Surface Modification Surface modification is still one of the most effective approaches to improve rate capability, and many studies have shown that solid electrolytes and ion conductive coating materials can improve the interfacial stability and rate capability of LLOs as compared with other surface coating materials that possess low Li conductivity and electronic conductivity and can block Li transport channels. Researchers have reported that carbon and other electronic conductive coating materials on LLOs can exhibit superior rate performance, mainly due to their high electronic conductivities and reduced charge transfer resistances [137–145, 217] and that surface coating with ionic conductive $AlPO_4$ can retain O vacancies and stabilize electrode/electrolyte interface side reactions due to the high stability of $AlPO_4$ (stemming from the high electronegativity of polyanions with Al ions) [150]. For example, Ahn et al. [155] reported that nanoscaled Zr-abundant nanolayers grown along the $(20\bar{2})_m$ plane which are along the Li diffusion facets can exhibit a capacity of ~ 110 mAh g^{-1} even at a high rate of 30 C in which Zr can prevent the segregation of TM ions along the $(20\bar{2})_m$ plane and was believed to influence the electrochemical performance. In addition, the researchers also suggested that this surface modification can induce O vacancies in the surface regions. Normally, cation-disordered structures impede Li diffusion [4, 206]; however, this study suggests the unexpected formation of percolation networks with facile Li transport in Li-disordered rock-salt structures [218, 219]. Based on this, surface modification can not only refer to coatings for protection and higher conductivity, but also refer to the pre-activation of Li_2MnO_3, surface structure tuning and surface gradient doping through pre-cycling treatments.

Pre-cycling treatments on LLO surfaces have been shown to improve rate performance, and surface treatments with H_2SO_4 [220], AlF_3 [221, 222], $NH_4H_2PO_4$ [117], $(NH_4)_2HPO_4$ [223], $Na_2S_2O_8$ [224, 225], $(NH_4)_2SO_4$ [226] and NH_4HF_2 [227] have been used to activate Li_2MnO_3 components and induce the formation of the spinel-like phase on the surface, which enhance Li diffusion (Fig. 17). For example, Wu et al. [228] pre-treated LLOs with $Mn(Ac)_2$ to achieve an encapsulating layer and annealed the samples to achieve a heterostructured spinel layer with three-dimensional (3D) Li diffusion channels that facilitated rapid Li diffusion and reported that the treated cathode exhibited improved cycling stability and rate capability (Fig. 18).

Aside from activating Li_2MnO_3 with acidic species and facilitating fast Li diffusion channels, surface treatments with polyaniline [229], Super P [230], hydrazine [231] and reduced graphene oxide (rGO) [180] have all been shown to

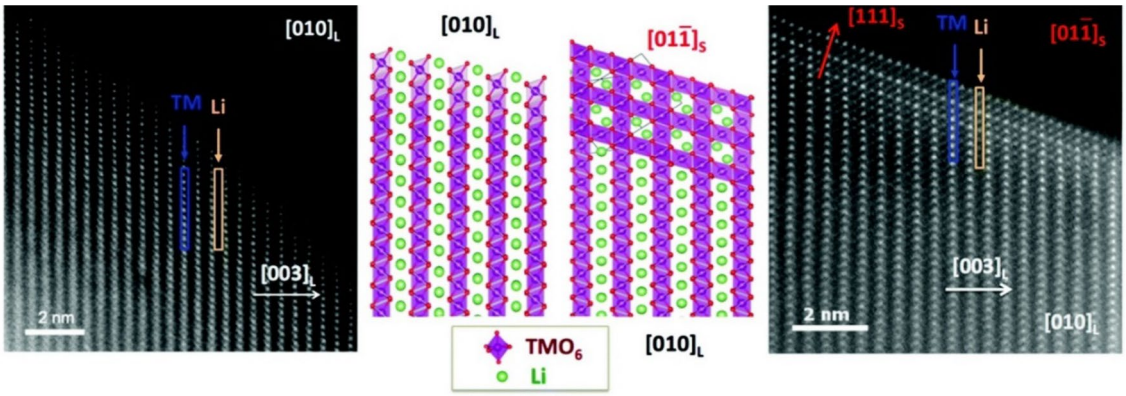

Fig. 17 Spinel-like formations after surface treatment in LLOs. *Source*: Reproduced with permission from Ref. [117]

be able to prevent layered-spinel transitions in LLOs through limiting the formation of Li and O vacancies at the surface and thereby preventing induced structural instability in these materials. For example, Zhang et al. [232] introduced surface nitridation to $Li(Li_{0.17}Ni_{0.25}Mn_{0.58})O_2$ through sintering in NH_4OH atmosphere at 400 °C and reported that the nitrogen introduction improved interfacial stability and Li diffusion. Here, the researchers reported that the improved rate capability (164.7 mAh g^{-1} discharge capacity at 5 C rate) can be associated with the presence of surface nitrogen; however, explanations and findings related to the effects of surface nitridation are obscure. Furthermore, surface morphology tuning is also a possible approach to enhance the rate capability of LLOs. For example, Qing et al. [116] adopted a surface doping strategy to achieve surface gradient Na^+ doping by soaking LLOs in molten NaCl before heat treatment. Here, the researchers reported that some of the Li^+ layers were occupied by Na^+, resulting in a pinning effect that stabilized the structure and improved Li^+ diffusion kinetics.

In addition, Ding et al. [64] investigated gradient surface doping using Si/Sn in which the interplanar spacings of the TM ions were expanded as Sn/Si atoms were doped into the lattice of LLO near the crystal surface and reported that such doping can result in structural stabilization and enhanced cycling performances in which the rate capability of their LLO was improved by improving Li^+ diffusion through the enlargement of the interslab spacing of the TM layer. A similar gradient doping approach was conducted by Zhao et al. [117] in which polyanion doping resulted in a surface spinel transformation similar to that in acid treatments, which enhanced ionic and electronic conductivities through electrode surfaces and improved rate kinetics. Here, the researchers reported that a Mn-depleted surface layer can limit HF acid attacks and Mn dissolution and improve the stability of the electrode/electrolyte interface. In addition, these researchers also reported that PO_4^{3-} doping can restrain TM-ion migration because the smaller ^{V}P cations tend to occupy tetrahedral interstitial sites. In another study, Liu et al. [118] also reported that surface doping with Nb^{5+} and other heavy element ions such as Ti^{4+} and Zr^{4+} can improve LLO capacity retention rates and rate capability. Here, the researchers suggested that these elements possess stronger bonds to oxygen as compared with Mn–O bonds and can limit oxygen evolution through surface oxygen deactivation and that doped Nb^{5+}, Ti^{4+} and Zr^{4+} ions can enter the surface Li layers to inactivate Mn^{4+} ions and retain them in the TM layers, thus retarding migration and phase transformation. Surface gradient doping strategies have also been reported to improve LLO cycling stability and rate capabilities through the stabilization of LLO structures during electrochemical cycling. For example, Hu et al. [25] recently had suggested that AlF_3 coatings can thermally stabilize LLO surface structures and restrict O release, thereby limiting structural instability and impedance build-up at the interface caused by electrolyte decomposition.

The surface coating of LLO cathode materials is an effective method to enhance rate performances through the passivation of electrode surfaces during cycling, the enhancement of LLO surface electronic and ionic conductivities and the ability to act as a protective barrier. Here, surface coating layers can act as protective layers to suppress side reactions, reduce interfacial resistances and stabilize interfaces, and some surface coatings can stabilize structural stability of LLO by partially removing Li_2O or enhance structural stability by limiting O release. Researchers also reported that the effectiveness of the surface coating approach depends on the thickness, uniformity, stability (thermal and mechanical), electronic and ionic conductivity of the coating layer and that these parameters are linked to the type of coating materials and methods adopted. For example, Qiu et al. [15] introduced O vacancies into the surface of LLOs through the interfacial modification of LLO surfaces using gas-solid interface reactions (GSIR) between LLOs and CO_2 gas.

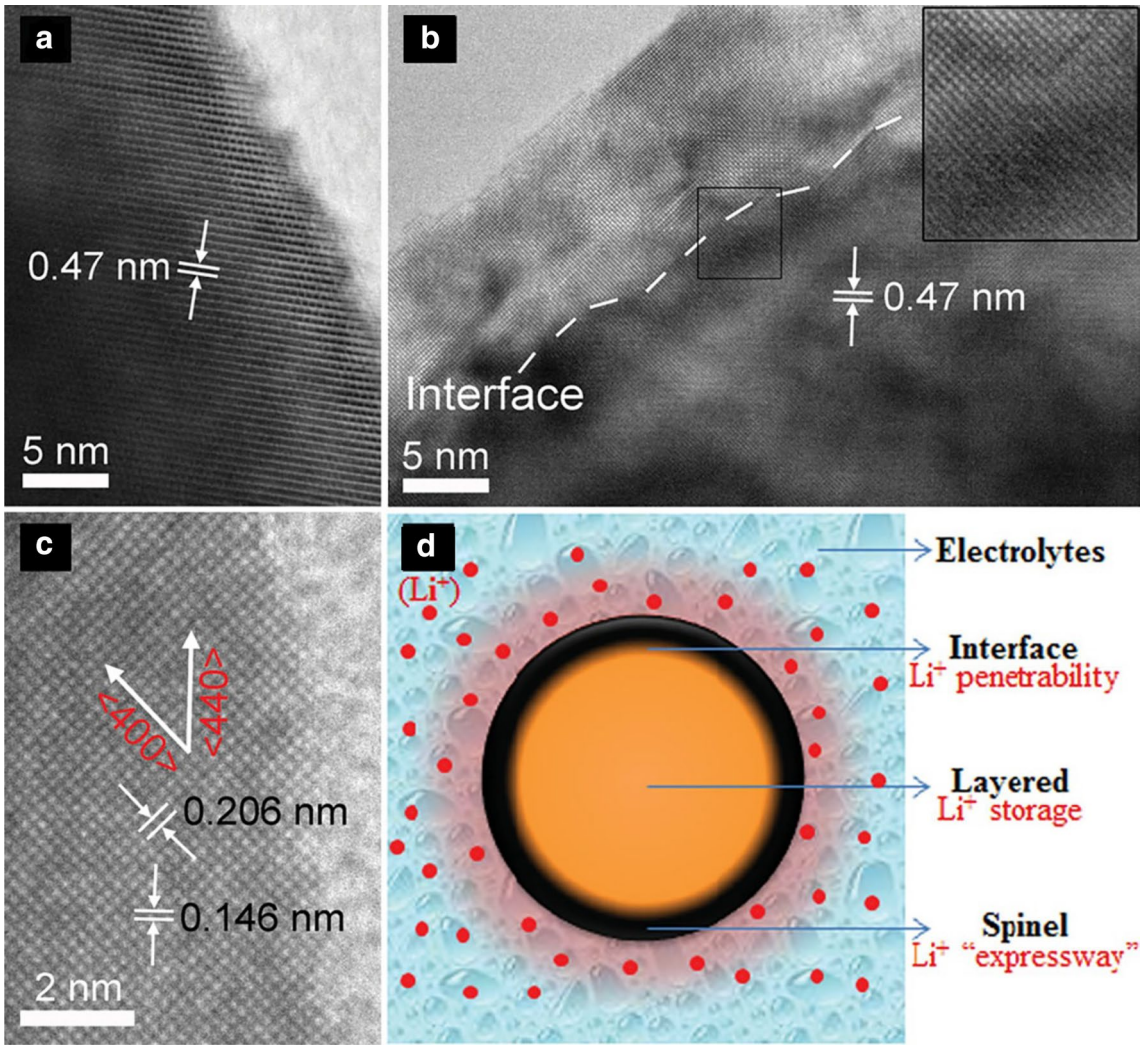

Fig. 18 HRTEM images of treated and untreated samples with spinel heterostructure surfaces. *Source*: **a–d** Reproduced with permission from Ref. [228]

Here, the researchers reported that the induced O vacancies at the LLO surface suppressed O evolution and limited electrolyte decomposition due to the highly reactive O species (Fig. 19a–e). In addition, the researchers also reported that the presence of O vacancies destabilized the tetrahedral sites, which reduced the chance of Li atoms becoming trapped in the tetrahedral sites, impeding Li diffusion and affecting rate performances and capacity.

The surface of electrode materials can also influence the electrode/electrolyte contact, the reactivity of particles and the surface reactions and reactivity, and researchers suggest that hierarchical nanostructures with exposed (110), (100) and (010) planes with better Li intercalation kinetics can demonstrate improved rate capabilities [233, 234]. For example, Xia et al. [139] fabricated a layered-spinel carbon heterostructure using the carbothermal reduction method and reported significantly enhanced rate performances. Here, the researchers suggested that the high-capacity Li-rich core with the spinel interlayer and the outside carbon-coated shell took advantage of the 3D Li^+ diffusion channels favoured by the spinel interlayer and demonstrated improved electrical conductivity due to the nanocarbon coating layer, in which a capacity of > 120 mAh g^{-1} even at 20 C was obtained. In another example, Li et al. [235] synthesized a core-shell structure with a Ni-rich material as the core and a Mn-rich material as the shell and reported that the Ni-rich core contributed to high energy densities and the Mn-rich shell hindered electrolyte oxidation. A similar heterogeneous design was also adopted to enhance the rate capability of LLOs in other studies and was reported to also possess high capacity inner cores and structurally stable outer shells [236, 237]. Overall, all these presented strategies aim at limiting voltage fade and

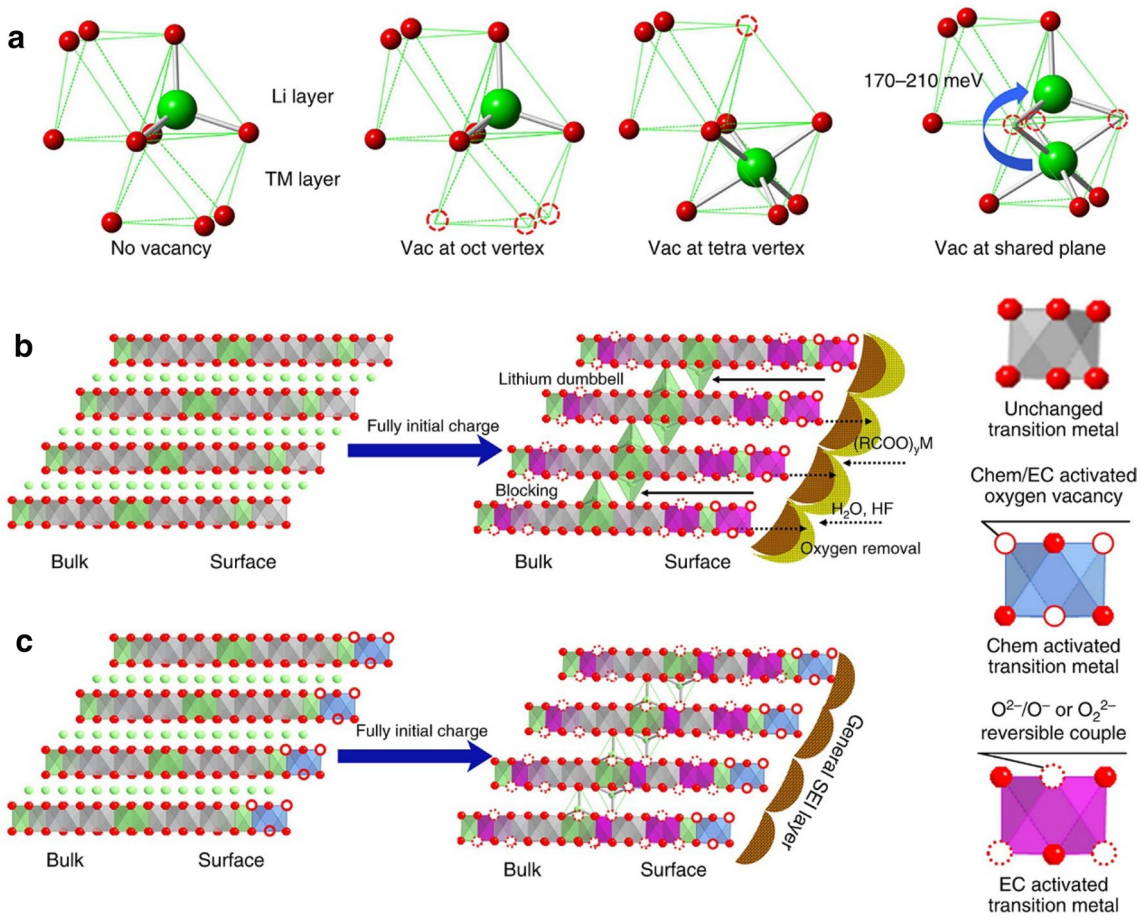

Fig. 19 **a** Schematic of the site stability and Li migration barrier under conditions of no oxygen vacancy and oxygen vacancies at different site vertexes. Schematic of LLOs **b** without induced oxygen vacancies and **c** with surface oxygen vacancies before and after initial charging. *Source*: **a**–**c** Reproduced with permission from Ref. [15]

have achieved improved rate performances as well because the origin of both issues is related to O activities in LLOs.

3.3.2.2 Lattice Doping Lattice doping with alkali metals such as Na^+ [163, 208], K^+ [164, 165] and Mg^{2+} [166] with large ionic radii has proved to enhance LLO rate performances. For example, Zheng et al. [165] synthesized K-doped $Li_{1.212}K_{0.02}Mn_{0.615}Ni_{0.154}O_2$ which exhibited enhanced rate performances and suggested that K^+ can restrict TM-ion migration and accompanying spinel formation in subsequent cycles. In another example, Yu et al. [166] doped Mg^{2+} ions into $Li_{1.5}(Mn_{0.75}Ni_{0.25})O_{2+\delta}$ and reported stronger Mg–O bonds as compared with Li–O bonds, allowing for the suppression of irreversible Li extraction and subsequent oxygen loss. As a result, this Mg-doped cathode exhibited good capacity retention of 94% even after 200 cycles at 0.5 C and 92% after 100 cycles if cycled at 5 C. Overall, improvements in rate performance through lattice doping can be mainly attributed to the stabilization of LLO crystal structures through the suppression of O evolution and accompanying phase transitions in subsequent cycles. Here, large dopant elements can hinder TM-ion migration and promote lattice expansion, favouring Li diffusion kinetics. In addition, researchers reported that the partial substitution of Ti^{4+} ions into Li sites of the Li_2MnO_3 component can create Li vacancies and increase interlayer spacing, allowing for better Li diffusion kinetics [171] and that doping with anions such as F^- can improve rate kinetics in which F^- doping into O sites can result in larger crystal lattices and improved Li diffusion [51] along with restricted spinel-phase transformation [238]. Furthermore, 4d TMs such as Sn [170], Ru [174], Nb [175], Y [169], Zr [172] and Sb [63], and 5d metals such as W [176] have also been used as dopants in LLOs and have shown improved cycling stability and rate capabilities. Here, the observed enhanced electrochemical performances can mainly be attributed to reduced O loss due to strong 4d–O and 5d–O bonds as compared with 3d–O bonds. Moreover, researchers suggest that the strengthening of M–O covalent bonds can promote

reversible anionic redox instead of irreversible O loss that results from the breaking of M–O bonds [239].

3.3.2.3 Particle Morphology Control and Other Strategies for LLO Rate Enhancements Architectures of nanosized LLOs that provide shorter Li diffusion pathways and more exposed surface sites for lithium intercalation/deintercalation can also enhance LLO rate capabilities [63, 240]. Here, the morphology of LLO plays a critical role in electrochemical performance in which hierarchial nanostructures with exposed (110), (100) and (010) planes favour Li intercalation kinetics, and LLOs possessing hierarchial porous structures can exhibit enhanced rate performances [233, 241–244]. Researchers also report that the formation of undesirable surface passivation layers due to organic electrolyte oxidation at higher voltage can cause poor rate capabilities due to increased Li diffusion resistances at the electrode/electrolyte interface [229, 245, 246]. In one study, Ming et al. [243] synthesized LLO nanoplates with built-in spinel/rock-salt tunnels (OAN-ST) that exhibited highly exposed (010) planes and reported that the resulting cathode exhibited enhanced capacity retention rates (92% after 100 cycles at 1 C), delivering high discharge capacities and ICE. Here the researchers attributed the performance enhancements to enhanced Li diffusion and intercalation kinetics as well as structural reinforcements through the accommodation of volume change during electrochemical cycling due to the peculiar structural design. In another study, Lin et al. [245] reported that other than the formation of surface passivation layers, progressive structural transitions can occur at the LLO surface depending on the crystal orientation and can result in impedance build-up and affect Li diffusion kinetics.

One reason for poor rate capability and irreversible capacity fading in LLOs is the formation of undesirable SEI layers (e.g. Li_2CO_3, LiF) on cathode surfaces, which can generate resistance to Li diffusion, and O species extracted during the Li_2MnO_3 activation process can oxidize organic solvents and result in the formation of this surface passivation layer at the cathode/electrolyte interphase [247]. In addition, at higher voltages above 4.6 V, carbonate-based electrolytes can decompose and contribute to SEI layer formations as well. Based on this, researchers have reported that electrolyte additives such as TPFPB [192], tris(2,2,2-trifluoro ethyl)phosphite [202] and LiBOB [193] can be useful to improve LLO rate capability by forming protective films at the cathode surface without impeding Li diffusion or by preventing undesirable parasitic reactions at the cathode/electrolyte interphase and therefore avoid the formation of undesirable surface passivating layers. For example, TPFPB with B atoms located at the centre has been found to be effective in the capture of active oxygen species and thus can limit side reactions at the interphase and assist in the dissolution of by-products of these parasitic reactions [192]. Alternatively, LiBOB is an electrolyte additive that can slow down Li_2MnO_3 activation and although studies report poor performances and an initial discharge capacity of only 215 mAh g^{-1}, cycling stability and rate performances can be enhanced with less discharge voltage fade [193]. However, the mechanisms behind the stabilization achieved by this additive have not yet been elucidated. Furthermore, with its stable chemical structure, PVS as an electrolyte additive can form a stable and ion conductive film on cathode surfaces to improve the capacity and rate performance of $Li(Li_{0.2}Mn_{0.54}Ni_{0.13}Co_{0.13})O_2$ [248]. Lastly, lithium difluoro(oxolato) borate (LiODFB) can also be employed as an electrolyte additive in full cells with $Li_{1.17}Ni_{0.17}Mn_{0.5}Co_{0.17}O_2$ cathodes and graphite anodes to achieve better rate capabilities due to the improved electronic and ionic conductivities of the SEI layer at the anode surface and the alleviated metal-ion dissolution of the cathode surface [249].

Overall, lattice changes and phase transformations originating from the activation process of Li_2MnO_3 are the major causes of poor rate capability; therefore, the optimization of the TM content and stabilization of TM lattices, especially Mn, are potential strategies to improve LLO rate capabilities.

4 Summary and Future Perspectives

Lithium-rich layered oxides (LLOs) possess high energy densities and are ideal for large-scale energy storage applications such as EVs and PHEVs. However, intrinsic weaknesses such as low initial Coulombic efficiency (ICE), severe capacity/voltage fade and poor rate capabilities impede further application. Therefore, in this review, fundamental origins of these issues and corresponding solutions are summarized along with opinions and perspectives.

Since the introduction of LLOs by Thackeray et al. in 1993, their electrochemical performances have continuously improved. And although the practical capacity of LLOs has reached ~ 330 mAh g^{-1} and many breakthroughs have been achieved, challenging issues remain and are closely connected with Li_2MnO_3 activation as well as the subsequent O release and evolution and the corresponding atomic (transition metal/cation migrations, mechanistic evolutions and valence drop cation redox reactions) and macroscopic (porogenic behaviours, surface cracking and pulverization) responses. To address these, commonly used strategies that have proved to be useful include particle size control, electrolyte and binder formulations, surface modifications and lattice doping. Although these strategies can partially mitigate some issues posed by LLOs, intrinsic issues that limit practical application have not been fully resolved. Here, many recent studies on LLOs have been able to find the root causes of these issues with the aid of advanced

characterization techniques, but more efforts are needed to obtain reliable conclusions and solutions. This is because none of these studies have been able to deliver clear and conclusive results regarding the fundamental origins of the challenges, especially the voltage fade, as well as the fact that many of the proposed solutions, such as surface modification, involve additional costs. Overall, an ICE greater than 90% for LLOs is required for communalization, and to achieve this, more intensive full-cell studies need to be conducted. In addition, volumetric energy densities of LLOs need to be improved through the improvement of LLO tap densities through the exploration of facile routes for low-cost large-scale synthesis.

Overall, an in-depth understanding of the correlation between O redox reactions and O release with respect to how it is affected by local structures is required and a promising and challenging approach is to create more triggering anionic redox reactions while lowering O release in which a noteworthy example is the use of electroactive cations such as Ru while maintaining strong d-sp hybridization to harvest additional capacity from $O^{2-} \rightarrow O_2^{2-}$ redox. In addition, new cutting-edge probing techniques need to be developed to investigate redox origins such as the direct measurement of O activities in LLOs during lithiation/delithiation to provide clearer and more precise pictures of mechanistic behaviours along with currently available characterization tools and approaches. And from a material design perspective, achieving coupled cationic and anionic redox processes can be a good solution, in which the fast kinetics of cationic redox reactions can act as redox mediators for sluggish anionic processes. Overall, there has been clear progress in the commercialization of LLOs; however, intrinsic challenges remain for practical application. To address these challenges, this review has presented many promising strategies in the hope that LLOs will eventually become optimized enough to meet the demands of commercial and industrial applications.

Acknowledgements This review was conducted with the support of the Australian Research Council (ARC) through the Future Fellowship projects (FT150100109 and FT160100251) and funding from the NSFC (51474110), the Natural Science Foundation of Hubei Province (2018CFB192) and the CSC (201608420205). We would also like to thank Dr. Tania Silver for her critical review of the manuscript and her valuable feedback.

References

1. Bunsen, T., Cazzola, P., Gorner, M., et al.: Global EV Outlook 2018: towards cross-modal electrification. International Energy Agency, Paris (2018)
2. Li, M., Lu, J., Chen, Z., et al.: 30 Years of lithium-ion batteries. Adv. Mater. **30**, 1800561 (2018)
3. Howell, D., Duong, T.Q., Faguy, P.W., et al.: FY 2016 annual progress report for advanced batteries. In: Energy Efficiency & Renewable Energy, U.S. Department of Energy, Washington, DC (2017)
4. Liu, W., Oh, P., Liu, X., et al.: Nickel-rich layered lithium transition-metal oxide for high-energy lithium-ion batteries. Angew. Chem. Int. Edit. **54**, 4440–4457 (2015)
5. Julien, C., Mauger, A.: Review of 5-V electrodes for Li-ion batteries: Status and trends. Ionics **19**, 951–988 (2013)
6. Hu, M., Pang, X., Zhou, Z.: Recent progress in high-voltage lithium ion batteries. J. Power Sources **237**, 229–242 (2013)
7. Xu, B., Qian, D., Wang, Z., et al.: Recent progress in cathode materials research for advanced lithium ion batteries. Mater. Sci. Eng. R-Rep. **73**, 51–65 (2012)
8. Ellis, B.L., Lee, K.T., Nazar, L.F.: Positive electrode materials for Li-ion and Li-batteries. Chem. Mater. **22**, 691–714 (2010)
9. Choi, J.W., Aurbach, D.: Promise and reality of post-lithium-ion batteries with high energy densities. Nat. Rev. Mater. **1**, 16013 (2016)
10. Croguennec, L., Palacin, M.R.: Recent achievements on inorganic electrode materials for lithium-ion batteries. J. Am. Chem. Soc. **137**, 3140–3156 (2015)
11. Kraytsberg, A., Ein-Eli, Y.: Higher, stronger, better… A review of 5 volt cathode materials for advanced lithium-ion batteries. Adv. Energy Mater. **2**, 922–939 (2012)
12. Li, W., Song, B., Manthiram, A.: High-voltage positive electrode materials for lithium-ion batteries. Chem. Soc. Rev. **46**, 3006–3059 (2017)
13. Rossouw, M.H., Liles, D.C., Thackeray, M.M.: Synthesis and structural characterization of a novel layered lithium manganese oxide, $Li_{0.36}Mn_{0.91}O_2$, and its lithiated derivative, $Li_{1.09}Mn_{0.91}O_2$. J. Solid State Chem. **104**, 464-466 (1993)
14. Thackeray, M.M., Kang, S.H., Johnson, C.S., et al.: Li_2MnO_3-stabilized $LiMO_2$ (M = Mn, Ni, Co) electrodes for lithium-ion batteries. J. Mater. Chem. **17**, 3112–3125 (2007)
15. Qiu, B., Zhang, M., Wu, L., et al.: Gas–solid interfacial modification of oxygen activity in layered oxide cathodes for lithium-ion batteries. Nat. Commun. **7**, 12108 (2016)
16. Lu, Z., Dahn, J.R.: Understanding the anomalous capacity of Li/Li $[Ni_xLi_{(1/3-2x/3)}Mn_{(2/3-x/3)}]O_2$ cells using in situ X-ray diffraction and electrochemical studies. J. Electrochem. Soc. **149**, A815–A822 (2002)
17. Croy, J., Kang, S.H., Balasubramanian, M., et al.: Li_2MnO_3-based composite cathodes for lithium batteries: a novel synthesis approach and new structures. Electrochem. Commun. **13**, 1063–1066 (2011)
18. Yu, X., Lyu, Y., Gu, L., et al.: Understanding the rate capability of high-energy-density Li-rich layered $Li_{1.2}Ni_{0.15}Co_{0.1}Mn_{0.55}O_2$ cathode materials. Adv. Energy Mater. **4**, 1300950 (2014)
19. Kalluri, S., Yoon, M., Jo, M., et al.: Feasibility of cathode surface coating technology for high-energy lithium-ion and beyond-lithium-ion batteries. Adv. Mater. **29**, 1605807 (2017)
20. Wang, Y., Yang, Z., Qian, Y., et al.: New insights into improving rate performance of lithium-rich cathode material. Adv. Mater. **27**, 3915–3920 (2015)
21. Zhang, X.D., Shi, J.L., Liang, J.Y., et al.: Structurally modulated Li-rich cathode materials through cooperative cation doping and anion hybridization. Sci. China Chem. **60**, 1554–1560 (2017)
22. Assat, G., Tarascon, J.M.: Fundamental understanding and practical challenges of anionic redox activity in Li-ion batteries. Nat. Energy **3**, 373 (2018)
23. Gent, W.E., Lim, K., Liang, Y., et al.: Coupling between oxygen redox and cation migration explains unusual electrochemistry in lithium-rich layered oxides. Nat. Commun. **8**, 2091 (2017)
24. Assat, G., Foix, D., Delacourt, C., et al.: Fundamental interplay between anionic/cationic redox governing the kinetics and thermodynamics of lithium-rich cathodes. Nat. Commun. **8**, 2219 (2017)

25. Hu, E., Yu, X., Lin, R., et al.: Evolution of redox couples in Li- and Mn-rich cathode materials and mitigation of voltage fade by reducing oxygen release. Nature Energy **3**, 690 (2018)
26. Singer, A., Zhang, M., Hy, S., et al.: Nucleation of dislocations and their dynamics in layered oxide cathode materials during battery charging. Nat. Energy **3**, 641–647 (2018)
27. Myeong, S., Cho, W., Jin, W., et al.: Understanding voltage decay in lithium-excess layered cathode materials through oxygen-centred structural arrangement. Nat. Commun. **9**, 3285 (2018)
28. Xu, J., Sun, M., Qiao, R., et al.: Elucidating anionic oxygen activity in lithium-rich layered oxides. Nat. Commun. **9**, 947 (2018)
29. Rozier, P., Tarascon, J.M.: Li-rich layered oxide cathodes for next-generation Li-ion batteries: chances and challenges. J. Electrochem. Soc. **162**, A2490–A2499 (2015)
30. Thackeray, M., Croy, J., Lee, E., et al.: The quest for manganese-rich electrodes for lithium batteries: strategic design and electrochemical behavior. Sustain. Energy Fuels **2**, 1375–1397 (2018)
31. Nayak, P.K., Erickson, E.M., Schipper, F., et al.: Review on challenges and recent advances in the electrochemical performance of high capacity Li-and Mn-rich cathode materials for Li-ion batteries. Adv. Energy Mater. **8**, 1702397 (2018)
32. Hu, E., Wang, X., Yu, X., et al.: Probing the complexities of structural changes in layered oxide cathode materials for Li-ion batteries during fast charge-discharge cycling and heating. Acc. Chem. Res. **51**, 290–298 (2018)
33. Thackeray, M.M., Johnson, C.S., Vaughey, J.T., et al.: Advances in manganese-oxide 'composite' electrodes for lithium-ion batteries. J. Mater. Chem. **15**, 2257–2267 (2005)
34. Lu, Z., Beaulieu, L., Donaberger, R., et al.: Synthesis, structure, and electrochemical behavior of $Li[Ni_xLi_{1/3-2x/3}Mn_{2/3-x/3}]O_2$. J. Electrochem. Soc. **149**, A778–A791 (2002)
35. Lu, Z., Chen, Z., Dahn, J.R.: Lack of cation clustering in $Li[Ni_xLi_{1/3-2x/3}Mn_{2/3-x/3}]O_2$ $(0 < x \leqslant 1/2)$ and $Li[Cr_xLi_{(1-x)/3}Mn_{(2-2x)/3}]O_2$ $(0 < x < 1)$. Chem. Mater. **15**, 3214–3220 (2003)
36. Li, X., Qiao, Y., Guo, S., et al.: Direct visualization of the reversible O^{2-}/O^{-} redox process in Li-rich cathode materials. Adv. Mater. **30**, 1705197 (2018)
37. Hong, J., Gwon, H., Jung, S.K., et al.: Review—lithium-excess layered cathodes for lithium rechargeable batteries. J. Electrochem. Soc. **162**, A2447–A2467 (2015)
38. Yu, H., Ishikawa, R., So, Y.G., et al.: Direct atomic-resolution observation of two phases in the $Li_{1.2}Mn_{0.567}Ni_{0.166}Co_{0.067}O_2$ cathode material for lithium-ion batteries. Angew. Chem. Int. Edit. **125**, 6085–6089 (2013)
39. Radin, M.D., Hy, S., Sina, M., et al.: Narrowing the gap between theoretical and practical capacities in Li-ion layered oxide cathode materials. Adv. Energy Mater. **7**, 1602888 (2017)
40. Mohanty, D., Huq, A., Payzant, E.A., et al.: Neutron diffraction and magnetic susceptibility studies on a high-voltage $Li_{1.2}Mn_{0.55}Ni_{0.15}Co_{0.10}O_2$ lithium ion battery cathode: insight into the crystal structure. Chem. Mater. **25**, 4064–4070 (2013)
41. Wang, D., Belharouak, I., Zhang, X., et al.: Insights into the phase formation mechanism of $[0.5Li_2MnO_3{\cdot}0.5LiNi_{0.5}Mn_{0.5}O_2]$ battery materials. J. Electrochem. Soc. **161**, A1–A5 (2014)
42. Boulineau, A., Simonin, L., Colin, J.F., et al.: Evolutions of $Li_{1.2}Mn_{0.61}Ni_{0.18}Mg_{0.01}O_2$ during the initial charge/discharge cycle studied by advanced electron microscopy. Chem. Mater. **24**, 3558–3566 (2012)
43. Cho, S.W., Kim, G.O., Ryu, K.S.: Sulfur anion doping and surface modification with $LiNiPO_4$ of a $Li[Co_{0.1}Ni_{0.15}Li_{0.2}Mn_{0.55}]O_2$ cathode material for Li-ion batteries. Solid State Ion. **206**, 84–90 (2012)
44. Gummow, R.J., Sharma, N., Feng, R., et al.: High performance composite lithium-rich nickel manganese oxide cathodes for lithium-ion batteries. J. Electrochem. Soc. **160**, A1856–A1862 (2013)
45. Devaraj, A., Gu, M., Colby, R., et al.: Visualizing nanoscale 3D compositional fluctuation of lithium in advanced lithium-ion battery cathodes. Nat. Commun. **6**, 8014 (2015)
46. Bareño, J., Balasubramanian, M., Kang, S.H., et al.: Long-range and local structure in the layered oxide $Li_{1.2}Co_{0.4}Mn_{0.4}O_2$. Chem. Mater. **23**, 2039–2050 (2011)
47. McCalla, E., Lowartz, C.M., Brown, C.R., et al.: Formation of layered-layered composites in the Li–Co–Mn oxide pseudoternary system during slow cooling. Chem. Mater. **25**, 912–918 (2013)
48. Zheng, J., Gu, M., Xiao, J., et al.: Corrosion/fragmentation of layered composite cathode and related capacity/voltage fading during cycling process. Nano Lett. **13**, 3824–3830 (2013)
49. Zheng, J., Gu, M., Xiao, J., et al.: Functioning mechanism of AlF_3 coating on the Li-and Mn-rich cathode materials. Chem. Mater. **26**, 6320–6327 (2014)
50. Nayak, P.K., Grinblat, J., Levi, M., et al.: Al doping for mitigating the capacity fading and voltage decay of layered Li and Mn-rich cathodes for Li-ion batteries. Adv. Energy Mater. **6**, 1502398 (2016)
51. Pang, W.K., Lin, H.F., Peterson, V.K., et al.: Effects of fluorine and chromium doping on the performance of lithium-rich $Li_{1+x}MO_2$ (M = Ni, Mn, Co) positive electrodes. Chem. Mater. **29**, 10299–10311 (2017)
52. Gu, M., Genc, A., Belharouak, I., et al.: Nanoscale phase separation, cation ordering, and surface chemistry in pristine $Li_{1.2}Ni_{0.2}Mn_{0.6}O_2$ for Li-ion batteries. Chem. Mater. **25**, 2319–2326 (2013)
53. Lei, C.H., Bareño, J., Wen, J.G., et al.: Local structure and composition studies of $Li_{1.2}Ni_{0.2}Mn_{0.6}O_2$ by analytical electron microscopy. J. Power Sour. **178**, 422–433 (2008)
54. Armstrong, A.R., Holzapfel, M., Novák, P., et al.: Demonstrating oxygen loss and associated structural reorganization in the lithium battery cathode $Li[Ni_{0.2}Li_{0.2}Mn_{0.6}]O_2$. J. Am. Chem. Soc. **128**, 8694–8698 (2006)
55. Zheng, J., Shi, W., Gu, M., et al.: Electrochemical kinetics and performance of layered composite cathode material $Li[Li_{0.2}Ni_{0.2}Mn_{0.6}]O_2$. J. Electrochem. Soc. **160**, A2212–A2219 (2013)
56. Kikkawa, J., Akita, T., Tabuchi, M., et al.: Coexistence of layered and cubic rocksalt structures with a common oxygen sublattice in $Li_{1.2}Mn_{0.4}Fe_{0.4}O_2$ particles: a transmission electron microscopy study. J. Appl. Phys. **103**, 104911 (2008)
57. Jacob, C., Jian, J., Zhu, Y., et al.: A new approach to investigate Li_2MnO_3 and $Li(Ni_{0.5}Mn_{0.3}Co_{0.2})O_2$ mixed phase cathode materials. J. Mater. Chem. A **2**, 2283–2289 (2014)
58. Shi, J.L., Zhang, J.N., He, M., et al.: Mitigating voltage decay of Li-rich cathode material via increasing Ni content for lithium-Ion batteries. ACS Appl. Mater. Interfaces **8**, 20138–20146 (2016)
59. Sun, Y.K., Lee, M.J., Yoon, C.S., et al.: The role of AlF_3 coatings in improving electrochemical cycling of Li-enriched nickel-manganese oxide electrodes for Li-ion batteries. Adv. Mater. **24**, 1192–1196 (2012)
60. Zhang, S., Gu, H., Tang, T., et al.: Insight into the synergistic effect mechanism between the Li_2MO_3 phase and the $LiMO_2$ phase (M = Ni Co, and Mn) in Li- and Mn-rich layered oxide cathode materials. Electrochim. Acta **266**, 66–77 (2018)
61. Ito, A., Li, D., Sato, Y., et al.: Cyclic deterioration and its improvement for Li-rich layered cathode material $Li[Ni_{0.17}Li_{0.2}Co_{0.07}Mn_{0.56}]O_2$. J. Power Sources **195**, 567–573 (2010)
62. Shojan, J., Chitturi, V.R., Soler, J., et al.: High energy xLi_2MnO_3–$(1\text{-}x)LiNi_{2/3}Co_{1/6}Mn_{1/6}O_2$ composite cathode for advanced Li-ion batteries. J. Power Sources **274**, 440–450 (2015)
63. Yu, R., Zhang, Z., Jamil, S., et al.: Effects of nanofiber architecture and antimony doping on the performance of lithium-rich

layered oxides: enhancing lithium diffusivity and lattice oxygen stability. ACS Appl. Mater. Interfaces **10**, 16561–16571 (2018)
64. Ding, F., Li, J., Deng, F., et al.: Surface heterostructure induced by $PrPO_4$ modification in $Li_{12}[Mn_{0.54}Ni_{0.13}Co_{0.13}]O_2$ cathode material for high-performance lithium-ion batteries with mitigating voltage decay. ACS Appl. Mater. Interfaces **9**, 27936–27945 (2017)
65. Ghanty, C., Basu, R.N., Majumder, S.B.: Performance of wet chemical synthesized $xLi_2MnO_{3-(1-x)}Li(Mn_{0.375}Ni_{0.375}Co_{0.25})O_2$ ($0.0 \leqslant x \leqslant 1.0$) integrated cathode for lithium rechargeable battery. J. Electrochem. Soc. **159**, A1125–A1134 (2012)
66. Nomura, F., Liu, Y., Tanabe, T., et al.: Elucidation of key factors of water-resistance of Li-rich solid-solution layered oxide cathode materials applicable to a water-based cathode preparation process for Li-ion battery. Electrochim. Acta **283**, 478–487 (2018)
67. Bréger, J., Jiang, M., Dupré, N., et al.: High-resolution X-ray diffraction, DIFFaX, NMR and first principles study of disorder in the Li_2MnO_3-$Li[Ni_{1/2}Mn_{1/2}]O_2$ solid solution. J. Solid State Chem. **178**, 2575–2585 (2005)
68. Jarvis, K.A., Deng, Z., Allard, L.F., et al.: Atomic structure of a lithium-rich layered oxide material for lithium-ion batteries: evidence of a solid solution. Chem. Mater. **23**, 3614–3621 (2011)
69. Shukla, A.K., Ramasse, Q.M., Ophus, C., et al.: Unravelling structural ambiguities in lithium-and manganese-rich transition metal oxides. Nat. Commun. **6**, 8711 (2015)
70. Zheng, J., Gu, M., Genc, A., et al.: Mitigating voltage fade in cathode materials by improving the atomic level uniformity of elemental distribution. Nano Lett. **14**, 2628–2635 (2014)
71. Komatsu, H., Minato, T., Matsunaga, T., et al.: Site-selective analysis of nickel-substituted Li-rich layered material: migration and role of transition metal at charging and discharging. J. Phys. Chem. C **122**, 20099–20107 (2018)
72. Zheng, J., Xu, P., Gu, M., et al.: Structural and chemical evolution of Li-and Mn-rich layered cathode material. Chem. Mater. **27**, 1381–1390 (2015)
73. Ozawa, K., Nakao, Y., Mochiku, T., et al.: Electrochemical characteristics of layered $Li_{1.95}Mn_{0.9}Co_{0.15}O_3$ (*C2/m*) as a lithium-battery cathode. J. Electrochem. Soc. **159**, A300–A304 (2012)
74. Liu, H., Harris, K.J., Jiang, M., et al.: Unraveling the rapid performance decay of layered high-energy cathodes: from nanoscale degradation to drastic bulk evolution. ACS Nano **12**, 2708–2718 (2018)
75. Wang, J.X.: Structure and delithiation/lithiation of the lithium-rich layered oxide $Li[Li_{0.23}Ni_{0.15}Mn_{0.62}]O_2$ as cathode material. Int. J. Electrochem. Sci. **12**, 8095–8105 (2017)
76. Pimenta, V., Sathiya, M., Batuk, D., et al.: Synthesis of Li-rich NMC: a comprehensive study. Chem. Mater. **29**, 9923–9936 (2017)
77. Fujii, H., Ozawa, K., Mochiku, T.: Electron diffraction and high-resolution electron microscopy studies on layered $Li_{2-\delta}(Mn_{1-x}Co_x)_{1+\delta}O_3$. J. Solid State Chem. **203**, 345–352 (2013)
78. Nomura, F., Tanabe, T., Gunji, T., et al.: Effect of the cooling process on the structure and charge/discharge cycling performance in $Li[Li_{0.20}Mn_{0.58}Ni_{0.18}Co_{0.04}]O_2$ Li-rich solid-solution layered oxide cathode materials for Li-ion battery. ECS Trans. **85**, 1497–1505 (2018)
79. Koga, H., Croguennec, L., Mannessiez, P., et al.: $Li_{1.20}Mn_{0.54}Co_{0.13}Ni_{0.13}O_2$ with different particle sizes as attractive positive electrode materials for lithium-ion batteries: insights into their structure. J. Phys. Chem. C **116**, 13497–13506 (2012)
80. Numata, K., Sakaki, C., Yamanaka, S.: Synthesis and characterization of layer structured solid solutions in the system of $LiCoO_2$-Li_2MnO_3. Solid State Ion. **117**, 257–263 (1999)
81. Yoon, W.-S., Iannopollo, S., Grey, C.P., et al.: Local structure and cation ordering in O3 lithium nickel manganese oxides with stoichiometry $Li[Ni_xMn_{(2-x)/3}Li_{(1-2x)/3}]O_2$ NMR studies and first principles calculations. Electrochem. Solid-State Lett. **7**, A167–A171 (2004)
82. Meng, Y.S., Ceder, G., Grey, C.P., et al.: Cation ordering in layered O3 $Li[Ni_xLi_{1/3-2x/3}Mn_{2/3-x/3}]O_2$ ($0 \leqslant x \leqslant 1/2$) compounds. Chem. Mater. **17**, 2386–2394 (2005)
83. Genevois, C., Koga, H., Croguennec, L., et al.: Insight into the atomic structure of cycled lithium-rich layered oxide $Li_{1.20}Mn_{0.54}Co_{0.13}Ni_{0.13}O_2$ using HAADF STEM and electron nanodiffraction. J. Phys. Chem. C **119**, 75–83 (2014)
84. Sun, Y., Shiosaki, Y., Xia, Y., et al.: The preparation and electrochemical performance of solid solutions $LiCoO_2$–Li_2MnO_3 as cathode materials for lithium ion batteries. J. Power Sources **159**, 1353–1359 (2006)
85. West, W.C., Soler, J., Smart, M.C., et al.: Electrochemical behavior of layered solid solution Li_2MnO_3-$LiMO_2$ (M = Ni, Mn, Co) Li-ion cathodes with and without alumina coatings. J. Electrochem. Soc. **158**, A883–A889 (2011)
86. Ohzuku, T., Nagayama, M., Tsuji, K., et al.: High-capacity lithium insertion materials of lithium nickel manganese oxides for advanced lithium-ion batteries: toward rechargeable capacity more than 300 mAh g^{-1}. J. Mater. Chem. **21**, 10179–10188 (2011)
87. Singh, G., Thomas, R., Kumar, A., et al.: Electrochemical behavior of Cr-doped composite Li_2MnO_3-$LiMn_{0.5}Ni_{0.5}O_2$ cathode materials. J. Electrochem. Soc. **159**, A410–A420 (2012)
88. Nomura, F., Liu, Y., Tanabe, T., et al.: Optimization of calcination temperature in preparation of a high capacity Li-rich solid-solution $Li[Li_{0.2}Ni_{0.18}Co_{0.03}Mn_{0.58}]O_2$ material and its cathode performance in lithium ion battery. Electrochim. Acta **269**, 321–330 (2018)
89. Thackeray, M., Kang, S.H., Johnson, C., et al.: Comments on the structural complexity of lithium-rich $Li_{1+x}M_{1-x}O_2$ electrodes (M = Mn, Ni, Co) for lithium batteries. Electrochem. Commun. **8**, 1531–1538 (2006)
90. Pan, H., Zhang, S., Chen, J., et al.: Li- and Mn-rich layered oxide cathode materials for lithium-ion batteries: a review from fundamentals to research progress and applications. Mol. Syst. Des. Eng. **3**, 748–803 (2018)
91. Hy, S., Felix, F., Rick, J., et al.: Direct In situ observation of Li_2O evolution on Li-Rich high-capacity cathode material, $Li[Ni_xLi_{(1-2x)/3}Mn_{(2-x)/3}]O_2$ ($0 \leqslant x \leqslant 0.5$). J. Am. Chem. Soc. **136**, 999–1007 (2014)
92. Arunkumar, T.A., Alvarez, E., Manthiram, A.: Structural, chemical, and electrochemical characterization of layered $Li[Li_{0.17}Mn_{0.33}Co_{0.5-y}Ni_y]O_2$ cathodes. J. Electrochem. Soc. **154**, A770–A775 (2007)
93. Koga, H., Croguennec, L., Ménétrier, M., et al.: Operando X-ray absorption study of the redox processes involved upon cycling of the Li-rich layered oxide $Li_{1.20}Mn_{0.54}Co_{0.13}Ni_{0.13}O_2$ in Li ion batteries. J. Phys. Chem. C **118**, 5700–5709 (2014)
94. Koga, H., Croguennec, L., Ménétrier, M., et al.: Reversible oxygen participation to the redox processes revealed for $Li_{1.20}Mn_{0.54}Co_{0.13}Ni_{0.13}O_2$. J. Electrochem. Soc. **160**, A786–A792 (2013)
95. Seo, D.H., Lee, J., Urban, A., et al.: The structural and chemical origin of the oxygen redox activity in layered and cation-disordered Li-excess cathode materials. Nat. Chem. **8**, 692 (2016)
96. Muhammad, S., Kim, H., Kim, Y., et al.: Evidence of reversible oxygen participation in anomalously high capacity Li-and Mn-rich cathodes for Li-ion batteries. Nano Energy **21**, 172–184 (2016)
97. Chen, C.J., Pang, W.K., Mori, T., et al.: The origin of capacity fade in the $Li_2MnO_3{\cdot}LiMO_2$ (M = Li, Ni Co, Mn) microsphere positive electrode: an operando neutron diffraction and transmission X-ray microscopy study. J. Am. Chem. Soc. **138**, 8824–8833 (2016)

98. Wu, Y., Manthiram, A.: Effect of surface modifications on the layered solid solution cathodes $_{(1-z)}Li[Li_{1/3}Mn_{2/3}]O_{2-(z)}Li[Mn_{05-y}Ni_{0.5-y}Co_{2y}]O_2$. Solid State Ion. **180**, 50–56 (2009)
99. West, W.C., Staniewicz, R.J., Ma, C., et al.: Implications of the first cycle irreversible capacity on cell balancing for Li_2MnO_3-$LiMO_2$ (M = Ni, Mn, Co) Li-ion cathodes. J. Power Sources **196**, 9696–9701 (2011)
100. van Bommel, A., Krause, L.J., Dahn, J.R.: Investigation of the irreversible capacity loss in the lithium-rich oxide $Li[Li_{1/5}Ni_{1/5}Mn_{3/5}]O_2$. J. Electrochem. Soc. **158**, A731–A735 (2011)
101. Shunmugasundaram, R., Senthil Arumugam, R., Harris, K.J., et al.: A search for low-irreversible capacity and high-reversible capacity positive electrode materials in the Li–Ni–Mn–Co pseudoquaternary system. Chem. Mater. **28**, 55–66 (2015)
102. Kang, S.H., Johnson, C., Vaughey, J., et al.: The effects of acid treatment on the electrochemical properties of $0.5Li_2MnO_3$•$0.5LiNi_{0.44}Co_{0.25}Mn_{0.31}O_2$ electrodes in lithium cells. J. Electrochem. Soc. **153**, A1186–A1192 (2006)
103. Gao, J., Kim, J., Manthiram, A.: High capacity $Li[Li_{0.2}Mn_{0.54}Ni_{0.13}Co_{0.13}]O_2$-$V_2O_5$ composite cathodes with low irreversible capacity loss for lithium ion batteries. Electrochem. Commun. **11**, 84–86 (2009)
104. Zhou, L., Yin, Z., Ding, Z., et al.: Bulk and surface reconstructed Li-rich Mn-based cathode material for lithium ion batteries with eliminating irreversible capacity loss. J. Electroanal. Chem. **829**, 7–15 (2018)
105. Shunmugasundaram, R., Senthil Arumugam, R., Dahn, J.R.: High capacity Li-rich positive electrode materials with reduced first-cycle irreversible capacity loss. Chem. Mater. **27**, 757–767 (2015)
106. Lu, J., Chen, Z., Ma, Z., et al.: The role of nanotechnology in the development of battery materials for electric vehicles. Nat. Nanotechnol. **11**, 1031 (2016)
107. Malik, R., Burch, D., Bazant, M., et al.: Particle size dependence of the ionic diffusivity. Nano Lett. **10**, 4123–4127 (2010)
108. Liu, J., Chen, H., Xie, J., et al.: Electrochemical performance studies of Li-rich cathode materials with different primary particle sizes. J. Power Sources **251**, 208–214 (2014)
109. Wang, J., Yuan, G., Zhang, M., et al.: The structure, morphology, and electrochemical properties of $Li_{1+x}Ni_{1/6}Co_{1/6}Mn_{4/6}O_{2.\,25+x/2}$ ($0.1 \leqslant x \leqslant 0.7$) cathode materials. Electrochim. Acta **66**, 61–66 (2012)
110. Li, J., Shunmugasundaram, R., Doig, R., et al.: In situ x-ray diffraction study of layered Li–Ni–Mn–Co oxides: effect of particle size and structural stability of core–shell materials. Chem. Mater. **28**, 162–171 (2015)
111. Yabuuchi, N., Kubota, K., Aoki, Y., et al.: Understanding particle-size-dependent electrochemical properties of Li_2MnO_3-based positive electrode materials for rechargeable lithium batteries. J. Phys. Chem. C **120**, 875–885 (2016)
112. Kuppan, S., Duncan, H., Chen, G.: Controlling side reactions and self-discharge in high-voltage spinel cathodes: the critical role of surface crystallographic facets. Phys. Chem. Chem. Phys. **17**, 26471–26481 (2015)
113. Xu, J., Deshpande, R.D., Pan, J., et al.: Electrode side reactions, capacity loss and mechanical degradation in lithium-ion batteries. J. Electrochem. Soc. **162**, A2026–A2035 (2015)
114. Zhao, T., Li, L., Chen, R., et al.: Design of surface protective layer of LiF/FeF_3 nanoparticles in Li-rich cathode for high-capacity Li-ion batteries. Nano Energy **15**, 164–176 (2015)
115. Song, J.H., Kapylou, A., Choi, H.S., et al.: Suppression of irreversible capacity loss in Li-rich layered oxide by fluorine doping. J. Power Sources **313**, 65–72 (2016)
116. Qing, R.P., Shi, J.L., Xiao, D.D., et al.: Enhancing the kinetics of Li-rich cathode materials through the pinning effects of gradient surface Na^+ doping. Adv. Energy Mater. **6**, 1501914 (2016)
117. Zhao, Y., Liu, J., Wang, S., et al.: Surface structural transition induced by gradient polyanion-doping in Li-rich layered oxides: implications for enhanced electrochemical performance. Adv. Funct. Mater. **26**, 4760–4767 (2016)
118. Liu, S., Liu, Z., Shen, X., et al.: Surface doping to enhance structural integrity and performance of Li-rich layered oxide. Adv. Energy Mater. **8**, 1802105 (2018)
119. Zhang, X., Belharouak, I., Li, L., et al.: Structural and electrochemical study of Al_2O_3 and TiO_2 coated $Li_{1.2}Ni_{0.13}Mn_{0.54}Co_{0.13}O_2$ cathode material using ALD. Adv. Energy Mater. **3**, 1299–1307 (2013)
120. Zhang, X., Yin, Y., Hu, Y., et al.: Zr-containing phosphate coating to enhance the electrochemical performances of Li-rich layer-structured Li $[Li_{0.2}Ni_{0.17}Co_{0.07}Mn_{0.56}]O_2$. Electrochim. Acta **193**, 96–103 (2016)
121. Seteni, B., Rapulenyane, N., Ngila, J.C., et al.: Coating effect of $LiFePO_4$ and Al_2O_3 on $Li_{1.2}Mn_{0.54}Ni_{0.13}Co_{0.13}O_2$ cathode surface for lithium ion batteries. J. Power Sources **353**, 210–220 (2017)
122. Kim, I.T., Knight, J.C., Celio, H., et al.: Enhanced electrochemical performances of Li-rich layered oxides by surface modification with reduced graphene oxide/$AlPO_4$ hybrid coating. J. Mater. Chem. A **2**, 8696–8704 (2014)
123. Wang, Z., Liu, E., He, C., et al.: Effect of amorphous $FePO_4$ coating on structure and electrochemical performance of $Li_{1.2}Ni_{0.13}Co_{0.13}Mn_{0.54}O_2$ as cathode material for Li-ion batteries. J. Power Sour. **236**, 25–32 (2013)
124. Liu, B., Zhang, Q., He, S., et al.: Improved electrochemical properties of $Li_{1.2}Ni_{0.18}Mn_{0.59}Co_{0.03}O_2$ by surface modification with $LiCoPO_4$. Electrochim. Acta **56**, 6748–6751 (2011)
125. Liu, X., Liu, J., Huang, T., et al.: CaF_2-coated $Li_{1.2}Mn_{0.54}Ni_{0.13}Co_{0.13}O_2$ as cathode materials for Li-ion batteries. Electrochim. Acta **109**, 52–58 (2013)
126. Xiao, B., Wang, B., Liu, J., et al.: Highly stable $Li_{1.2}Mn_{0.54}Co_{0.13}Ni_{0.13}O_2$ enabled by novel atomic layer deposited $AlPO_4$ coating. Nano Energy **34**, 120–130 (2017)
127. Wu, F., Li, N., Su, Y., et al.: Can surface modification be more effective to enhance the electrochemical performance of lithium rich materials? J. Mater. Chem. **22**, 1489–1497 (2012)
128. Gan, Y., Wang, Y., Han, J., et al.: Synthesis and electrochemical performance of nano TiO_2(B)-coated Li $[Li_{0.2}Mn_{0.54}Co_{0.13}Ni_{0.13}]O_2$ cathode materials for lithium-ion batteries. New J. Chem. **41**, 12962–12968 (2017)
129. Shi, S., Tu, J., Zhang, Y., et al.: Effect of Sm_2O_3 modification on $Li[Li_{0.2}Mn_{0.56}Ni_{0.16}Co_{0.08}]O_2$ cathode material for lithium ion batteries. Electrochim. Acta **108**, 441–448 (2013)
130. Wang, Z., Liu, E., Guo, L., et al.: Cycle performance improvement of Li-rich layered cathode material Li $[Li_{0.2}Mn_{0.54}Ni_{0.13}Co_{0.13}]O_2$ by ZrO_2 coating. Surf Coat Technol **235**, 570–576 (2013)
131. Li, C.D., Xu, J., Xia, J.S., et al.: Influences of FeF_3 coating layer on the electrochemical properties of Li $[Li_{0.2}Mn_{0.54}Ni_{0.13}Co_{0.13}]O_2$ cathode materials for lithium-ion batteries. Solid State Ion. **292**, 75–82 (2016)
132. Zhou, L., Tian, M., Deng, Y., et al.: La_2O_3-coated $Li_{1.2}Mn_{0.54}Ni_{0.13}Co_{0.13}O_2$ as cathode materials with enhanced specific capacity and cycling stability for lithium-ion batteries. Ceram. Int. **42**, 15623–15633 (2016)
133. Lu, C., Wu, H., Zhang, Y., et al.: Cerium fluoride coated layered oxide $Li_{1.2}Mn_{0.54}Ni_{0.13}Co_{0.13}O_2$ as cathode materials with improved electrochemical performance for lithium ion batteries. J. Power Sources **267**, 682–691 (2014)
134. Li, J., Li, J., Yu, T., et al.: Stabilizing the structure and suppressing the voltage decay of $Li[Li_{0.2}Mn_{0.54}Co_{0.13}Ni_{0.13}]O_2$ cathode materials for Li-ion batteries via multifunctional Pr oxide surface modification. Ceram. Int. **42**, 18620–18630 (2016)

135. Sun, S., Wan, N., Wu, Q., et al.: Surface-modified $Li[Li_{0.2}Ni_{0.17}Co_{0.07}Mn_{0.56}]O_2$ nanoparticles with MgF_2 as cathode for Li-ion battery. Solid State Ion. **278**, 85–90 (2015)
136. Bian, X., Fu, Q., Pang, Q., et al.: Multi-functional surface engineering for Li-excess layered cathode material targeting excellent electrochemical and thermal safety properties. ACS Appl. Mater. Interfaces **8**, 3308–3318 (2016)
137. Mun, J., Park, J.H., Choi, W., et al.: New dry carbon nanotube coating of over-lithiated layered oxide cathode for lithium ion batteries. J. Mater. Chem. A **2**, 19670–19677 (2014)
138. Song, B., Zhou, C., Chen, Y., et al.: Role of carbon coating in improving electrochemical performance of Li-rich $Li(Li_{0.2}Mn_{0.54}Ni_{0.13}Co_{0.13})O_2$ cathode. RSC Adv. **4**, 44244–44252 (2014)
139. Xia, Q., Zhao, X., Xu, M., et al.: A Li-rich layered@ spinel@ carbon heterostructured cathode material for high capacity and high rate lithium-ion batteries fabricated via an in situ synchronous carbonization-reduction method. J. Mater. Chem. A **3**, 3995–4003 (2015)
140. Qiu, B., Wang, J., Xia, Y., et al.: Enhanced electrochemical performance with surface coating by reactive magnetron sputtering on lithium-rich layered oxide electrodes. ACS Appl. Mater. Interfaces **6**, 9185–9193 (2014)
141. Lee, J., Choi, W.: Surface modification of over-lithiated layered oxides with PEDOT: PSS conducting polymer in lithium-ion batteries. J. Electrochem. Soc. **162**, A743–A748 (2015)
142. Wu, F., Liu, J., Li, L., et al.: Surface modification of Li-rich cathode materials for lithium-ion batteries with a PEDOT: PSS conducting polymer. ACS Appl. Mater. Interfaces **8**, 23095–23104 (2016)
143. Jiang, K.C., Wu, X.L., Yin, Y.X., et al.: Superior hybrid cathode material containing lithium-excess layered material and graphene for lithium-ion batteries. ACS Appl. Mater. Interfaces **4**, 4858–4863 (2012)
144. Xue, Q., Li, J., Xu, G., et al.: In situ polyaniline modified cathode material $Li[Li_{0.2}Mn_{0.54}Ni_{0.13}Co_{0.13}]O_2$ with high rate capacity for lithium ion batteries. J. Mater. Chem. A **2**, 18613–18623 (2014)
145. Song, B., Lai, M.O., Liu, Z., et al.: Graphene-based surface modification on layered Li-rich cathode for high-performance Li-ion batteries. J. Mater. Chem. A **1**, 9954–9965 (2013)
146. Bian, X., Fu, Q., Bie, X., et al.: Improved electrochemical performance and thermal stability of Li-excess $Li_{1.18}Co_{0.15}Ni_{0.15}Mn_{0.52}O_2$ cathode material by Li_3PO_4 surface coating. Electrochim. Acta **174**, 875–884 (2015)
147. Liu, H., Chen, C., Du, C., et al.: Lithium-rich $Li_{1.2}Ni_{0.13}Co_{0.13}Mn_{0.54}O_2$ oxide coated by Li_3PO_4 and carbon nanocomposite layers as high performance cathode materials for lithium ion batteries. J. Mater. Chem. A **3**, 2634–2641 (2015)
148. Xu, G., Li, J., Xue, Q., et al.: Elevated electrochemical performance of $(NH_4)_3AlF_6$-coated $0.5Li_2MnO_3{\cdot}0.5LiNi_{1/3}Co_{1/3}Mn_{1/3}O_2$ cathode material via a novel wet coating method. Electrochim. Acta **117**, 41–47 (2014)
149. Kang, S.H., Thackeray, M.M.: Enhancing the rate capability of high capacity $xLi_2MnO_3{\cdot}(1–x)$ $LiMO_2$ (M = Mn, Ni, Co) electrodes by Li-Ni-PO_4 treatment. Electrochem. Commun. **11**, 748–751 (2009)
150. Wu, F., Zhang, X., Zhao, T., et al.: Multifunctional $AlPO_4$ coating for improving electrochemical properties of low-cost $Li[Li_{0.2}Fe_{0.1}Ni_{0.15}Mn_{0.55}]O_2$ cathode materials for lithium-ion batteries. ACS Appl. Mater. Interfaces **7**(6), 3773–3781 (2015)
151. Sun, Y.Y., Li, F., Qiao, Q.Q., et al.: Surface modification of $Li(Li_{0.17}Ni_{0.2}Co_{0.05}Mn_{0.58})O_2$ with $LiAlSiO_4$ fast ion conductor as cathode material for Li-ion batteries. Electrochim. Acta **176**, 1464–1475 (2015)
152. Choi, W., Benayard, A., Park, J.H., et al.: Versatile coating of lithium conductive Li_2TiF_6 on over-lithiated layered oxide in lithium-ion batteries. Electrochim. Acta **117**, 492–497 (2014)
153. Meng, H., Li, L., Liu, J., et al.: Surface modification of Li-rich layered $Li[Li_{0.17}Ni_{0.17}Co_{0.10}Mn_{0.56}]O_2$ oxide with LiV_3O_8 as a cathode material for Li-ion batteries. J. Alloys Compd. **690**, 256–266 (2017)
154. Fu, Q., Du, F., Bian, X., et al.: Electrochemical performance and thermal stability of $Li_{1.18}Co_{0.15}Ni_{0.15}Mn_{0.52}O_2$ surface coated with the ionic conductor Li_3VO_4. J. Mater. Chem. A **2**, 7555–7562 (2014)
155. Ahn, J., Kim, J.H., Cho, B.W., et al.: Nanoscale zirconium-abundant surface layers on lithium-and manganese-rich layered oxides for high-rate lithium-ion batteries. Nano Lett. **17**, 7869–7877 (2017)
156. Qiao, Q., Zhang, H., Li, G., et al.: Surface modification of Li-rich layered $Li(Li_{0.17}Ni_{0.25}Mn_{0.58})O_2$ oxide with Li–Mn–PO_4 as the cathode for lithium-ion batteries. J. Mater. Chem. A **1**, 5262–5268 (2013)
157. Prakasha, K.R., Sathish, M., Bera, P., et al.: Mitigating the surface degradation and voltage decay of $Li_{1.2}Ni_{0.13}Mn_{0.54}Co_{0.13}O_2$ cathode material through surface modification using Li_2ZrO_3. ACS Omega **2**, 2308–2316 (2017)
158. Guo, S., Yu, H., Liu, P., et al.: Surface coating of lithium-manganese-rich layered oxides with delaminated MnO_2 nanosheets as cathode materials for Li-ion batteries. J. Mater. Chem. A **2**, 4422–4428 (2014)
159. Liu, Y., Wang, Q., Lu, Y., et al.: Enhanced electrochemical performances of layered cathode material $Li_{1.5}Ni_{0.25}Mn_{0.75}O_{2.5}$ by coating with $LiAlO_2$. J. Alloys Compd. **638**, 1–6 (2015)
160. Wu, F., Wang, Z., Su, Y., et al.: Li $[Li_{0.2}Mn_{0.54}Ni_{0.13}Co_{0.13}]O_2$-$MoO_3$ composite cathodes with low irreversible capacity loss for lithium ion batteries. J. Power Sources **247**, 20–25 (2014)
161. Kong, J.Z., Wang, C.L., Qian, X., et al.: Enhanced electrochemical performance of $Li_{1.2}Mn_{0.54}Ni_{0.13}Co_{0.13}O_2$ by surface modification with graphene-like lithium-active MoS_2. Electrochim. Acta **174**, 542–550 (2015)
162. Kong, J.Z., Xu, L.P., Wang, C.L., et al.: Facile coating of conductive poly (vinylidene fluoride-trifluoroethylene) copolymer on $Li_{1.2}Mn_{0.54}Ni_{0.13}Co_{0.13}O_2$ as a high electrochemical performance cathode for Li-ion battery. J. Alloys Compd. **719**, 401–410 (2017)
163. Du, K., Yang, F., Hu, G., et al.: Sodium additive to improve rate performance of $Li[Li_{0.2}Mn_{0.54}Ni_{0.13}Co_{0.13}]O_2$ material for Li-ion batteries. J. Power Sources **244**, 29–34 (2013)
164. Li, Q., Li, G., Fu, C., et al.: K^+-Doped $Li_{1.2}Mn_{0.54}Co_{0.13}Ni_{0.13}O_2$: a novel cathode material with an enhanced cycling stability for lithium-ion batteries. ACS Appl. Mater. Interfaces **6**, 10330–10341 (2014)
165. Zheng, Z., Guo, X.D., Zhong, Y.J., et al.: Host structural stabilization of $Li_{1.232}Mn_{0.615}Ni_{0.154}O_2$ through K-doping attempt: toward superior electrochemical performances. Electrochim. Acta **188**, 336–343 (2016)
166. Yu, R., Wang, X., Fu, Y., et al.: Effect of magnesium doping on properties of lithium-rich layered oxide cathodes based on a one-step co-precipitation strategy. J. Mater. Chem. A **4**, 4941–4951 (2016)
167. Yan, W., Xie, Y., Jiang, J., et al.: Enhanced rate performance of Al-doped Li-rich layered cathode material via nucleation and post-solvothermal method. ACS Sustain. Chem. Eng. **6**, 4625–4632 (2018)
168. Ramesha, R.N., Laisa, C.P., Ramesha, K.: Improving electrochemical stability by transition metal cation doping for manganese in lithium-rich layered cathode, $Li_{1.2}Ni_{0.13}Co_{0.13}Mn_{0.54-x}M_xO_2$ (M = Co, Cr and Fe). Electrochim. Acta **249**, 377–386 (2017)
169. Li, N., An, R., Su, Y., et al.: The role of yttrium content in improving electrochemical performance of layered lithium-rich cathode materials for Li-ion batteries. J. Mater. Chem. A **1**, 9760–9767 (2013)

170. Qiao, Q.Q., Qin, L., Li, G.R., et al.: Sn-stabilized Li-rich layered $Li(Li_{0.17}Ni_{0.25}Mn_{0.58})O_2$ oxide as a cathode for advanced lithium-ion batteries. J. Mater. Chem. A **3**, 17627–17634 (2015)
171. Feng, X., Gao, Y., Ben, L., et al.: Enhanced electrochemical performance of Ti-doped $Li_{1.2}Mn_{0.54}Co_{0.13}Ni_{0.13}O_2$ for lithium-ion batteries. J. Power Sources **317**, 74–80 (2016)
172. He, Z., Wang, Z., Chen, H., et al.: Electrochemical performance of zirconium doped lithium rich layered $Li_{1.2}Mn_{0.54}Ni_{0.13}Co_{0.13}O_2$ oxide with porous hollow structure. J. Power Sources **299**, 334–341 (2015)
173. Shang, H., Ning, F., Li, B., et al.: Suppressing voltage decay of lithium-rich cathode material by surface enrichment with atomic ruthenium. ACS Appl. Mater. Interfaces **10**, 21349–21355 (2018)
174. Song, B., Lai, M.O., Lu, L.: Influence of Ru substitution on Li-rich $0.55Li_2MnO_3{\cdot}0.45\ LiNi_{1/3}Co_{1/3}Mn_{1/3}O_2$ cathode for Li-ion batteries. Electrochim. Acta **80**, 187–195 (2012)
175. Zhang, H.Z., Li, F., Pan, G.L., et al.: The effect of polyanion-doping on the structure and electrochemical performance of Li-rich layered oxides as cathode for lithium-ion batteries. J. Electrochem. Soc. **162**, A1899–A1904 (2015)
176. Huang, J., Liu, H., Hu, T., et al.: Enhancing the electrochemical performance of Li-rich layered oxide $Li_{1.13}Ni_{0.3}Mn_{0.57}O_2$ via WO_3 doping and accompanying spontaneous surface phase formation. J. Power Sources **375**, 21–28 (2018)
177. Kleiner, K., Strehle, B., Baker, A.R., et al.: Origin of high capacity and poor cycling stability of Li-rich layered oxides: a long-duration in situ synchrotron powder diffraction study. Chem. Mater. **30**, 3656–3667 (2018)
178. Johnson, C.S., Li, N., Lefief, C., et al.: Synthesis, characterization and electrochemistry of lithium battery electrodes: $xLi_2MnO_3{\cdot}(1-x)\ LiMn_{0.333}Ni_{0.333}Co_{0.333}O_2$ $(0 \leqslant x \leqslant 0.7)$. Chem. Mater. **20**, 6095–6106 (2008)
179. Croy, J.R., Kim, D., Balasubramanian, M., et al.: Countering the voltage decay in high capacity $xLi_2MnO_3{\bullet}(1-x)\ LiMO_2$ electrodes (M = Mn, Ni, Co) for Li^+-Ion batteries. J. Electrochem. Soc. **159**, A781–A790 (2012)
180. Oh, P., Ko, M., Myeong, S., et al.: A novel surface treatment method and new insight into discharge voltage deterioration for high-performance $0.4\ Li_2MnO_3{-}0.6\ LiNi_{1/3}Co_{1/3}Mn_{1/3}O_2$ cathode materials. Adv. Energy Mater. **4**, 1400631 (2014)
181. Sathiya, M., Abakumov, A.M., Foix, D., et al.: Origin of voltage decay in high-capacity layered oxide electrodes. Nat. Mater. **14**, 230 (2015)
182. Wei, Z., Xia, Y., Qiu, B., et al.: Correlation between transition metal ion migration and the voltage ranges of electrochemical process for lithium-rich manganese-based material. J. Power Sources **281**, 7–10 (2015)
183. Yan, P., Zheng, J., Lv, D., et al.: Atomic-resolution visualization of distinctive chemical mixing behavior of Ni Co, and Mn with Li in layered lithium transition-metal oxide cathode materials. Chem. Mater. **27**, 5393–5401 (2015)
184. Dogan, F., Long, B.R., Croy, J.R., et al.: Re-entrant lithium local environments and defect driven electrochemistry of Li-and Mn-rich Li-ion battery cathodes. J. Am. Chem. Soc. **137**, 2328–2335 (2015)
185. Yan, P., Zheng, J., Gu, M., et al.: Intragranular cracking as a critical barrier for high-voltage usage of layer-structured cathode for lithium-ion batteries. Nat. Commun. **8**, 14101 (2017)
186. Luo, K., Roberts, M.R., Hao, R., et al.: Charge-compensation in 3d-transition-metal-oxide intercalation cathodes through the generation of localized electron holes on oxygen. Nat. Chem. **8**, 684 (2016)
187. Yan, P., Nie, A., Zheng, J., et al.: Evolution of lattice structure and chemical composition of the surface reconstruction layer in $Li_{1.2}Ni_{0.2}Mn_{0.6}O_2$ cathode material for lithium ion batteries. Nano Lett. **15**, 514–522 (2014)
188. Wang, H., Jang, Y.I., Huang, B., et al.: TEM study of electrochemical cycling-induced damage and disorder in $LiCoO_2$ cathodes for rechargeable lithium batteries. J. Electrochem. Soc. **146**, 473–480 (1999)
189. Jena, A., Lee, C.H., Pang, W.K., et al.: Capacity enhancement of the quenched Li–Ni–Mn–Co oxide high-voltage li-ion battery positive electrode. Electrochim. Acta **236**, 10–17 (2017)
190. Dong, L., Liang, F., Wang, D., et al.: Safe ionic liquid-sulfolane/LiDFOB electrolytes for high voltage $Li_{1.15}\ (Ni_{0.36}Mn_{0.64})_{0.85}O_2$ lithium ion battery at elevated temperatures. Electrochim. Acta **270**, 426–433 (2018)
191. Ji, Y., Zhang, Z., Gao, M., et al.: Electrochemical behavior of suberonitrile as a high-potential electrolyte additive and co-solvent for $Li[Li_{0.2}Mn_{0.56}Ni_{0.16}Co_{0.08}]O_2$ cathode material. J. Electrochem. Soc. **162**, A774–A780 (2015)
192. Zheng, J., Xiao, J., Gu, M., et al.: Interface modifications by anion receptors for high energy lithium ion batteries. J. Power Sources **250**, 313–318 (2014)
193. Nayak, P.K., Grinblat, J., Levi, M., et al.: Understanding the effect of lithium bis(oxalato) borate (LiBOB) on the structural and electrochemical aging of Li and Mn rich high capacity $Li_{1.2}Ni_{0.16}Mn_{0.56}Co_{0.08}O_2$ cathodes. J. Electrochem. Soc. **162**, A596–A602 (2015)
194. Zhu, Y., Luo, X., Zhi, H., et al.: Structural exfoliation of layered cathode under high voltage and its suppression by interface film derived from electrolyte additive. ACS Appl. Mater. Interfaces **9**, 12021–12034 (2017)
195. Zhu, Y., Li, Y., Bettge, M., et al.: Electrolyte additive combinations that enhance performance of high-capacity $Li_{1.2}Ni_{0.15}Mn_{0.55}Co_{0.1}O_2$-graphite cells. Electrochim. Acta **110**, 191–199 (2013)
196. Wu, Q., Lu, W., Miranda, M., et al.: Effects of lithium difluoro (oxalate) borate on the performance of Li-rich composite cathode in Li-ion battery. Electrochem. Commun. **24**, 78–81 (2012)
197. Tu, W., Xia, P., Zheng, X., et al.: Insight into the interaction between layered lithium-rich oxide and additive-containing electrolyte. J. Power Sources **341**, 348–356 (2017)
198. Birrozzi, A., Laszczynski, N., Hekmatfar, M., et al.: Beneficial effect of propane sultone and tris (trimethylsilyl) borate as electrolyte additives on the cycling stability of the lithium rich nickel manganese cobalt (NMC) oxide. J. Power Sources **325**, 525–533 (2016)
199. Lim, S.H., Cho, W., Kim, Y.J., et al.: Insight into the electrochemical behaviors of 5 V-class high-voltage batteries composed of lithium-rich layered oxide with multifunctional additive. J. Power Sources **336**, 465–474 (2016)
200. Wang, L., Ma, Y., Li, Q., et al.: 1,3,6-Hexanetricarbonitrile as electrolyte additive for enhancing electrochemical performance of high voltage Li-rich layered oxide cathode. J. Power Sources **361**, 227–236 (2017)
201. Chen, Z., Liu, J., Amine, K.: Impact of tripropyl borate on life and impedance of lithium-ion cells. Electrochim. Acta **53**, 3267–3270 (2008)
202. Pires, J., Castets, A., Timperman, L., et al.: Tris (2, 2, 2-trifluoroethyl) phosphite as an electrolyte additive for high-voltage lithium-ion batteries using lithium-rich layered oxide cathode. J. Power Sources **296**, 413–425 (2015)
203. Tan, S., Zhang, Z., Li, Y., et al.: Tris(hexafluoro-iso-propyl) phosphate as an SEI-forming additive on improving the electrochemical performance of the $Li[Li_{0.2}Mn_{0.56}Ni_{0.16}Co_{0.08}]O_2$ cathode material. J. Electrochem. Soc. **160**, A285–A292 (2013)
204. Pham, H.Q., Kim, G., Jung, H.M., et al.: Fluorinated polyimide as a novel high-voltage binder for high-capacity cathode of lithium-ion batteries. Adv. Funct. Mater. **28**, 1704690 (2018)
205. Zhang, S., Gu, H., Pan, H., et al.: A novel strategy to suppress capacity and voltage fading of Li-and Mn-rich layered oxide

cathode material for lithium-ion batteries. Adv. Energy Mater. **7**, 1601066 (2017)
206. Liu, W., Oh, P., Liu, X., et al.: Countering voltage decay and capacity fading of lithium-rich cathode material at 60 C by hybrid surface protection layers. Adv. Energy Mater. **5**, 1500274 (2015)
207. Kim, S., Cho, W., Zhang, X., et al.: A stable lithium-rich surface structure for lithium-rich layered cathode materials. Nat. Commun. **7**, 13598 (2016)
208. Ates, M.N., Jia, Q., Shah, A., et al.: Mitigation of layered to spinel conversion of a Li-rich layered metal oxide cathode material for Li-ion batteries. J. Electrochem. Soc. **161**, A290–A301 (2014)
209. Wang, D., Huang, Y., Huo, Z., et al.: Synthesize and electrochemical characterization of Mg-doped Li-rich layered $Li[Li_{0.2}Ni_{0.2}Mn_{0.6}]O_2$ cathode material. Electrochim. Acta **107**, 461–466 (2013)
210. Yu, Z., Shang, S.L., Gordin, M.L., et al.: Ti-substituted $Li[Li_{0.26}Mn_{0.6-x}Ti_xNi_{0.07}Co_{0.07}]O_2$ layered cathode material with improved structural stability and suppressed voltage fading. J. Mater. Chem. A **3**, 17376–17384 (2015)
211. Li, L., Song, B.H., Chang, Y.L., et al.: Retarded phase transition by fluorine doping in Li-rich layered $Li_{1.2}Mn_{0.54}Ni_{0.13}Co_{0.13}O_2$ cathode material. J. Power Sources **283**, 162–170 (2015)
212. Li, Z., Du, F., Bie, X., et al.: Electrochemical kinetics of the $Li[Li_{0.23}Co_{0.3}Mn_{0.47}]O_2$ cathode material studied by GITT and EIS. J. Phys. Chem. C **114**, 22751–22757 (2010)
213. Ates, M.N., Mukerjee, S., Abraham, K.: A Li-rich layered cathode material with enhanced structural stability and rate capability for Li-on batteries. J. Electrochem. Soc. **161**, A355–A363 (2014)
214. Nayak, P.K., Grinblat, J., Levi, E., et al.: Remarkably improved electrochemical performance of Li-and Mn-rich cathodes upon substitution of Mn with Ni. ACS Appl. Mater. Interfaces **9**, 4309–4319 (2016)
215. Massarotti, V., Capsoni, D., Bini, M., et al.: Electric and magnetic properties of $LiMn_2O_4$-and Li_2MnO_3-type oxides. J. Solid State Chem. **131**, 94–100 (1997)
216. Vendra, V.K., Nguyen, T.Q., Thapa, A.K., et al.: Scalable synthesis and surface stabilization of Li_2MnO_3 NWs as high rate cathode materials for Li-ion batteries. RSC Adv. **5**, 36906–36912 (2015)
217. Liu, J., Reeja-Jayan, B., Manthiram, A.: Conductive surface modification with aluminum of high capacity layered $Li[Li_{0.2}Mn_{0.54}Ni_{0.13}Co_{0.13}]O_2$ cathodes. J. Phys. Chem. C **114**, 9528–9533 (2010)
218. Urban, A., Matts, I., Abdellahi, A., et al.: Computational design and preparation of cation-disordered oxides for high-energy-density Li-ion batteries. Adv. Energy Mater. **6**, 1600488 (2016)
219. Lee, J., Urban, A., Li, X., et al.: Unlocking the potential of cation-disordered oxides for rechargeable lithium batteries. Science **343**, 519–522 (2014)
220. Johnson, C.S., Kim, J.S., Lefief, C., et al.: The significance of the Li_2MnO_3 component in "composite" $xLi_2MnO_3\cdot(1-x)$ $LiMn_{0.5}Ni_{0.5}O_2$ electrodes. Electrochem. Commun. **6**, 1085–1091 (2004)
221. Oh, P., Oh, S.M., Li, W., et al.: High-performance heterostructured cathodes for lithium-ion batteries with a Ni-rich layered oxide core and a Li-rich layered oxide shell. Adv. Sci. **3**, 1600184 (2016)
222. Kim, D., Sandi, G., Croy, J.R., et al.: Composite "layered-layered-spinel" cathode structures for lithium-ion batteries. J. Electrochem. Soc. **160**, A31–A38 (2013)
223. Cheng, F., Chen, J., Zhou, H., et al.: Structural and electrochemical characterization of $(NH_4)HPO_4$-treated lithium-rich layered $Li_{1.2}Ni_{0.2}Mn_{0.6}O_2$ cathodes for lithium-ion batteries. J. Electrochem. Soc. **160**, A1661–A1667 (2013)
224. Zheng, J., Deng, S., Shi, Z., et al.: The effects of persulfate treatment on the electrochemical properties of $Li[Li_{0.2}Mn_{0.54}Ni_{0.13}Co_{0.13}]O_2$ cathode material. J. Power Sources **221**, 108–113 (2013)
225. Han, S., Qiu, B., Wei, Z., et al.: Surface structural conversion and electrochemical enhancement by heat treatment of chemical pre-delithiation processed lithium-rich layered cathode material. J. Power Sources **268**, 683–691 (2014)
226. Denis, Y., Yanagida, K., Nakamura, H.: Surface modification of Li-excess Mn-based cathode materials. J. Electrochem. Soc. **157**, A1177–A1182 (2010)
227. Liu, H., Du, C., Yin, G., et al.: An Li-rich oxide cathode material with mosaic spinel grain and a surface coating for high performance Li-ion batteries. J. Mater. Chem. A **2**, 15640–15646 (2014)
228. Wu, F., Li, N., Su, Y., et al.: Spinel/layered heterostructured cathode material for high-capacity and high-rate Li-ion batteries. Adv. Mater. **25**, 3722–3726 (2013)
229. Wang, D., Wang, X., Yang, X., et al.: Polyaniline modification and performance enhancement of lithium-rich cathode material based on layered-spinel hybrid structure. J. Power Sources **293**, 89–94 (2015)
230. Song, B., Liu, H., Liu, Z., et al.: High rate capability caused by surface cubic spinels in Li-rich layer-structured cathodes for Li-ion batteries. Sci. Rep. **3**, 3094 (2013)
231. Oh, P., Myeong, S., Cho, W., et al.: Superior long-term energy retention and volumetric energy density for Li-rich cathode materials. Nano Lett. **14**, 5965–5972 (2014)
232. Zhang, H.Z., Qiao, Q.Q., Li, G.R., et al.: Surface nitridation of Li-rich layered $Li(Li_{0.17}Ni_{0.25}Mn_{0.58})O_2$ oxide as cathode material for lithium-ion battery. J. Mater. Chem. **22**, 13104–13109 (2012)
233. Wei, G.Z., Lu, X., Ke, F.S., et al.: Crystal habit-tuned nanoplate material of $Li[Li_{1/3-2x/3}Ni_xMn_{2/3-x/3}]O_2$ for high-rate performance lithium-ion batteries. Adv. Mater. **22**, 4364–4367 (2010)
234. Zhang, L., Li, N., Wu, B., et al.: Sphere-shaped hierarchical cathode with enhanced growth of nanocrystal planes for high-rate and cycling-stable li-ion batteries. Nano Lett. **15**, 656–661 (2014)
235. Li, J., Camardese, J., Shunmugasundaram, R., et al.: Synthesis and characterization of the lithium-rich core-shell cathodes with low irreversible capacity and mitigated voltage fade. Chem. Mater. **27**, 3366–3377 (2015)
236. Noh, J.K., Kim, S., Kim, H., et al.: Mechanochemical synthesis of Li_2MnO_3 shell/$LiMO_2$ (M = Ni Co, Mn) core-structured nanocomposites for lithium-ion batteries. Sci. Rep. **4**, 4847 (2014)
237. Pajot, S., Feydi, P., Weill, F., et al.: Synthesis of Li and Mn-rich layered oxides as concentration-gradients for lithium-ion batteries. J. Electrochem. Soc. **165**, A425–A433 (2018)
238. Zheng, J., Wu, X., Yang, Y.: Improved electrochemical performance of $Li[Li_{0.2}Mn_{0.54}Ni_{0.13}Co_{0.13}]O_2$ cathode material by fluorine incorporation. Electrochim. Acta **105**, 200–208 (2013)
239. Sathiya, M., Rousse, G., Ramesha, K., et al.: Reversible anionic redox chemistry in high-capacity layered-oxide electrodes. Nat. Mater. **12**, 827 (2013)
240. Jiang, Y., Yang, Z., Luo, W., et al.: Hollow $0.3Li_2MnO_3\cdot0.7$ $LiNi_{0.5}Mn_{0.5}O_2$ microspheres as a high-performance cathode material for lithium-ion batteries. Phys. Chem. Chem. Phys. **15**, 2954–2960 (2013)
241. Fu, F., Tang, J., Yao, Y., et al.: Hollow porous hierarchical-structured $0.5Li_2MnO_3\cdot0.5LiMn_{0.4}Co_{0.3}Ni_{0.3}O_2$ as a high-performance cathode material for lithium-ion batteries. ACS Appl. Mater. Interfaces **8**, 25654–25659 (2016)
242. Chen, L., Su, Y., Chen, S., et al.: Hierarchical $Li_{1.2}Ni_{0.2}Mn_{0.6}O_2$ nanoplates with exposed {010} planes as high-performance cathode material for lithium-ion batteries. Adv. Mater. **26**, 6756–6760 (2014)
243. Xu, M., Fei, L., Zhang, W., et al.: Tailoring anisotropic Li-Ion transport tunnels on orthogonally arranged Li-rich layered oxide

nanoplates toward high-performance Li-ion batteries. Nano Lett. **17**, 1670–1677 (2017)
244. He, X., Wang, J., Wang, R., et al.: A 3D porous Li-rich cathode material with an in situ modified surface for high performance lithium ion batteries with reduced voltage decay. J. Mater. Chem. A **4**, 7230–7237 (2016)
245. Lin, F., Markus, I.M., Nordlund, D., et al.: Surface reconstruction and chemical evolution of stoichiometric layered cathode materials for lithium-ion batteries. Nat. Commun. **5**, 3529 (2014)
246. Martha, S.K., Nanda, J., Veith, G.M., et al.: Electrochemical and rate performance study of high-voltage lithium-rich composition: $Li_{1.2}Mn_{0.525}Ni_{0.175}Co_{0.1}O_2$. J. Power Sources **199**, 220–226 (2012)
247. Yabuuchi, N., Yoshii, K., Myung, S.T., et al.: Detailed studies of a high-capacity electrode material for rechargeable batteries, Li_2MnO_3-$LiCo_{1/3}Ni_{1/3}Mn_{1/3}O_2$. J. Am. Chem. Soc. **133**, 4404–4419 (2011)
248. Zheng, X., Wang, X., Cai, X., et al.: Constructing a protective interface film on layered lithium-rich cathode using an electrolyte additive with special molecule structure. ACS Appl. Mater. Interfaces **8**, 30116–30125 (2016)
249. Cha, J., Han, J.G., Hwang, J., et al.: Mechanisms for electrochemical performance enhancement by the salt-type electrolyte additive, lithium difluoro (oxalato) borate, in high-voltage lithium-ion batteries. J. Power Sources **357**, 97–106 (2017)

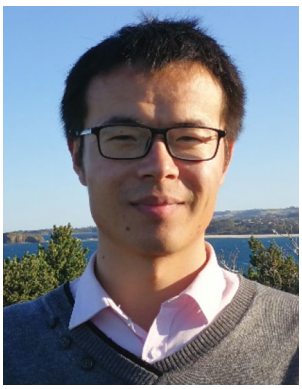

Dr. Sijiang Hu received his M.Sc. in Physical Chemistry at Guangxi Normal University, China, in 2010. Then he got a lecture position at Huanggang Normal University. Dr. Hu received his Ph.D. from China University of Geosciences in 2015 and then moved to Institute for Superconducting and Electronic Materials (ISEM), University of Wollongong (UOW), as a postdoctoral research fellow with Professor Zaiping Guo. His current research interests focus on advanced materials and technologies for energy conversion and storage devices (e.g. Li-ion batteries, supercapacitors).

Anoop. S. Pillai recieved his Bachelor's degree from University of Kerala and Master's degree from Amrita Viswa Vidyapeetham University in India. He joined as a Ph.D. student at Institute of Superconducting and electronic Materials (ISEM), University of Wollongong, under supervision of Dr. Wei Kong Pang and Prof. Zaiping Guo in July 2017. His research focuses on synthesis, characterization and mechanical investigation of high-voltage positive electrode materials for Li-ion batteries.

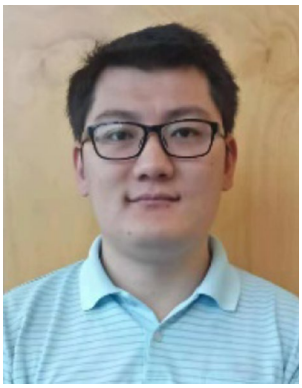

Gemeng Liang received his Bachelor's degree from Shandong University in 2014 and Master's degree from Tsinghua University in 2017. Currently he is a Ph.D. candidate at the Institute for Superconducting and Electronic Materials (ISEM), University of Wollongong, Australia, under the supervision of Dr. Wei Kong Pang, Prof. Vanessa Peterson and Prof. Zaiping Guo. His research focuses on the high-voltage cathode materials and their mechanistic behaviour in lithium-ion batteries.

Dr. Wei Kong Pang received his Ph.D. in Applied Physics from Curtin University, Western Australia, in 2011. As a joint postdoctoral research fellow, he then focused on the research and development of Li-ion batteries at the National Taiwan University and the Department of Materials Engineering at Tatung University. Since June 2013, he has been a joint postdoctoral fellow at University of Wollongong and Australian Nuclear Science and Technology Organization. Currently he was awarded with an Australian Future Fellowship and works as a senior research fellow at Institute for Superconducting and Electronic Materials, University of Wollongong since 2016. His main focus is the crystallography of materials for energy storage applications and understanding their structure–function relationships. This includes understanding the insertion/extraction mechanism and working principles of the electrode materials for both Li- and Na-ion batteries by using a variety of in situ techniques.

Dr. Hongqiang Wang received his Ph.D. in metallurgical physical chemistry from Central South University (China) in 2003. After his Ph.D., he joined the Guangxi Normal University and was promoted to Professor in 2009. Dr. Wang's expertise areas include (1) supercapacitors; (2) lithium-ion batteries, lithium–air batteries and battery technology; (3) electroplating technique and aluminium electrolysis. Dr. Wang has conducted in total 15 projects funded by Chinese Government including National Natural Science Foundation of China (NSFC) and the Key Research and Development Program of Guangxi Province. He authored 80+ publications in peer-reviewed journals and 30+ patents in the areas of energy materials, particularly in lithium-ion battery, supercapacitors and aluminium electrolysis.

Dr. Qinyu Li is a professor of School of Chemistry and Pharmaceutical Sciences at the Guangxi Normal University, leader of Guangxi Key Laboratory for New Energy Material and Technology. He received his Ph.D. in non-ferrous metallurgy from the Central South University in 2003. He is a committee member of Chinese Society of Electrochemistry (CSE) and a board committee member of the International Academy of Electrochemical Energy Science (IAOEES). His researches aim to bring technology innovations and practical applications for materials and new energy. More specifically, his current works focus on (a) new energy material-based energy storage systems, including batteries and supercapacitors; and (b) functional materials for energy conservation and environmental protection, particularly for aluminium electrolysis and battery recycling.

Prof. Zaiping Guo is a distinguished professor and an Australian Research Council (ARC) Future Fellow (FT3) at School of Mechanical, Materials, Mechatronic, and Biomedical Engineering, and Institute for Superconducting and Electronic Materials, University of Wollongong, Australia. She received her Ph.D. degree from University of Wollongong in 2003. Her current research interest mainly focuses on the energy storage such as lithium-ion batteries, sodium-ion batteries, potassium-ion batteries and hydrogen storage, as well as electrochemistry characterization and computer modelling.